GEO-3900

# MASTER'S THESIS IN GEOLOGY

## *Shallow gas accumulation in glacigenic sedimentary formation of the mid-Norwegian margin north of Storegga slide (Helland Hansen 3D cube)*

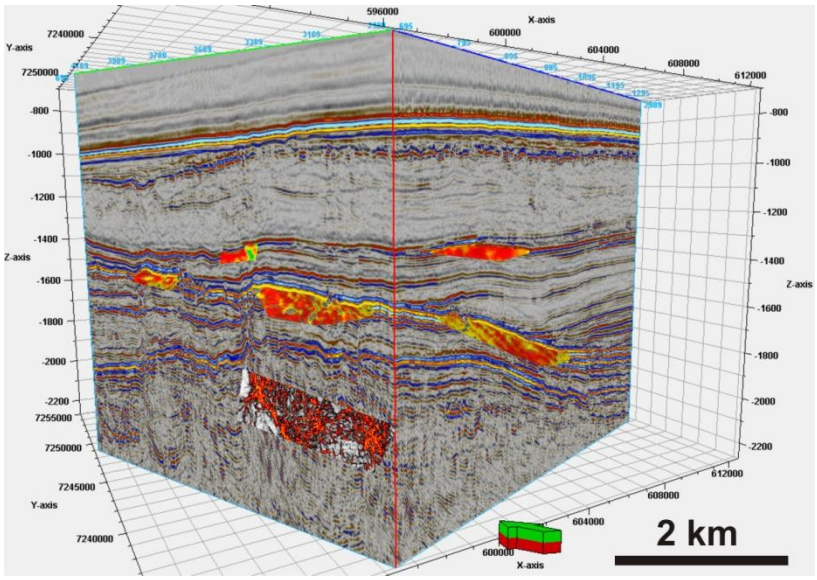


Tanveer Ahmad

June, 2012

Faculty of Science and Technology

Department of Geology

University of Tromsø

GEO-3900

# MASTER'S THESIS IN GEOLOGY

## Shallow gas accumulation in glacigenic sedimentary formation of the mid-Norwegian margin north of Storegga slide (Helland Hansen 3D cube)

Tanveer Ahmad

June, 2012

Faculty of Science and Technology

Department of Geology

University of Tromsø

## Abstract

My master thesis concentrates on the distribution of gas accumulation to infer vertical fluid migration in sedimentary formations of Eocene-Oligocene (Brygge Formation) and Pliocene-Pleistocene (Naust Formation) in the mid-Norwegian margin at the Helland Hansen Arch, north of the Storegga slide. The seismic interpretation is based on "Helland Hansen 3D cube SH9602". The N-S oriented Helland Hansen Arch (HHA) has a hydrocarbon potential where both tectonic and thermal subsidence has played a role in forming hydrocarbon traps. The oozes and debris flow deposit seal off the vertical migrating fluids allowing them to accumulate along the HHA. At the crest of HHA seismic bright spots are delineated by using acoustic attributes. The area beneath the bright spots shows the depletion of higher frequencies due to absorption of seismic energy. Beneath the bright spot vertical fluid migration features appear as disturbed and distorted wipe-out seismic zone and velocity sags (push down). The vertical fluid migration features occur along major faults and are identified by the low coherency values on variance attribute maps. Gas accumulation zones are extensively disturbed by faulting along the eastern flanks of HHA where polygonal faults provide routes for vertical gas migration. The polygonal faults were reactivated by sediment loading from submarine slides. Pipe structures provide further pathways for vertical gas migration from reactivated polygonal faults. The presence of gas in the glacigenic sedimentary formation of Naust A and U unit is identified by the distinct reduction of P-wave velocities.

*Behold! In the creation of the heavens and the earth; in the alternation of the Night and the Day; in the sailing of the ships through the Ocean for the profit of mankind; in the rain which Allah sends down from the skies, and the life which He gives there with to an earth that is dead; in the beasts of all kinds that He scatters through the earth; in the change of the winds and the clouds which they trail like their slaves between the sky and the earth, (here) indeed are Signs for a people that are wise (HOLY QURAN 2: 164).*

## Acknowledgements

My master thesis would not have been possible without the support and assistance of many people. I would like to express my gratitude to supervisor, Prof. Dr. Jurgen Mienert who was abundantly helpful and offered invaluable assistance, support and guidance. Deepest gratitude is also due to the co-supervision of Assoc. Prof. Dr. Stefan Bunz, without his guidance and assistance this study would not have been successful. I have learnt a lot from their knowledge and experience. Special thanks to all Geophysics group members; Alxandros, Sunil, Peter, Malin, Yasir, Krishna, Torgeir for sharing the literature, experience and guidance. I also wish my gratitude to best friends, Ibrahim, Amir, Haroon, Atif, Munawar, Kenneth, Morten, Kjtil, Alexy who rendered their support and guidance during the period of my thesis. I would also like to convey my thanks to Andreia Plaza and Leif Rise for their guidance in carrying out this thesis work and to solve the problems.

I wish to express my love and gratitude to my beloved family specially my mother for her prayers & endless love, through the duration of my studies.

Tanveer Ahmad

June, 2012.

# Contents

# 1 Introduction

## 1.1 Objectives

The main objective of my master thesis is to determine and understand the distribution of shallow gas accumulations in glacigenic sedimentary formations of the mid–Norwegian margin at the Helland Hansen Arch (HHA) north of the Storegga slide (Fig. 1.1). For this investigation I shall use a 3D seismic cube (Helland Hansen 3D cube) and seismic attribute interpretation tools. Acoustic sub-seabed imaging tools allow to determine pathways of migrating fluids, their accumulation areas and their relation to various sedimentary formations. The acoustic attribute (amplitude, frequency) are generated to infer fluid pathways, accumulation area and potentially over pressurized horizons.

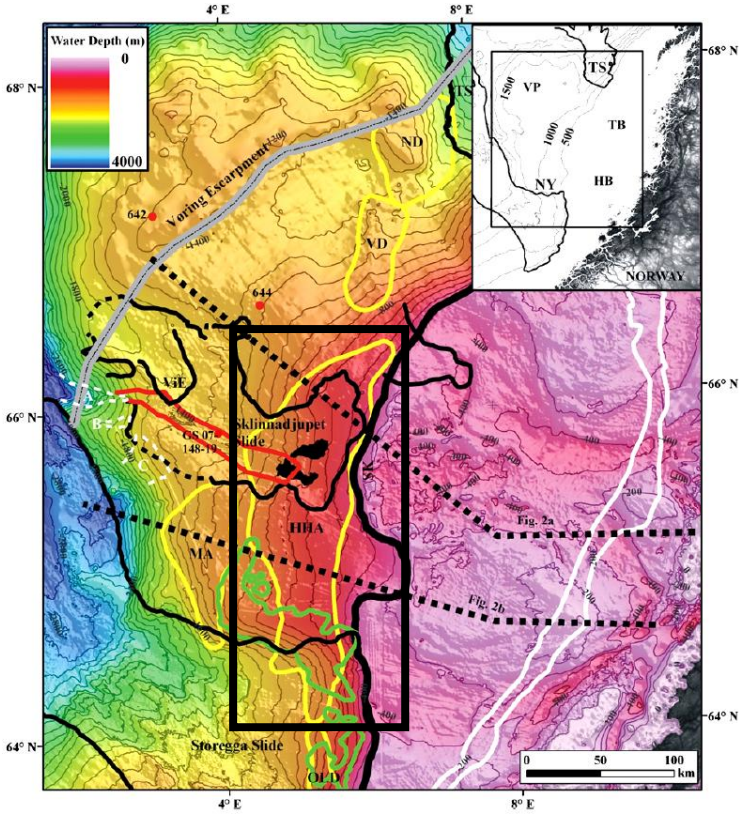


**Figure 1.1: Shaded relief bathymetry map of mid-Norwegian margin showing five prominent dome structures represented by yellow polygons; Helland-Hansen Arch (HHA); Modgunn Arch (MA); Vema Dome (VD); Nagelfar Dome (ND); Ormen Lange Dome (OLD ); Large slides (black polygons), slides A, B, C(Dashed white polygons), evacuation craters (black area), gas hydrate Bottom Simulating Reflector( BSR, green polygon), ODP bore holes are marked by red dots, shelf edge(thick black line) and mound area (red polygon), subcrop Molo Formation (white polygon) and locations of regional seismo-geological sections in Fig.2.6. The location of the study area is indicated by a black rectangle. (Figure from Rise et al., 2010).**

## 1.2 Motivation

Shallow gas in marine sediments may contain appreciable amounts of carbon dioxide, hydrogen sulphide, ethane and/or methane. There are mainly two sources for shallow gas accumulation in marine sediments: (1) biogenic gas produced by the bacterial activity within the top few hundred meters of sediments at 0-80°C temperature and (2) thermogenic gas produced by the degradation and cracking of organic matter at high temperature (90-250°C) and pressure at depth greater than 1000 m during catagenesis. Thermogenic gas may migrate towards the surface due to large enough hydraulic gradients. It may be barred by impermeable sediments from further movement to the seabed and thus trapped as shallow gas accumulation (Fig. 1.2). (Floodgate & Judd, 1992., Missiaen et al., 2002). Biological processes best explains the origin of most of the shallow gas which involve the intervention of dead organism decay and bacteria activity, which generate methane (Floodgate & Judd, 1992).

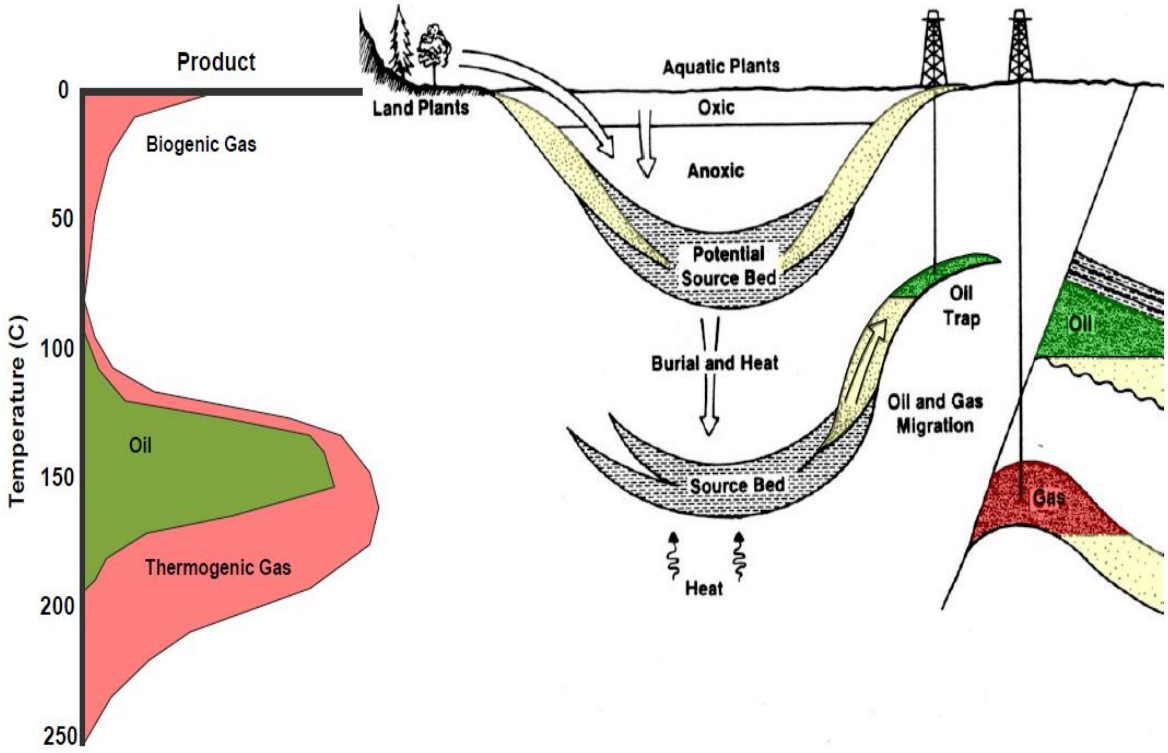


**Figure 1.2: Generation and accumulation of shallow gas in marine sediments. (Figure from petroleum geology notes, Statoil).**

In order to distinguish between shallow and deep sources one can apply geophysical imaging methods to identify fluid migration pathways. Migration pathways connected to

shallow gas accumulation areas may allow to infer biogenic and/or thermogenic source areas. This master thesis will use seismic interpretation tools to infer both fluid migration pathways and shallow gas accumulation areas connected to potential escape routes to the seabed. The natural release of gas to the ocean and atmosphere may contribute to changes in the acidification of water masses and/or to greenhouse gas increases in the atmosphere (Floodgate & Judd, 1992).

## 1.3 Petroleum System

A petroleum system encompasses a pod of active source rocks and all genetically related oil and gas accumulations. It also includes the geological elements such as source rock, reservoir rock, seal rock and overburden rock. The important processes involved are trap formation and the generation, migration and accumulation of hydrocarbons. These essential elements are time and space dependent where organic matter in the source rock provides the base for a hydrocarbon generation (Magoon & Dow 1994).

A source rock consists of enough reactive organic material to generate and expel petroleum (oil and gas). When organic material is preserved in anoxic conditions then it may result in the formation of hydrocarbons in the source rocks. The presence of an active source rock is essential for the presence of a petroleum system. A source rock of karogen may be derived from organic matter decay due to bacteria activity.

Reservoir rocks are porous and permeable formations that have the ability to concentrate oil and gas or both in commercial quantities. The reservoir can be of various shapes, size, origin and rock compositions such as sandstone, carbonate, and even some igneous and metamorphic rocks that exist near sedimentary rocks may act as reservoirs.

A seal is an impermeable rock above and around the reservoir that’s acts as barrier for hydrocarbon migration. It allows to accumulate hydrocarbons where shale and salt are one of the most common sealing rocks (Selley, 1998).

A play is a geological unit that can provide petroleum accumulations, in which the key elements are reservoir rock, source rock and seal. A prospect is a place where these elements may be combined inside a trapping geometry to provide a potential petroleum accumulation.

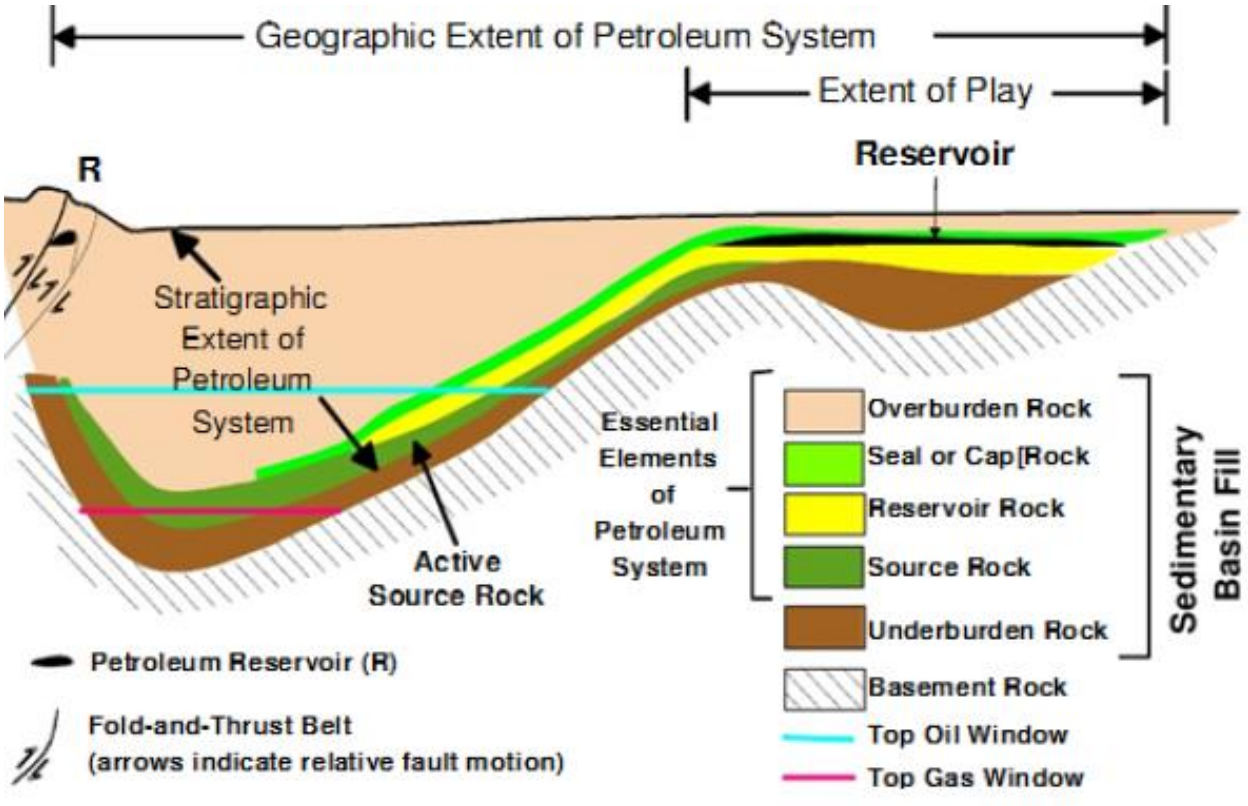


**Figure 1.3: Petroleum system and its elements in a sedimentary basin. (Figure from Magoon and Dow, 1994).**

## 1.4 Hydrocarbon Migration

During and after the diagenesis of organic matter water with oil and gas migrate from the source rock into the reservoir rock and accumulates. The migration takes place along faults, fractures and joints of various types and fluid pressure gradients. Oil and gas are trapped in the highest point (structural culmination) of a permeable rock which implies upward and lateral migration. Oil, gas and water occur stratified in porous, permeable reservoir rocks according to their decreases in densities from water to oil and gas. Their stratification from bottom to top with water, oil and gas implies that they were and are free to migrate vertically and laterally within the reservoir (Selley, 1998).

The fluid flow in permeable rocks is best explained by Darcy's Law (equation 1). It describes that the amount of fluid flowing through rocks depends on its ability to conduct fluid (permeability) and the pore water pressure difference (hydraulic potential difference) between two ends of this flow. Fluid flow is directly related to the permeability and pressure difference and inversely related to the viscosity of the fluid. During burial the pressure difference also increases with differential loading and compaction.

$$F = \kappa . \frac{\Delta P}{\mu} \qquad \text{(Equation 1)}$$

Where

Fluid Flux (F) = $m^3/s$

Permeability (k) = $m^2$

Pressure Gradient ($\Delta P$)= Pa

Viscosity ($\mu$) = $N.s/m^2$

Primary fluid migration occurs from source rocks to reservoir rocks. Diagenesis of organic material associated with compaction may cause squeeze out of fluids (water, oil and gas) from clays and shales into the reservoir rocks.

Secondary migration refers to the subsequent movement of oil and gas within permeable carriers and reservoirs. Secondary migration occurs by buoyancy due to different densities of respective fluids and in response to different pressure. There are many factors that contribute to the secondary migration through the reservoir rocks and accumulation within "pools", which are for example capillary pressure, buoyancy, dissolved gas, accumulation time of oil, tilted oil-water contacts and stratigraphic barriers.

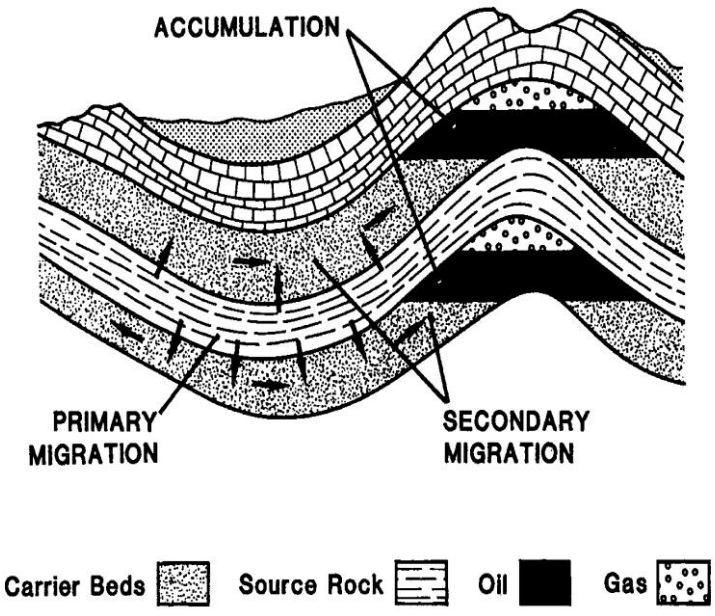


**Figure 1.4: A Sketch showing the petroleum migration and accumulation. (Figure from Tissot and Welte, 1984).**

## 1.5 Hydrocarbon accumulation

The updip migration of hydrocarbon continues as long as it does not encounter a structural configuration of strata where oil and gas are barred from further movement. This arrangement of strata that permits the accumulation of hydrocarbon in commercial amounts and prevents the further movement of hydrocarbon is known as reservoir trap (Figure 1.4) (Leverson, 1967). In a reservoir trap it is necessary that oil and gas are capable of accumulating and being captured within it. The presence of oil and gas in a trap depends upon the chemistry, PT (pressure temperature) conditions and the level of the maturation of source rocks. The most common traps are culminations folds (Anticlinal traps) comprising of gas, oil and water. Hydrocarbons are found from the top of the culmination and expanding to the flanks of the anticline. The boundaries between them may be sharp or transitional but are mostly horizontal. Gas accumulates in the apex of the structure due to highest buoyancy so-called gas cap. This gas cap overlies the oil zone which is known as oil leg or oil column (Fig. 1.5).

There are several terms used to describe the various parameters of petroleum accumulation in a trap as shown in figure 1.5.The highest point of the trap is the crest or culmination.

The lowest point at which the hydrocarbon may be contained in the trap is the spill point.

The vertical distance from crest to spill plane is the closure of the trap.

The water zone immediately beneath the petroleum is referred to as the bottom water and the water zone adjacent to trap is edge water (Selley, 1998).

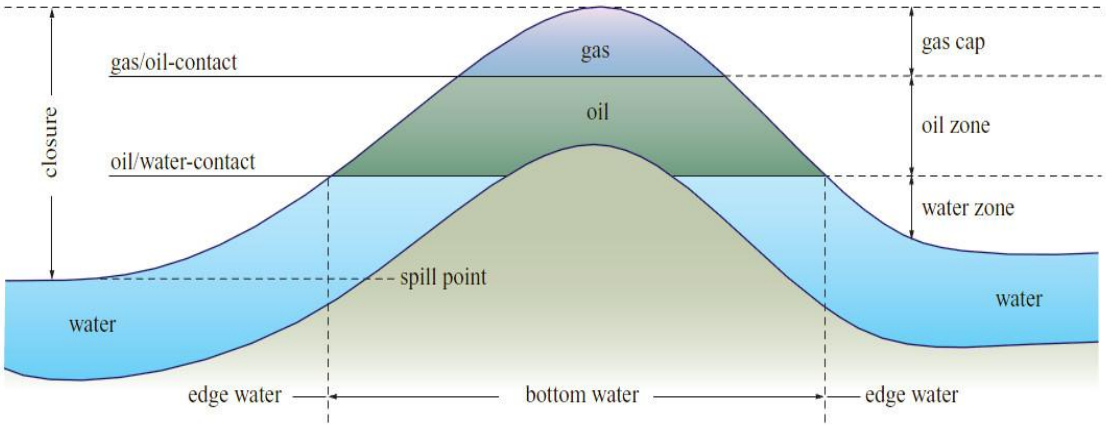


**Figure 1.5: Folded reservoir trap. At the apex of this anticline, natural gas and oil below has accumulated. In the pore space of the gas cap and the oil zone, the original pore water was displaced by gas and oil respectively. Below the oil/water-contact the water-saturated zone sustained. (Figure from Selley, 1998).**

## 1.6 Seismic evidence of shallow gas

A seismic reflection arises from lithological boundaries across which acoustic impedance (AI) changes significantly. Acoustic impedance (AI) is the product of density and P-wave velocity within a sediment layer. The presence of gas in the pore space of a sediment layer may produce a sufficient acoustic impedance contrast to create a seismic reflection due to a significantly reduced P-wave velocity in gassy sediments. The presence of gas can be observed in seismic data by different indicators such as i) amplitude anomaly ii) flat spot iii) polarity reversal iv) velocity effects v) loss of frequency (Figure 1.6). These indicators are also known as Direct Hydrocarbon Indicators (DHI).

**Amplitude anomaly**

Various amplitude anomalies exist due to marked density contrast in rocks, water, oil and gas (Figure 1.6). *Bright spot* is a seismic reflection with local anomalously high amplitude and a negative reflection coefficient. A bright spot can be observed right above leaky fault. (Figure 1.6 and 1.7).

*Dim spot* is the local decrease in reflection amplitude when the acoustic impedance (AI) of the rock is reduced in magnitude.

*Flat Spot* is caused by the interface between two different types of fluids in a reservoir such as gas-/oil and gas-/water. Flat spot is a good hydrocarbon indicator and normally appears at the base of gas filled portion of reservoir. Flat spots show a positive reflection coefficient and amplitude increase with offset. They always show tuning effects at the extremities of the fluid wedge (Figure 1.6 and 1.7). (Andreassen, 2009).

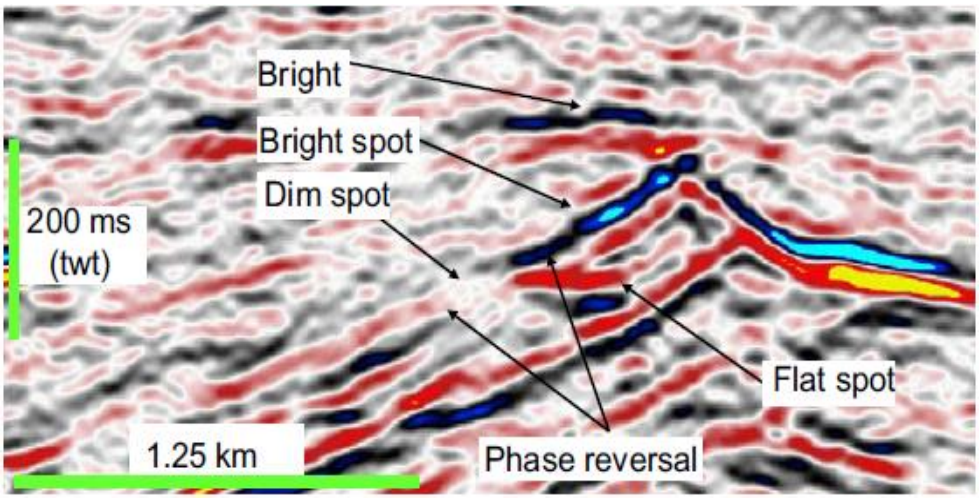


**Figure 1.6:**

**Hydrocarbon Indicators shown as bright spot, dim spot and flat spot in a reservoir (from Løseth et al., 2009).**

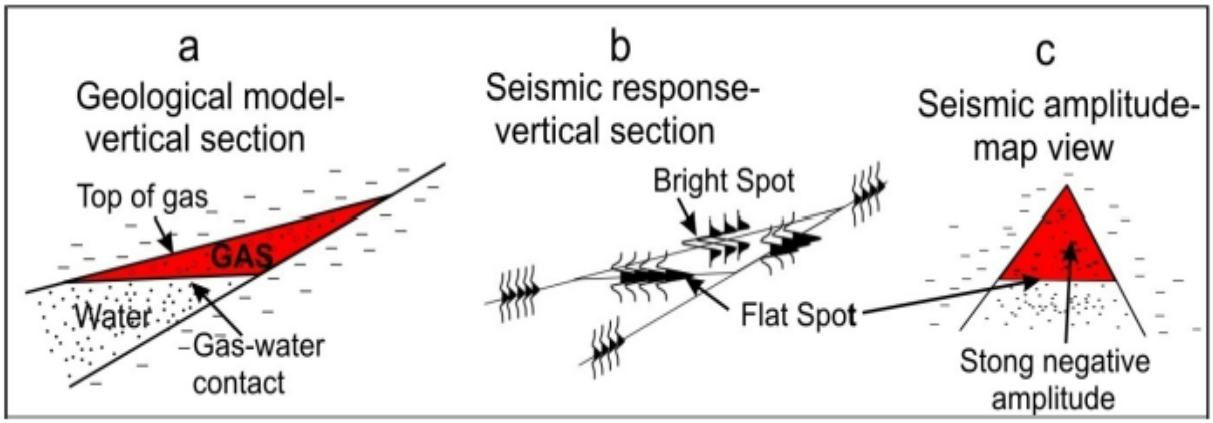


**Figure1.7: A sketch to showing the gas accumulation area prepared from seismic data. a) Vertical section of gas zone in geological model. b) Seismic response of vertical section of gas zone. c) Horizontal amplitude map view of vertical section of gas zone. (Figure from Andreassen et al., 2007).**

### Polarity Reversal/ Phase Reversal

There is negative reflection coefficient at the top of gas accumulation zone with a phase shift of 180° if compared to the seafloor. A polarity reversal is common indicator of a gas accumulation zone (Andreassen, 2009).

### Velocity effects

A thick gas accumulation zone significantly reduces the P-wave velocity within the formation resulting in longer two way travel times (TWT) of the seismic signal. It creates a pull down (smile) effect on the underlying reflectors (Andreassen, 2009).

### Loss of high frequencies

Beneath the gas accumulation zone there is loss of frequencies due to absorption and scattering of seismic energy in the gassy zone. This loss of frequency is sometimes observed within bright spots (Andreassen, 2009).

## 1.7 Seismic Expressions of Fluid Migrating Pathways

Seismic expressions of fluid migration pathways may allow locating zones of possible hydrocarbon expulsion. The zones recognized may be faults or segments of faults that are leaking. The fluid flow features are often visualized on the seismic section as they cause a change in acoustic impedance. Fluid migrating pathways and seepages are recognized both in the subsurface and at the seabed. Fluid seepage expressions at the sea bed include features such as carbonate mounds, mud volcanoes and pockmarks (e.g. Hovland & Judd, 1988). Subsurface fluid migrating features may consist of gas chimneys, mud diapers, bright spot, acoustic turbidity zones and palaeo-surface expressions such as buried mud volcanoes and pockmarks (Ligtenberg., et al., 2003., Hovland & Judd, 1988., Ligtenberg et al., 2005).

### Mud Volcanoes

Mud volcanoes are defined by Guliev (1992) as 'periodic expulsion from deep parts of the sediment cover of mixtures of water, various gases and solid material'. Mud flows are expelled from the volcanoes and appear on seismic sections as distinctive conical topographic structure. They may develop in active compressional tectonic regions in active continental margin settings but also in passive continental margins (e.g. Perez-Garcia et al., 2009., Perez-Garcia et al., 2011). The size of mud volcanoes ranges from several km to a meter. A reflection free and transparent zone in the center of mud volcanoes are interpreted as feeder pipe (Fig. 1.8). (Ligtenberg et al., 2005., Løseth et al., 2009).

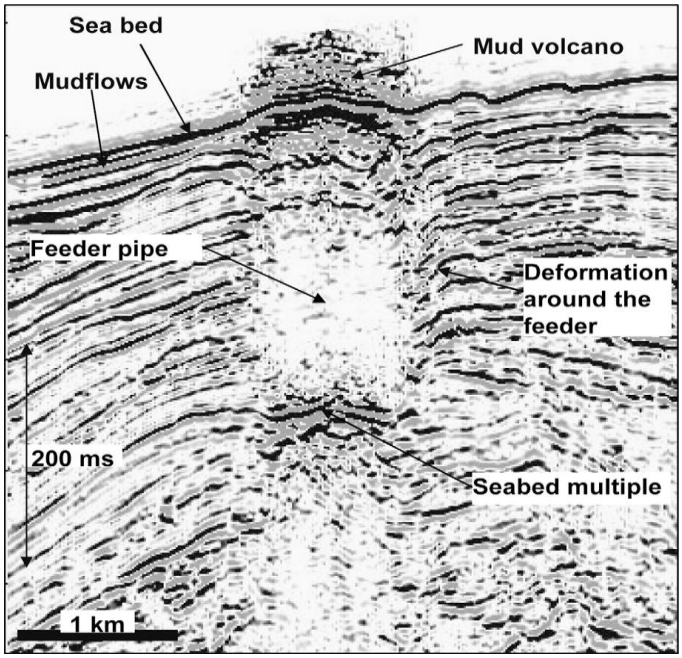


**Figure 1.8: Mud flows with feeder pipes. (Figure from Løseth et al., 2009).**

**Pockmarks**

Pockmarks are shallow concave crater like seabed depressions (Judd and Hovland, 2007). Their diameter ranges from a meter to several hundred meters and their depth from less than a meter to 100 meters. They generally form in fine grained sediments as fluid or gas escape into the water column (Fig. 1.9). Different types of pockmarks are identified on seismic such as circular, elliptical and in combined forms. Pockmarks are found directly above leaking faults or chaotic sub seabed reflections which may indicate hydrocarbon leakage from the subsurface in both marine and lacustrine environment. Pockmarks are also found above shallow gas reservoirs as the fluid can originate from any depth from subsurface (Ligtenberg et al., 2005., Løseth et al., 2009., Hovland et al., 2002).

It is shown in figure 4.9.

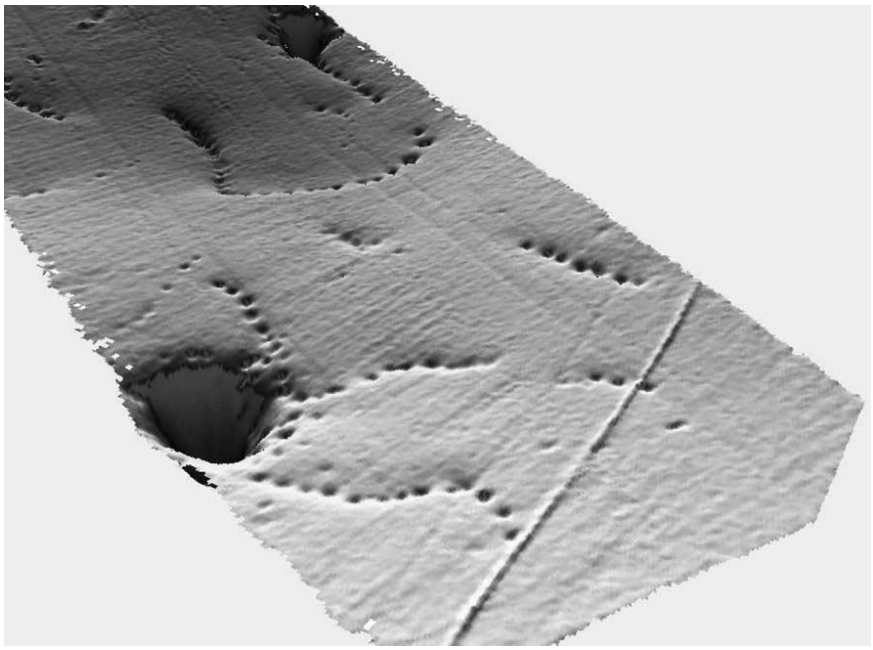

**Figure1.9: Multibeam bathymetry image showing the strings of pockmark on a soft sea bed at 300m water depth off Norway. (Figure from Hovland et al., 2002*).***

**Gas Chimney**

Gas chimneys are recognized in seismic data as vertical to near-vertical zones of distorted seismic reflections of low trace coherency (wipe-out zone), low reflection amplitude and high variable dip and azimuth of seismic reflection due to scattering and absorption of seismic energy along the zone (Fig. 1.10). Gas chimneys are interpreted to represent the migration of gas through sediments and high fluid flux paths caused by an overpressure regime. In some cases gas chimneys may terminate into mud volcanoes or pockmarks at the sea bed or at

shallow gas zones beneath it. Gas chimneys are also found above high pressure reservoirs tectonically fractured cap rocks and may be also locally present above salt pillows. They appears on seismic sections as diffuse shadow to well defined vertical zones associated with low velocity anomalies, velocity sags right below the chimney, bright and dim spot at the flanks and above the gas chimneys (Fig. 1.10) (Ligtenberg et al., 2005., Løseth et al., 2009., Andreassen , 2009).

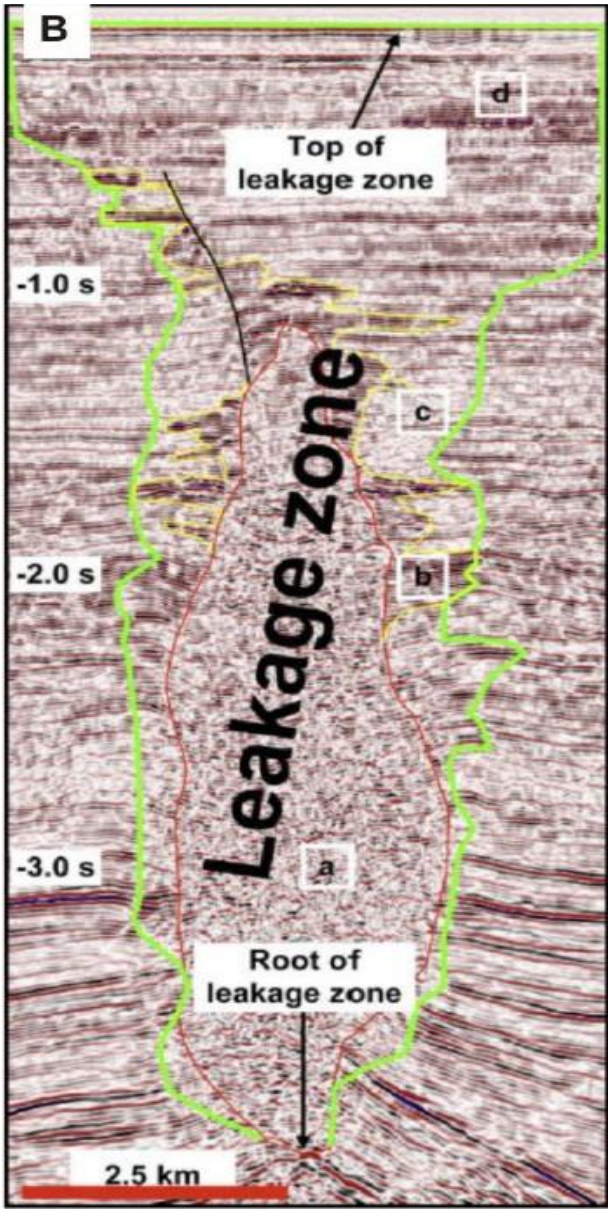


**Figure 1.10: Wipe-out zone indicate the existence of gas chimney with sharp outer boundary. Different acoustic features such as (a) distorted (wipe-out) zone (b) high amplitude anomaly appeared along the side of gas chimney. A dim zone (c) which is interpreted as acoustic transparent zone and a diffuse zone (d) comprising of bright spot, dim spot and pockmark on the sea bed.**

**(Figure from Løseth et al., 2009., Andreassen 2009).**

**Acoustic Turbidity Zone**

An acoustic turbidity zone is an area of diffuse and chaotic acoustic pattern observed on seismic sections (Fig. 1.11). It results from the scattering and absorption of seismic energy by the interstitial of gas bubbles and is also known as acoustic blanking that is useful to locate the presence of gas. It may also be generated by the absence of sediment layering and huge migrating of gas. Acoustic turbidity zones are observed at shallow depth interrupting the stratification. In acoustic turbidity zones reflections may undergo the ``pull-down`` effect (Ligtenberg et al., 2005., Missiaen et al., 2002).

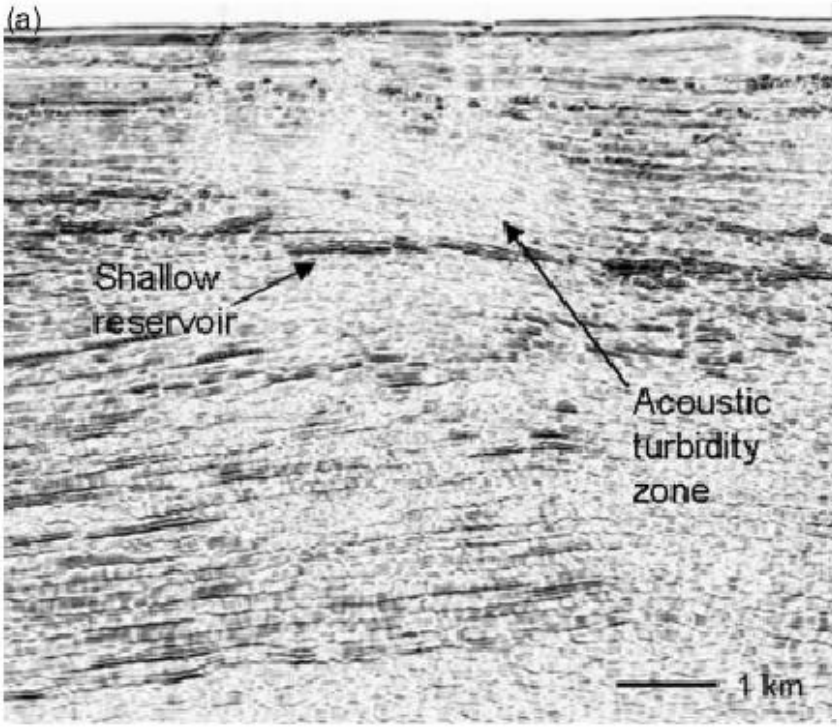


**Figure 1.11: Acoustic Turbidity zone indicate the gas leakage from shallow reservoir. (Figure from Ligtenberg et al., 2005)**

**Acoustic Pipes**

Acoustic pipes are comparatively narrow zones of acoustic masking but with often a large vertical extent (Fig. 1.12). Acoustic pipes indicate the vertical pathways for fluid migration associated with bright spots and some time they merge into pockmarks. (Andreassen et al., 2007).

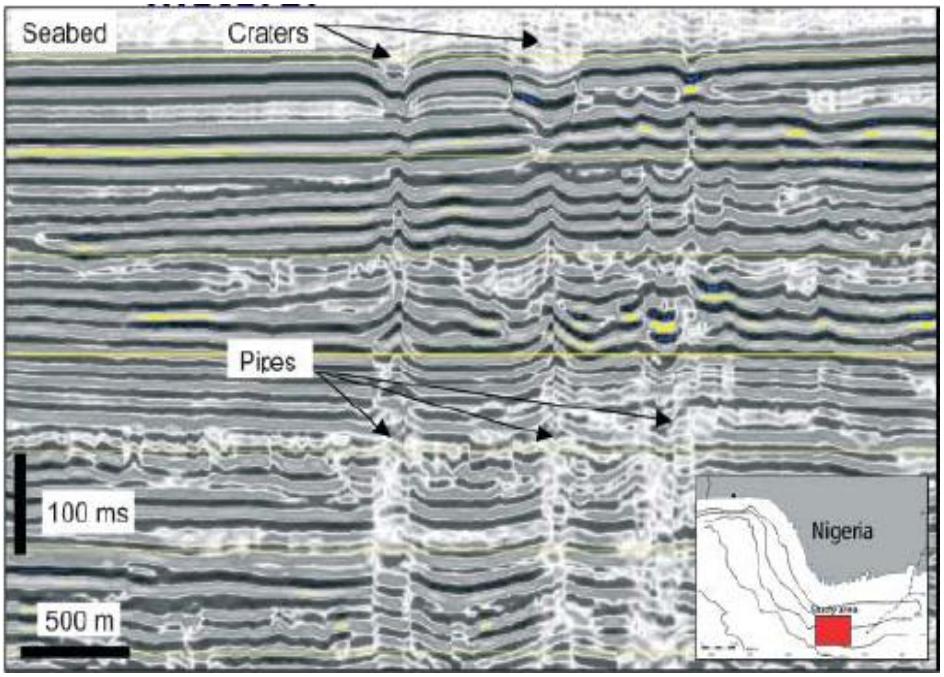


**Figure1.12: Acoustic pipes indicate the focused fluid flow from gas reservoir and some terminate at the seabed.**

**(from Berndt et al., 2005).**

**Faults zones**

A fault zone consists of interconnected fractures that act as good fluid conduits (Fig. 1.13). Especially pressure dependent open faults provide a good pathway for fluid migration. A faults zone is identified as line-ups of discontinuous reflections on a vertical seismic section (Fig. 1.13.). Hydrocarbon cannot be identified within the faults zone because of uneven distributions and limited extent of the fault zone. However, hydrocarbon may appear on the side of faults zone due to the migration into permeable strata adjacent to the fault zone, which is identified as a high amplitude anomaly (Fig. 1.13). Sometime faults terminate close to the seabed which appears as a line of pockmarks at the sub crops of the faults producing gas plumes in the water column. (Ligtenberg et al., 2005., Løseth et al., 2009., Andreassen, 2009).

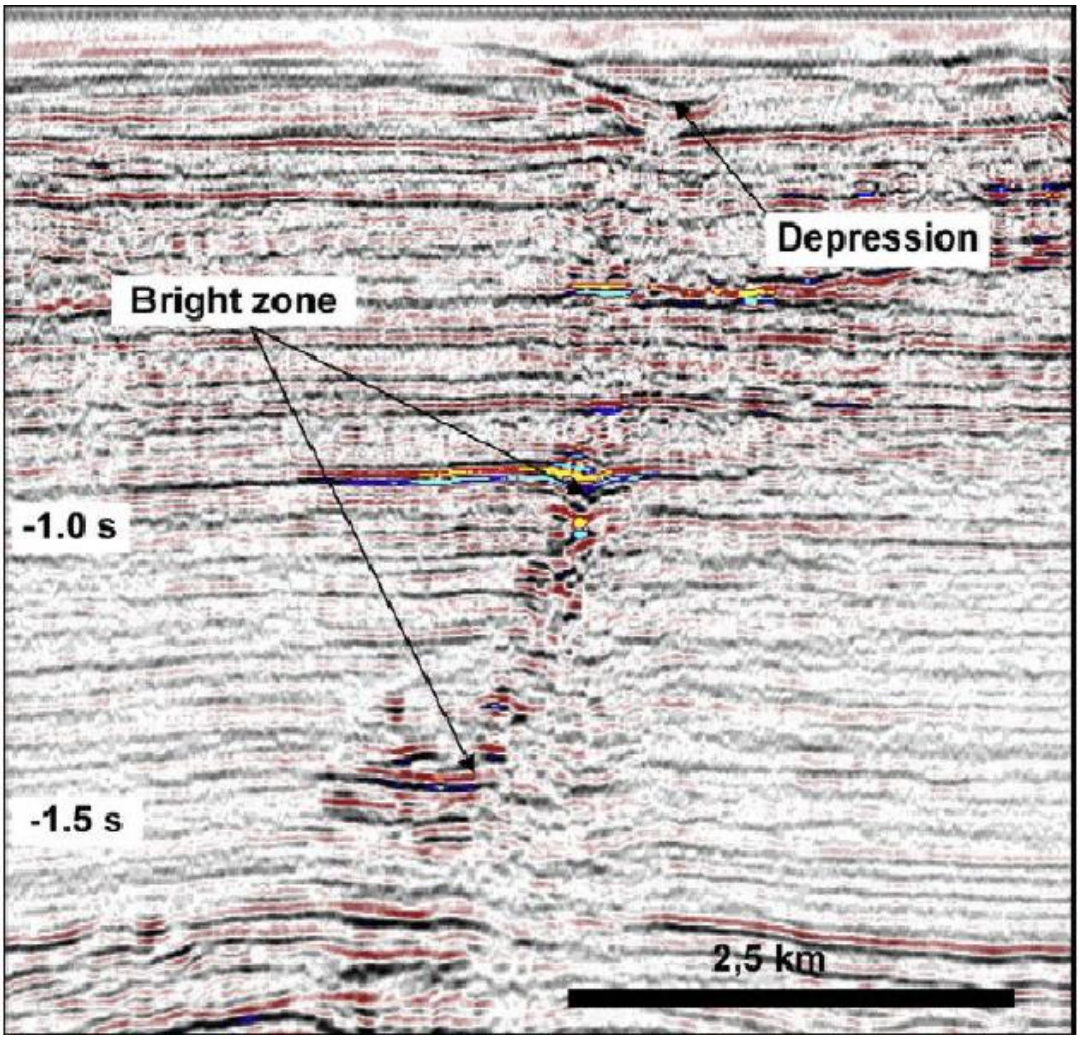


**Figure 1.13: Vertical bright zone consists of several high amplitude anomaly in the fault. These high amplitude anomalies indicate the fluid migration by gas charging permeable beds along the fault. (Figure modified from Løseth et al., 2009; Andreassen, 2009).**

## 1.8 Gas Hydrate

Gas hydrates (Fig. 1.14), also called clathrates, are naturally occurring solid ice like substance that traps the molecules of natural gas, mainly methane in the rigid lattice of water molecules due to hydrogen bonding. Gas hydrates occur preferably in continental margins in polar and permafrost regions but large amounts exists worldwide on passive and active continental margins if the temperature and pressure fall within the stability field of gas hydrates (Fig. 1.15). (Sloan, 1998). Gas hydrate forms in a complex hydrological system, which depends on the fluid flux, methane solubility, temperature, pressure and distribution of the sediment properties such as porosity and grain size. They also act as cementing material in the pore space of sediments, which reduces the porosity and permeability. They may occur as lamina, hydrate veins or nodules of pure hydrate (Nimblett and Ruppel, 2003). The change in bottom

water temperature causes the temporal variation in GHSZ, which in turn may change the slope stability of continental margin. (Mienert et al., 2001., Paul et al., 2000., Hustoft et al., 2007).

**Figure 1.14: Chunks of gas hydrate recovered from the giant piston coring in Gulf of Mexico in 2002 (Figure from Barth et al., 2006).**

On seismic reflection data the base of gas hydrate stability zone (GHSZ) is identified by an anomalous bottom simulating reflection (BSR), characterized by seismic amplitude polarity reversal if compared to the seabed (Fig.1.15).

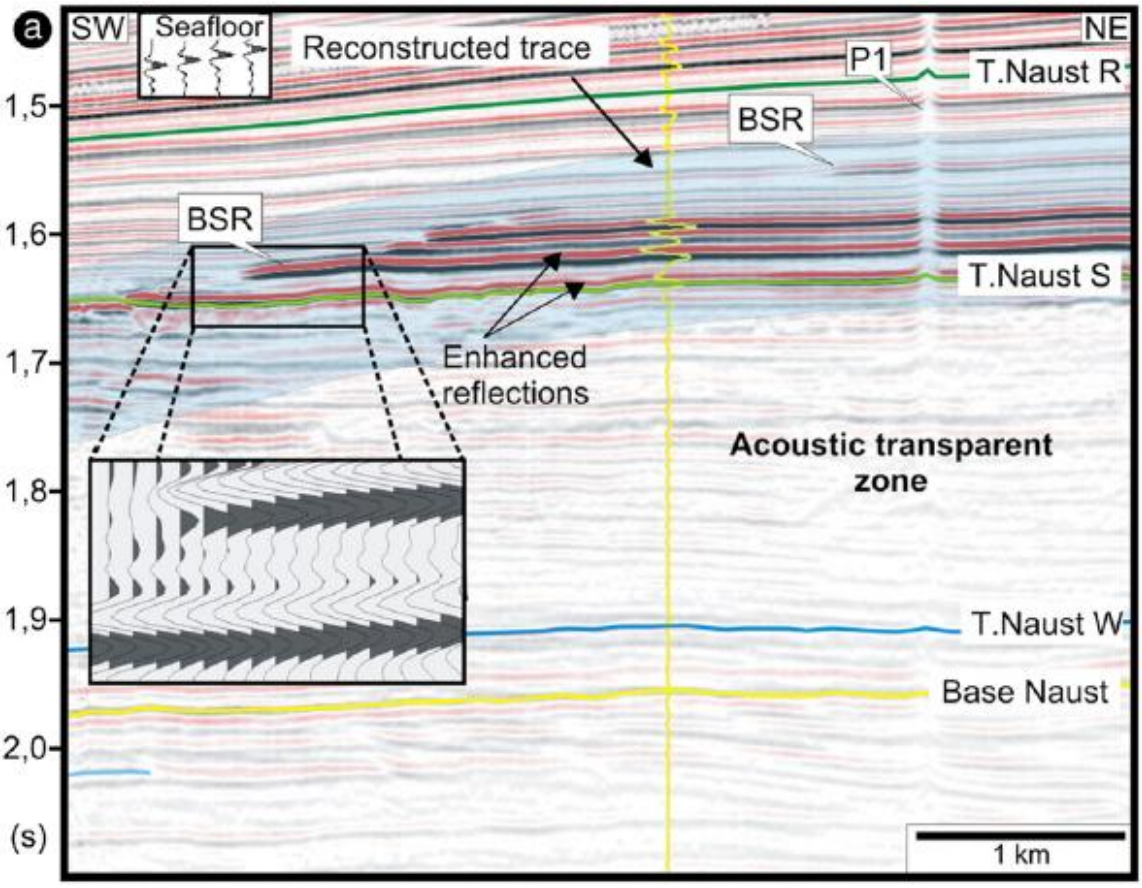


**Figure 1.15: The seismic cross-section shows the enhanced reflection of BSR with phase reversal across it. (Figure from Hustoft et al., 2007).**

BSR follows the iso temperature lines parallel to sea floor. This BSR is inferred be the result of the impedance contract between high velocity of hydrate cemented sediment and low velocity free gas layers beneath it (Shipley et al., 1979., Hustoft et al., 2007). BSR is the best geophysical indicator of gas hydrate at the base of gas hydrate stability zone (BGHSZ). (Bünz et al., 2003).

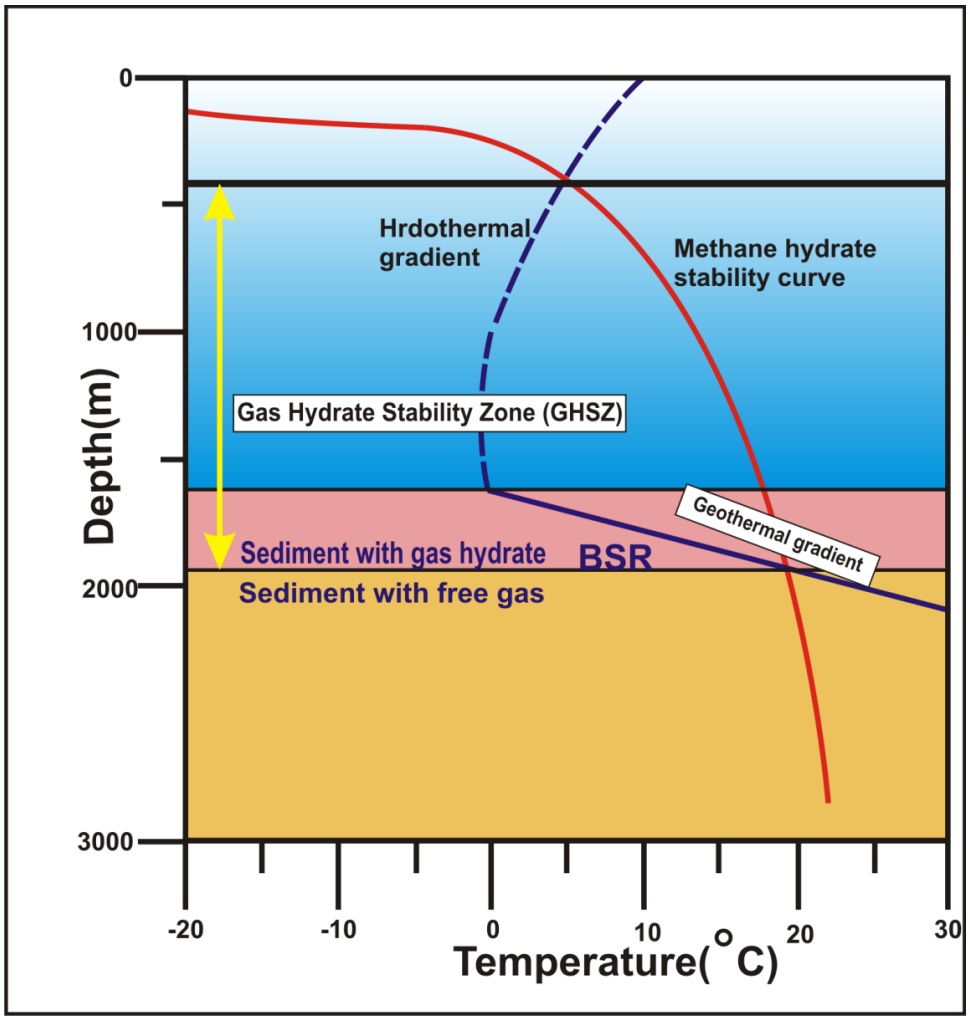


**Figure 1.16: A phase diagram indicates the gas hydrate stability zone using the geothermal gradient and the methane hydrate stability curve. . Blue dashed line indicates the stability zone of gas hydrate. . The base of GHSZ is indicated by a bottom simulating reflector which separates the sediments with gas hydrate from sediments without gas hydrate but free gas beneath it. (Figure from Chand and Minshull, 2003).**

The occurrence of gas hydrate along continental margins depends on the physical and chemical properties of the sedimentary formation (Figure 1.16). It is noted that the depth of the gas hydrate stability zone (GHSZ) increases with an increase in water depth and a decrease in seafloor temperature and geothermal gradient (Chand and Minshull, 2003., Dillon and Max, 2000).

# 2 Geology of the study area

## 2.1 Tectonic setting

Three major sedimentary basins characterize the continental margin offshore mid Norway, which are Møre, Vøring and Lofton Vesterålen basins (Fig. 2.1). The study area is the located within the transition from the Møre basin to the Vøring basins (Fig. 2.1). (Stuevold & Eldholm, 1996). The outer margin at the Vøring Plateau comprises the Vøring Marginal Highs and the Vøring Escarpment., all have a northern termination caused by the Bivoirst Lineament (NW-trending dislocation defined by the Blaystad et al (1995) which separates the Vøring and Lofoten-Vesterålen margin (Tsikalas et al., 2005).

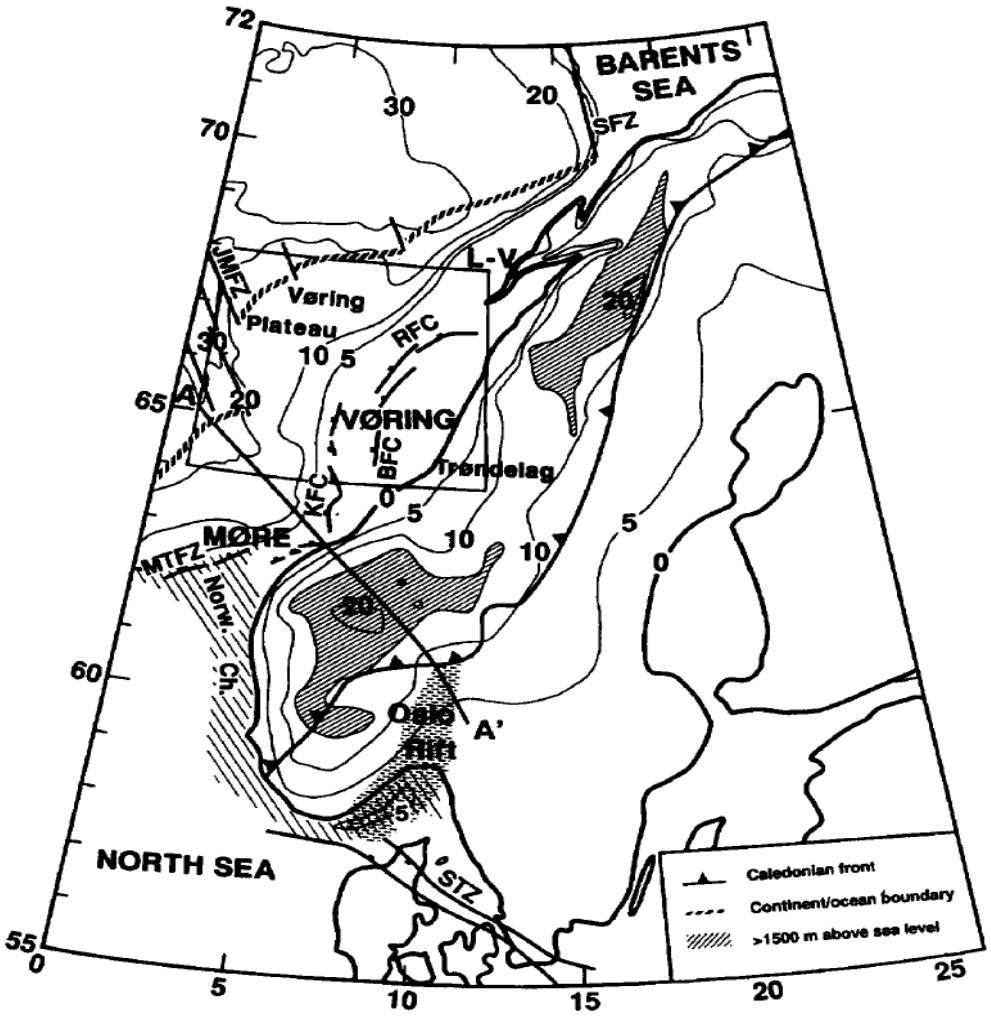


**Figure 2.1: The distribution of main structure elements on the Møre, Vøring and Lefton-Vesterålen margin segments off Norway. Box represents the study area. BFC= Bremstein Fault Complex, KFC=Klakk Fault Complex, MTFZ=Møre-Trøndelag Fault Zone, RFC=Revfallet Fault Complex, STZ= Sorgenfrei-Tornquist Zone, JMFC= Jan Mayen Fracture Zone, SFZ= Senja Fracture Zone. (Figure from Stuevold & Eldholm, 1996).**

Devonian strike slip movement influenced the post-Caledonian structural development by four main extensional tectonic events, which occurred during Permian, Triassic-Jurassic, Jurassic-Cretaceous, and the late Cretaceous-early Tertiary time (Larsen et al., 1987., Brekke and Riis, 1987., Skogseid et al., 1992). The entire mid Norwegian shelf has been affected during the Triassic-Jurassic Extensional episode (Gabrielsen et al., 1984., Bukovics and Ziegler, 1985) and the Trøndelag Platform was separated from the Møre and Vøring basins during Jurassic-Cretaceous. Subsequent thermal subsidence and deposition of large amounts of Cretaceous sediments resulted in a 10 km thick Møre and Vøring basins. The Jan Mayen Fracture Zone separates the Vøring basin from the Møre basin (Bünz et al., 2003). The margin has been faulted due to flexure deformation by post-rift subsidence and intraplate deformation events. In Vøring and Møre basins intraplate deformation structured the Helland-Hansen Arch (Fig. 2.2) (Stuevold & Eldholm, 1996., Eldholm et al., 1989).

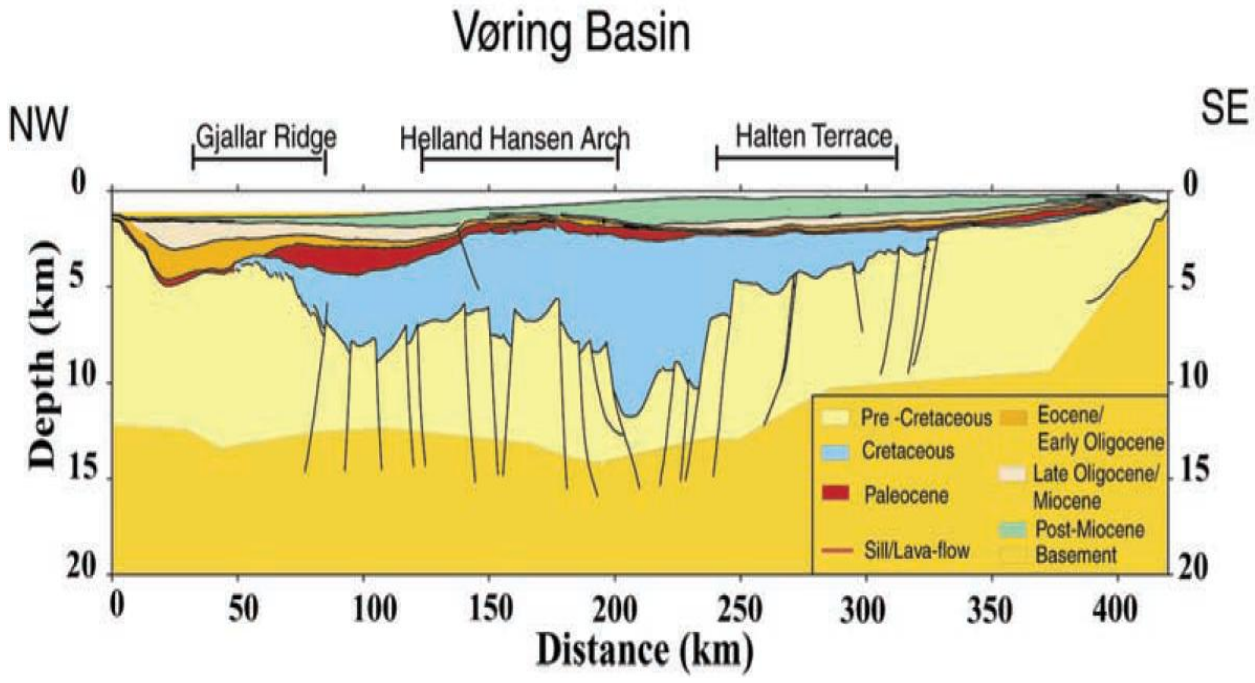


**Figure 2.2: Interpreted seismic section across the Vøring Basin and the arches in front of the Pliocene-Pleistocene deposit. (Figure from Kjeldstad et al., 2003).**

## 2.2 Post break up compression and arching

The mid Norwegian margin has undergone a post break up compressional deformation between Middle Eocene and Early Miocene (Lundin and Dore, 2002). The result is represented by the north-south oriented local domes, reverse movement of the normal faults and broad basin inversion as illustrated is figure 2.3.

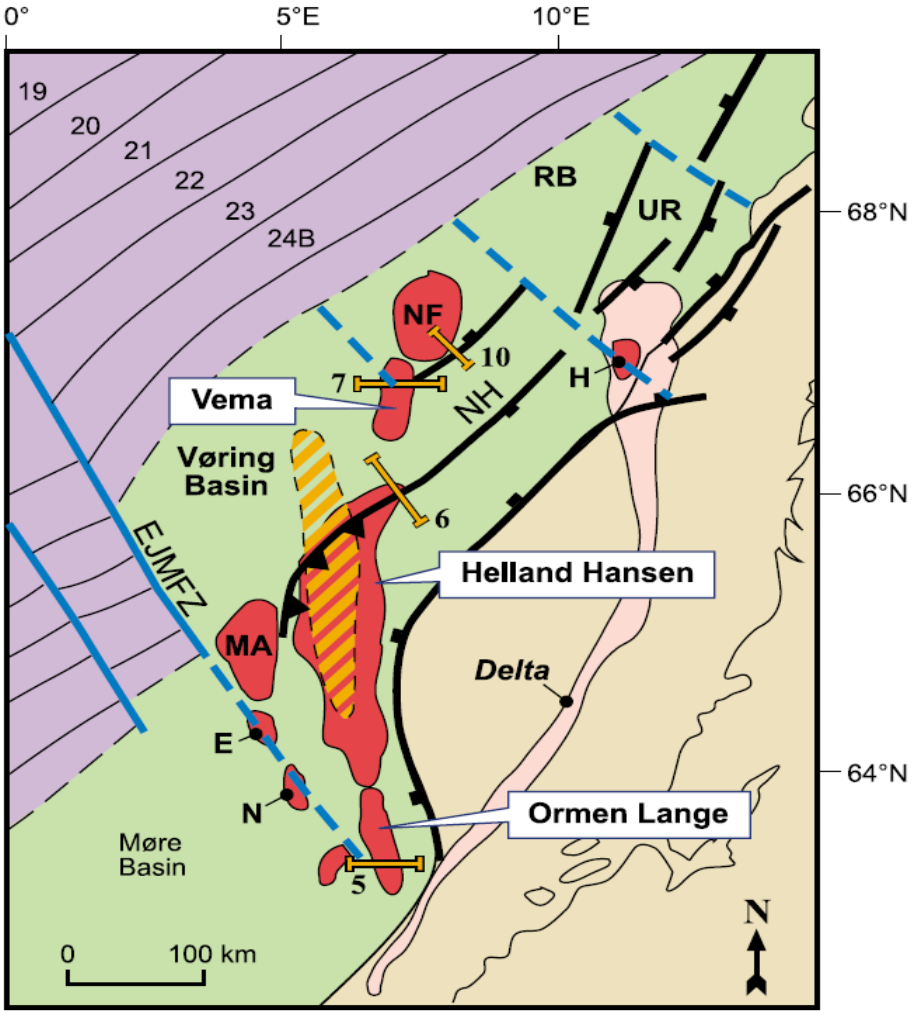


**Figure 2.3: Shows the index map of mid-Norway. Red color represents the mid Cenozoic dome, stripped section late Pliocene-Pleistocene high and pink color Lower Oligocene delta. BL:Bivrost Lineament; EJMFZ:East Jan Mayan Fracture Zone, H:Hedda Dome ,MA:Modgunn Arch, NF:Naglfar Doom, NH:Nyk High;RB:Røst Basin; and UR:Utrøst Ridge. (Figure from Lundin and Dore, 2002).**

Møre and Vøring basins offshore mid-Norway surround the regional domes, synclines and anticlines (Rønnevik & Navrestad , 1976., Jørgensen and Navrestad , 1981., Bøen et al., 1984., Bukovics and Ziegleret, 1985., Brekke and Riis, 1987). Some authors believed that volcanism or pre-Cenozoic salt structured these dome features (Hinz et al., 1982., Hamar and Hjelle, 1984), while other argued that differential subsidence and compaction played a role in

the formation of dome features (Skogseid and Eldholm, 1989., Stuevold et al., 1992). Recent work suggested that these dome features are originally developed by the contraction and that later the differential compaction modified them (Grunnaleite and Gabrielsen, 1995., Dore´ & Lundin, 1996., Vågnes et al., 1998).

Helland Hansen, Ormen Lange, Modgunn Arches, Vema and Nagelfar Domes are one of the largest dome structures described and named by Blystad et al (1995) (Fig. 2.4). In the central part of the Vøring basin these structures have N-S to NNE-SSW trends but close to eastern margin the trend varies from N-S to NE-SW. These domes are large and vary in shape and extent having 40-60km axial traces, 300m-600m amplitude and several tens of kilometers wavelengths (Vågnes et al., 1998).

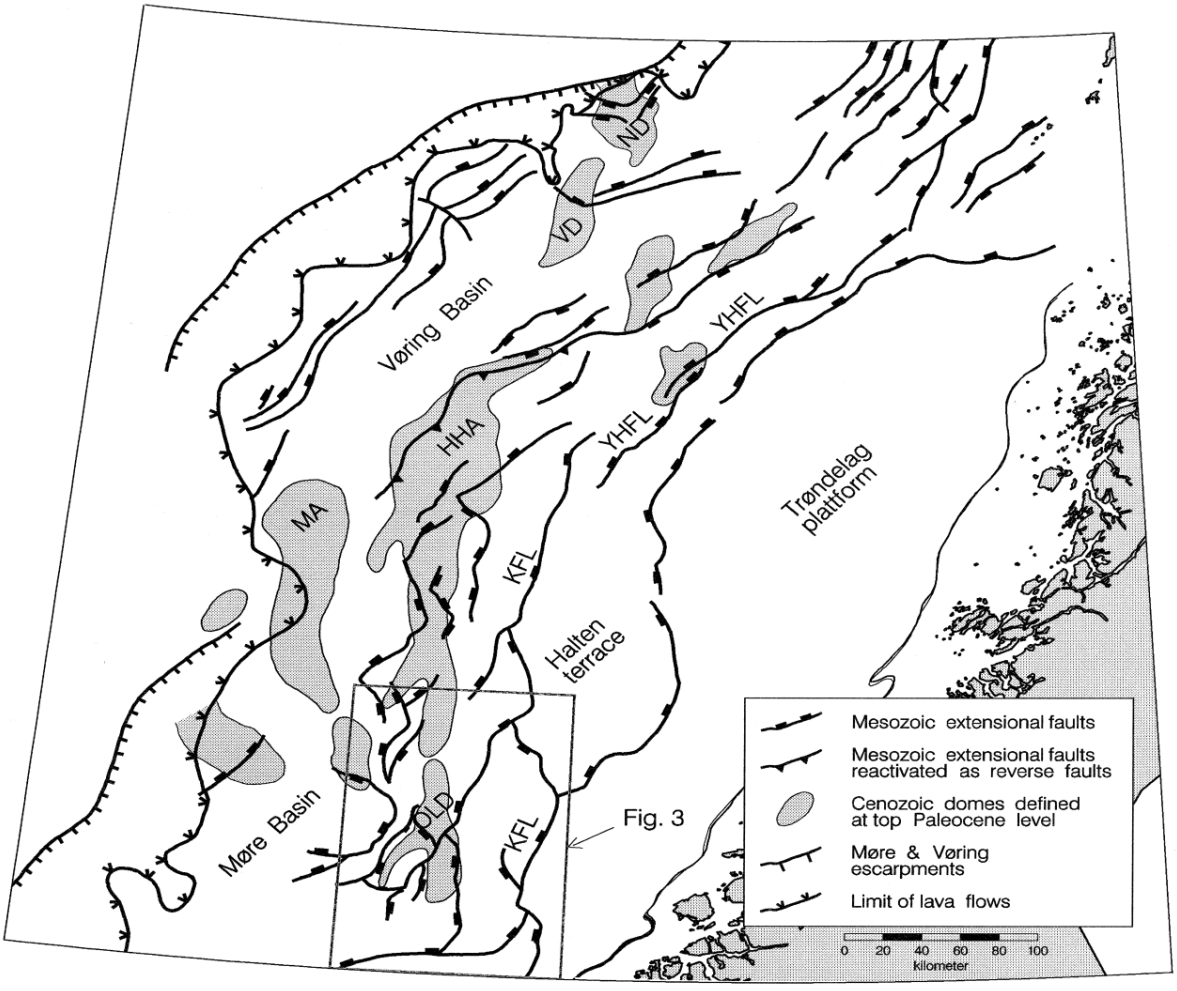


**Figure 2.4: Structural map of the mid-Norwegian margin showing the regional domes and anticlinal structures. Modified from Blystad et al. (1995). MA D Modgunn Arch; OLD D Ormen Lange Dome; HHA D Helland-Hansen Arch; VD D Vema Dome; ND D Nagelfar Dome; KFL D Klakk Fault Complex; YHFL D Ytreholmen Faul complex. (Figure from Vågnes et al 1998).**

The working area lies within the Helland Hansen Arch and therefore a more detailed description is given in the following.

## 2.3 The Helland Hansen Arch

The Helland Hansen Arch is the most well-developed high of Møre and Vøring Basins and was named by Blystad et al (1995). Before it was called ``Structure D`` by Hinz (Hinz et al., 1982) and ``Modal High`` by Hamar and Hjell (Hamar and Hjell, 1984). It is the largest anticlinal structure with axial trace more than 280km along its strike. Its amplitude is more than 600 m and the maximum wavelength is 60 km. It becomes narrow both in north and south direction and at the center it is approx. 100km in width, representing itself as a long arch whose eastern flank is more gentle than the western flank. The Helland Hansen Arch is symmetrical in the south and asymmetrical with a steeper northwestern flank in the north (Vågnes et al., 1998). The eastern flank developed by a prograding shelf with sediment loading and subsiding in the Late Pliocene and Pleistocene because of significant erosion during to the Neocene uplift of the Norwegian main land and erosion during the ice ages ( e.g Kjeldstad et al., 2003). The western flank of the Helland Hansen Arch might also have been shaped during Pliocene-Pleistocene loading. In the lower part of the wedge the Oligocene and Miocene sediment layers are forming on-lap structures both on eastern and western flanks of the arch.

Kjeldstad et al. (2003) suggested based on the interpretation of both elastic and ridge push models that the arch was formed by regional orthogonal compression early in Neogene time.

Both tectonic and thermal subsidence has played a role in forming the hydrocarbon traps, e.g for the Ormen Lange gas reservoir.

## 2.4 Stratigraphy of the Study Area

A thick sedimentary succession was deposited during both post break up and subsidence time along the Norwegian margin (e.g. Skogseid and Eldholm, 1989). The sediments were divided into three major units: the Eocene-Oligocene Brygge Fm, the Miocene-early Pliocene Kai Fm and the late Plio-Pleistocene Naust Fm (Fig. 2.5). (Dalland et al., 1988., Hjelstuen et al., 2004).

| Sequence boundary *(reflector name)* | Formation (Dalland et aL, 1988) | Seismic pattern | Lithology |
|---|---|---|---|
| | Naust | High amplitude reflectors separating sub-sequences of non-structurally, weakly layered and chaotic seismic facies. Well-stratified seismic units deposited outside the prograding wedge on the Vøring margin | Diamicton, hemipelagic/ glacimarine sediments, till |
| *Base Late Pliocene (BP)* | Kai | Parallel medium amplitude reflectors. Small-offset faults. | Siliceous ooze |
| *Lower Miocene (LM)* | Brygge | Parallel low to medium amplitude reflectors. Small-offset faults. | Clay |
| *Intra Oligocene (IO)* | | Chaotic/non-structural to weakly layered | |
| *Middle Oligocene (MO)* | | Band of parallel, non-faulted, high amplitude reflectors characterise the upper unit. An acoustic non-structural seismic pattern dominate the lower unit. | Clay |
| *Top Paleocene (TP)* | | | |

**Figure 2.5: Shows the sequence boundaries, seismic facies characteristics and lithologies of mapped mega sequences. (Figure from Hjelstuen et al., 2004).**

### Brygge Formation (Eocene-Oligocene)

Brygge Formation of variable thickness and mainly consists of clay ooze-dominated sediments in the Møre and Vøring Basins where it reaches maximum thicknesses (Eidvin et al., 2000., Rise et al., 2010). In the Møre margin it consist of fine grained sandstone layers (Martinsen et al., 1999)

### Kai Formation (Miocene–early Pliocene)

The Kai Formation consists of fine grained hemipelagic siliceous oozes (Rokoengen et al., 1995). The Kai Formation is characterized by polygonal faults. The polygonal faults may have developed under compaction and dewatering because of gravitational loading (Cartwright and Lonergan, 1996). The thickness of the Kai Formation decreases on the eastern side of the Helland Hansen Arch and does not exists in the upper part of the Helland-

Hansen Arch and Modgunn Arch where strong bottom currents controlled the depositional environment (Rise et al., 2010., Hjelstuen et al., 2004).

**Naust Formation (late Plio-Pleistocene)**

The Naust Formation represents glacial-interglacial climate cycles that resulted in the deposition of appreciable amounts of hemipelagic, glaciomarine and contouritic sediments controlled by the waxing and waning of the Fennoscandian ice sheet (Sejrup et al., 2004). Glacigenic Debris Flow (GDF) deposits are one of the characteristic sediment deposits (Dalland et al., 1988., Hjelstuen et al., 2005). They represent the periods of grounded ice sheets during maximum glaciations.

The Naust Formation is divided into five sequences Naust N (oldest), A, U, S and T with dominating progradational wedge formation (Figs. 2.6-2.8). (Rise et al., 2006).

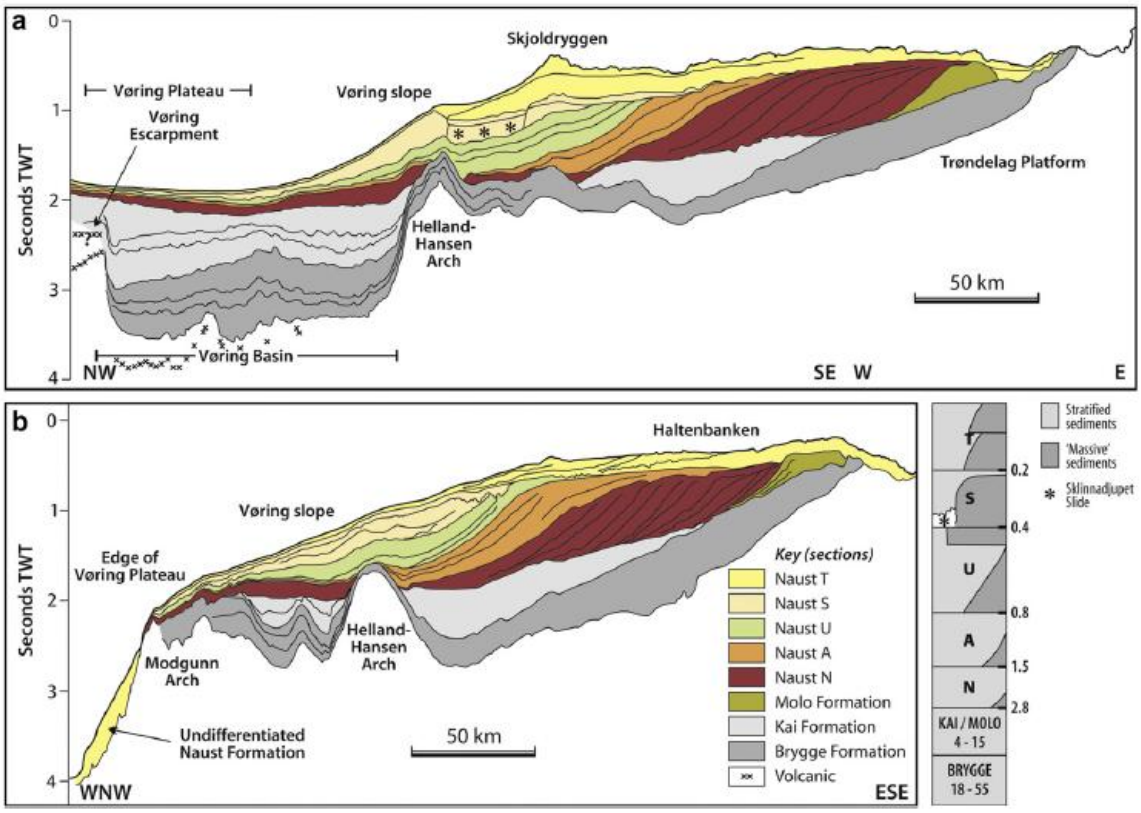


**Figure 2.6: Interpreted seismic section illustrating the general stratigraphy and inferred age in the region of the Vøring Plateau. (Figure from Rise et al., 2010).**

**Naust N** (2.8-1.5 Ma) is a westerly prograding wedge formed sequence that consists of clay-rich diamiction interbedded with subordinate sand layers documented by bore holes from

exploration wells. Ice rafted debris exists in the matrix which consist of sub angular to angular pebbles of crystalline rocks transported by calving icebergs along the Norwegian coast. During the Naust N-time (2.8-1.5 Ma BP) terrestrial glaciers acted as important agents for erosion and transportation of sediments documented in the deposition of the large amount of sediments along the mid Norwegian margin (Rise et al., 2006 & 2010).

**Naust A (1.5-0.8 Ma)** shows also wedge formed massive layered sequences which prograded close to the eastern flank of HHA. It shows the same pattern like Naust N but it is reduced in thickness (Rise et al., 2010). It also shows parallel mega scale glacial lineations produced by fast flowing ice streams at its base during 1.5-0.6 Ma BP when marine ice sheets occasionally reached the palaeo shelf edge (Rise et al., 2006).

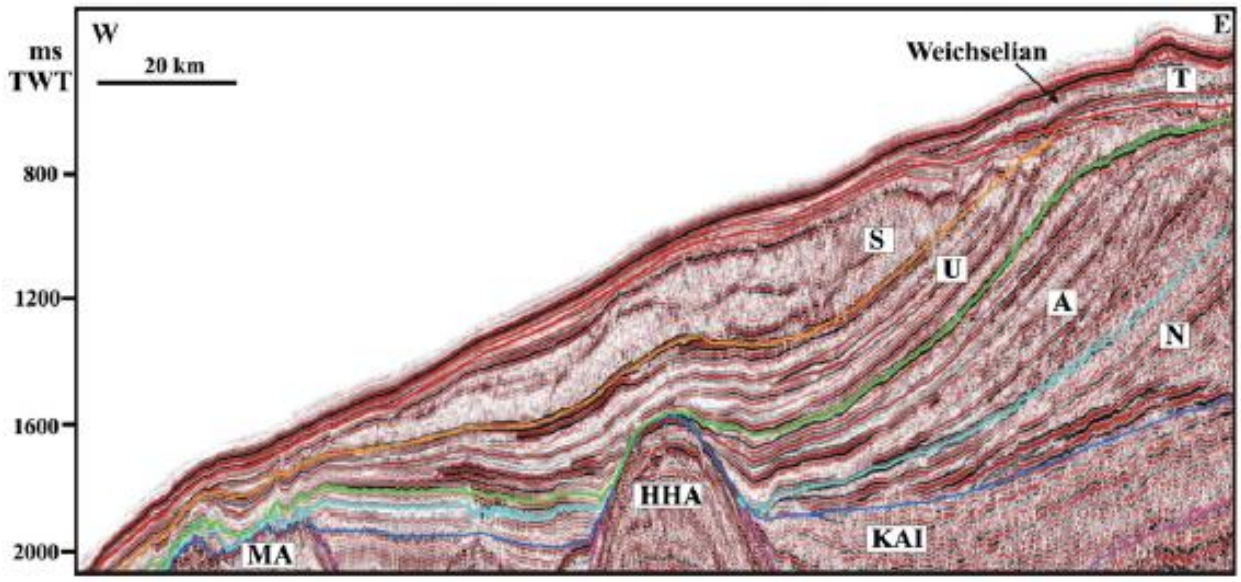


**Figure 2.7: seismic line indicating the prograded wedge formed units of Naust Formation across HHA. (Figure from Rise et al., 2010).**

**Naust U** (0.8-0.4 Ma) comprises several cycles of glacigenic debris flow deposits which have buried the whole crest of HHA and extended far west into the Vigrid depression (Rise et al., 2006 & 2010).

**Naust S** (0.4-0.2) consists of glacial debris flow which has prograded up to 50km westward to position directly above the crest of HHA. The units occur also north of Storegga slide scar.

Naust S has in the shallow part of the HHA may act as a seal rock of the entire anticline. Naust S sediments have been deposited during Elsterian glaciations and hence comprises mainly glacial debris, slide deposit and hemiplegic and contouritic sediments (Rise et al., 2006 &2010).

**Naust T** comprises mainly flat lying aggradational sediment units with some transparent character representing the last two glaciations Saalian and Weichselian, which have deposited till and massive glacial debris flow sediments on the shelf and uppermost slope (Rise et al., 2006 &2010).

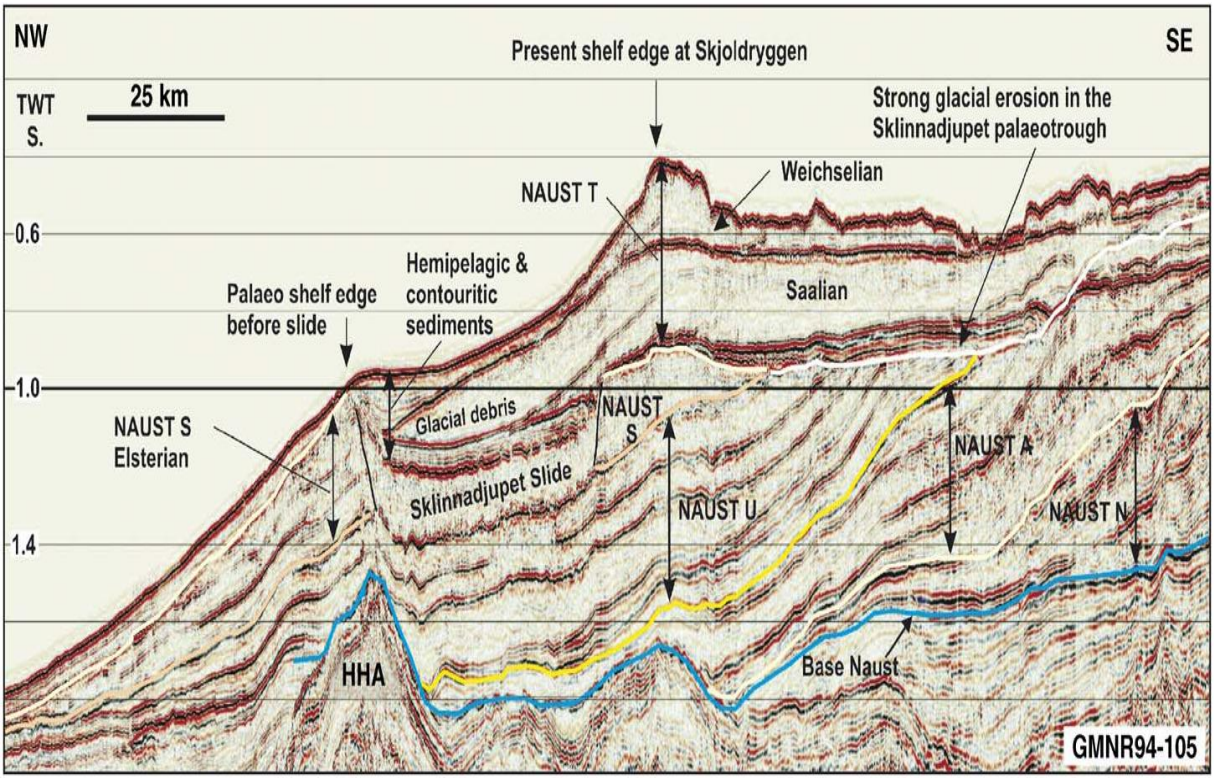


**Figur2.8: Regional seismic line showing the prograding wedges of the Naust Formation sequences-Naust N, A, U, S, T. (Figure from Rise et al., 2006).**

# 3 Data and Method

The 3D seismic survey ***SH9602*** is located in the area west of Skjolddryggen and north of Storegga Slide in mid-Norwegian margin (Fig. 3.1).

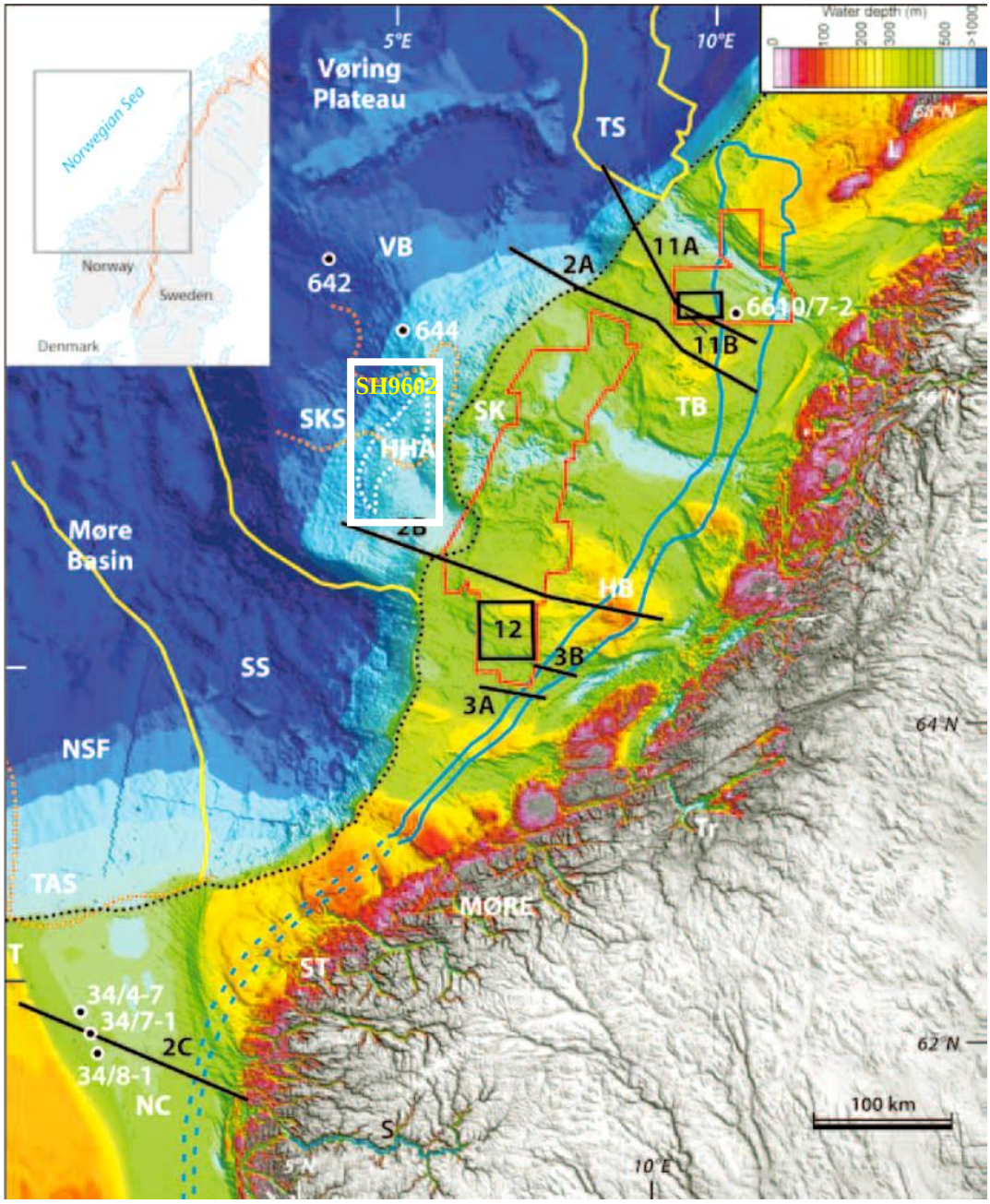


**Figure 3.1: Bathymetry map of the study area (from Ottesen et al., 2009). White rectangle shows the 3D survey SH9602 covering the HHA and NC-Norwegian Channel, NSF– North Sea Fan, ST – Stad, SKS – Sklinnadjupet Slide, SS – Storegga Slide, HHA – Helland-Hansen Arch (dotted white line marks the shallowest part of the dome), SK-Skjoldryggen, HB-Haltenbanken, TB-Trænabanken, VB-Vøring Basin,TS-Trænadjupet Slide, Tr-Trondheim, T-Tampen, TAS-The buried Tampen Slide.**

The master thesis is based on the 3D seismic interpretation of seismic data ***SH9602*** using petrel 2011.

The 3D seismic data are used for shallow-gas investigations of gas migration and accumulation areas. Gas accumulations are clearly visible on seismic sections and their corresponding attribute maps. A large number of seismic attributes are available for 3D studies for identifications of gas accumulations, related structures and the sedimentary facies in which they occur. The different seismic attributes characterize the different sedimentary environments and it is an effective way in identifying acoustic anomalies related to sub seabed gas occurrences (e.g. Plaza-Faverola, 2012).

## 3.1 Seismic Resolution

Seismic resolution is the ability to distinguish features that are close together (Sheriff, 2006). Seismic resolution comprises the vertical and horizontal resolution. The vertical resolution depends upon velocity (**v**), wavelength (**λ**) and frequency (**f**) of the wavelet given in a mathematical relation.

$$\lambda = v/f \qquad \text{Equation 1}$$

Seismic wave velocities are controlling factors of the acoustic impedance of rocks. Velocity increases with burial depth, diagenesis and compaction of sediments. At shallow depth the seismic response has a higher frequency (shorter wavelength) and therefore higher resolution but the frequency will be attenuated with depth resulting in a poorer resolution (Fig. 3.2). (Brown, 1999).

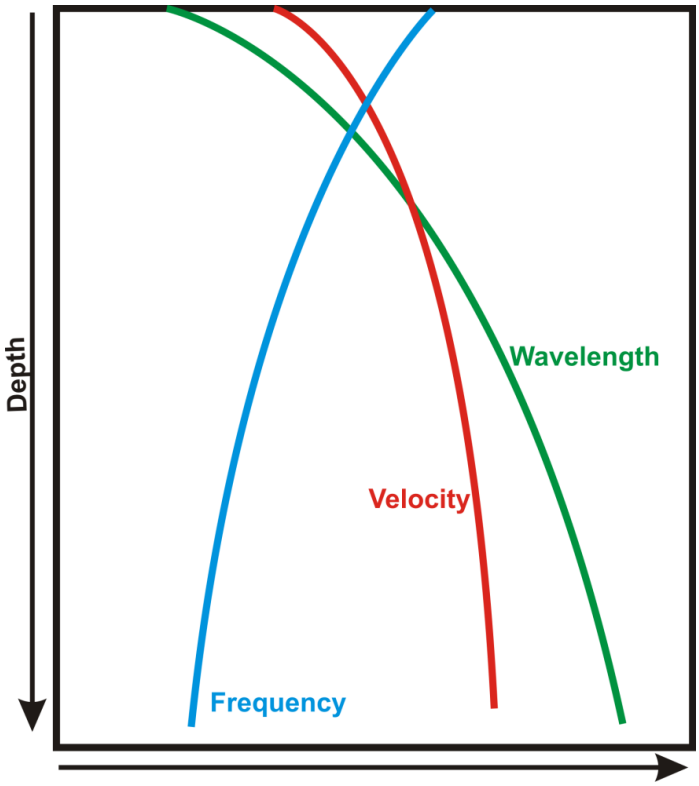


**Figure 3.2: The variation of velocity, frequency and wavelength with depth. Velocity and wavelength increases and frequency decreases with depth.**

**(Figure from Brown 1999).**

A spectrum analysis is performed to calculate the frequency spectrum and dominant frequency of the dataset SH9602. This is done by importing the inline 691 in a "SEG Y" format to landmark seismic processing software, Promax. The dominant frequency is figure out 28Hz from the frequency spectrum 16-48 Hz (Fig. 3.3).

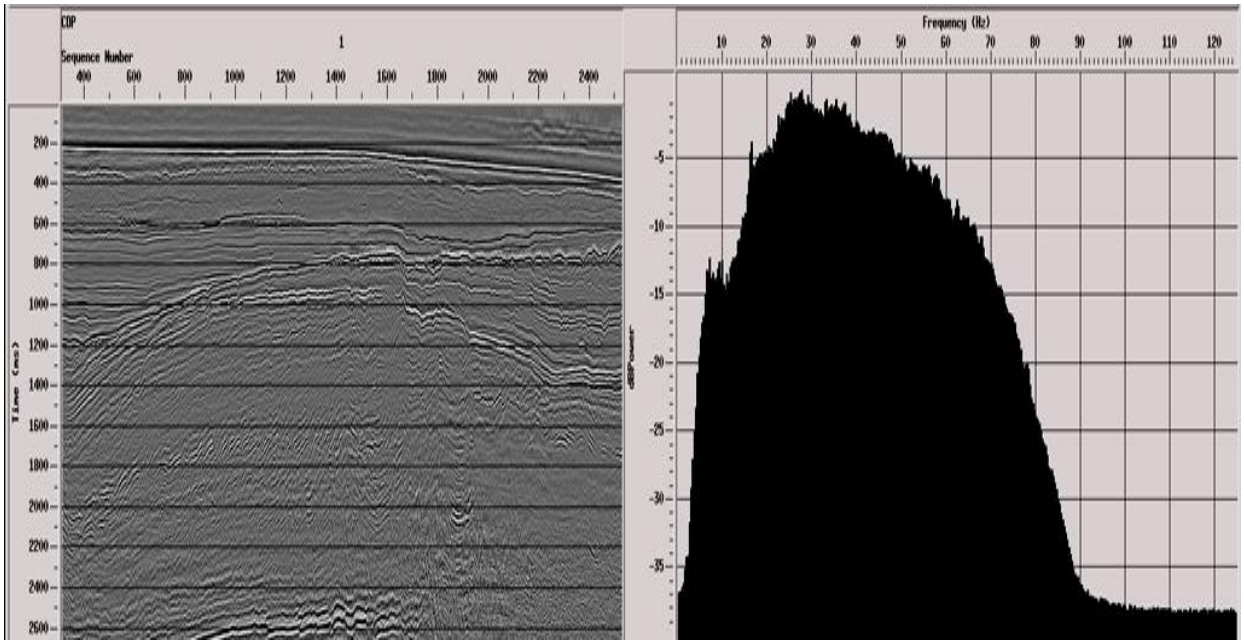


**Figure 3.3: The spectrum analysis of inline 691 shows the dominant frequency is 28Hz from frequency spectrum analysis 16-48Hz.**

An average p-wave velocity of 2000m/s is calculated from time-depth conversion of the surface (Ottesen et al., 2009) and the dominant frequency of 28Hz is estimated from the spectrum analysis. Accordingly, the vertical resolution is calculated:

$$\lambda = v/f$$

$$= 2000/28$$

$$=71.43$$

$$\text{Vertical Resolution}=1/4\ \lambda$$

$$\sim 17.85\text{m}$$

Horizontal resolution determines the position of two reflecting points horizontally and discriminates them. Horizontal resolution depends on the frequency and velocity of seismic waves (Yilmaz, 1987). It is determined by the width of first Fresnel Zone (FZ) on the unmigrated seismic section. Fresnel Zone (FZ) is the circular zone on the reflecting horizon and its diameter can be calculated from the mathematical relation.

$$rf = \frac{v}{2}\left(\frac{t}{f}\right)^{1/2} \qquad \text{Equation 2}$$

It is concluded from above relation that FZ increases with increasing depth and velocity, and with decreasing frequency. Migration improves the horizontal resolution by shifting the reflection to their accurate position in all direction and collapse the FZ into an ellipse. (Fig.3.4). On the 3D migrated seismic data lateral resolution can be estimated by $\frac{1}{4}\ \lambda$.

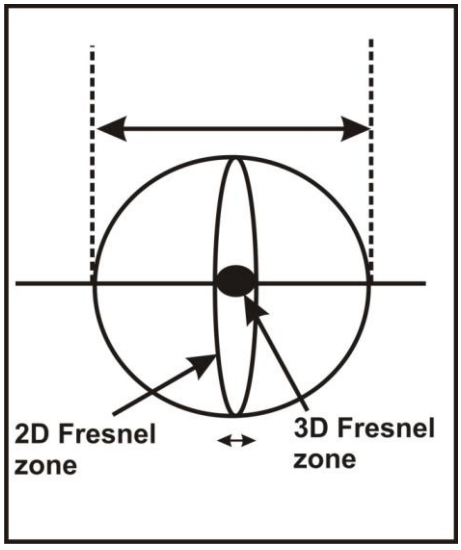


**Figure 3.4: The extension of Fresnel zone before and after the migration. Complete circle shows the Fresnel zone before migration, ellipse after 2-D migration and black dot after 3-D migration. (Figure from Brown, 1999).**

## 3.2 Description of the survey SH9602

3D seismic dataset SH9602 covers an area 6404 $km^2$ of the Helland Hansen Arch (Fig.3.1). SH9602 is a full-offset dataset acquired by Norske Shell and processed by Ensign Geophysics Ltd.UK in 1996/1997 (Tab. 1).

***Table 1 .Information about the Survey SH9602-3D***

| *Term* | *Description* |
|---|---|
| ***CDP fold*** | ***46*** |
| ***Sample Interval*** | ***4 ms*** |
| ***Recorded*** | ***SEGY-D 8015*** |
| ***Format*** | ***SEGY*** |
| ***Sample Code*** | ***Floating Point 32bit*** |
| ***Source*** | ***Airgun Arrays 25m Flip-Flop*** |
| ***Separation*** | ***50m Lateral Separation*** |
| ***Shot Point Interval*** | ***25m:50m per array;*** |
| | ***Depth:6m;Volum:3397cu*** |
| ***Spread*** | ***Near Trace Offset=173m*** |
| ***Traces Sorted*** | ***CDP*** |
| ***Hydrophone depth*** | ***7.0m*** |
| ***Number of Inlines*** | ***1319*** |
| ***Number of Crosslines*** | ***2641*** |
| ***Inline Interval*** | ***25.17*** |
| ***Crossline Interval*** | ***25.26*** |
| ***Datum*** | ***ED50*** |
| ***Projection*** | ***UTM Zone 32N*** |
| ***Central Meridian*** | ***9 Degree East*** |

### 3.2.1 Inline Noise

During the 3-D seismic data acquisition footprints such as strips existed (Fig. 3.5) that were difficult to remove by later data processing.

Acquisition footprints are clearly visible along the inline direction on the interpreted seabed reflection in 3D survey SH9602 (Fig.3.5).

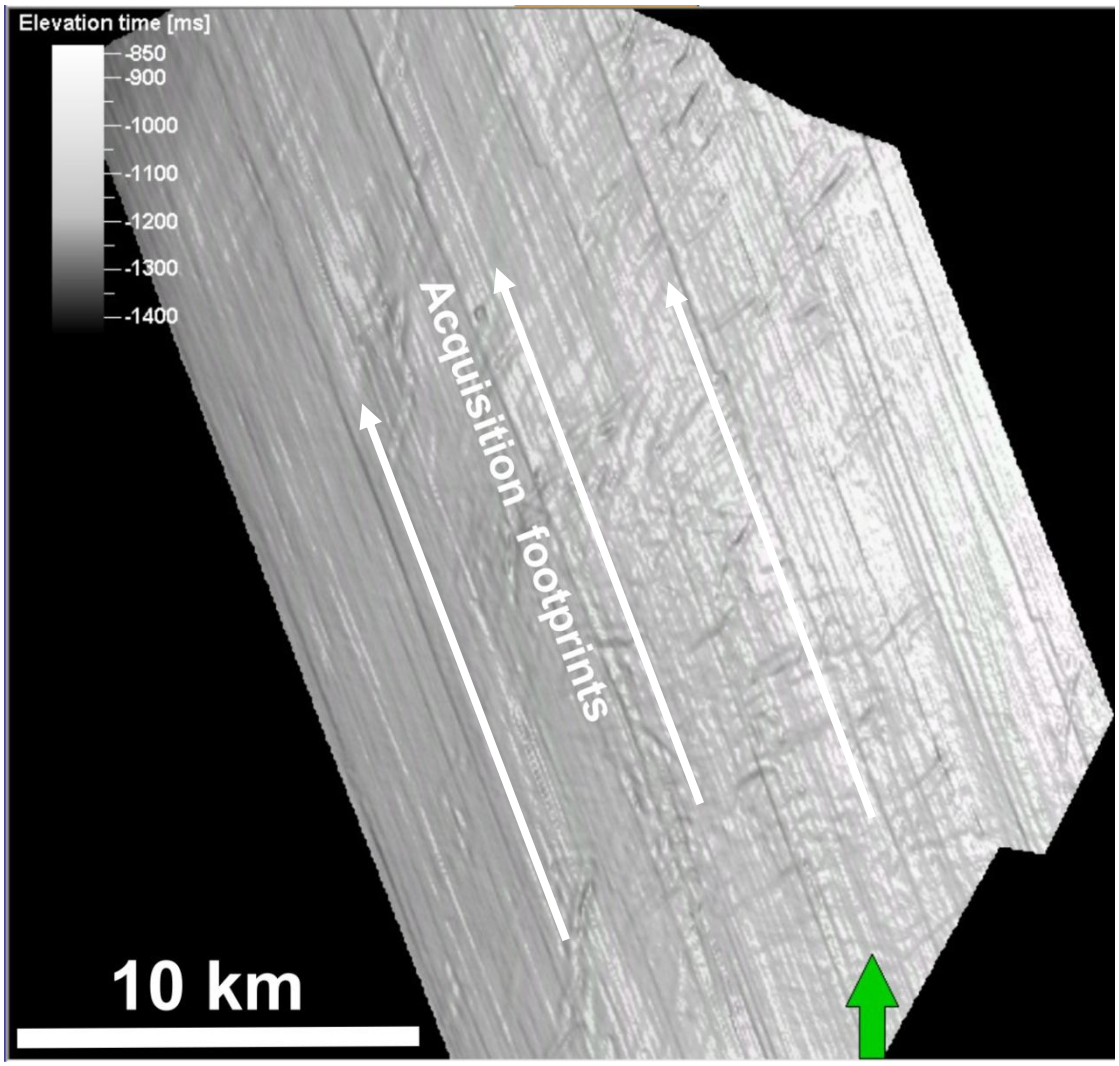


**Figure 3.5: Acquisition foot prints indicated by white arrows on the sea floor surface in 3D survey SH9602.**

### 3.2.2 Mapping of Fluid Migration pathways

It has been suggested by Løseth et al., (2009) to interpret fluid migration pathways in a three ways: (1) observe, describe and map the seismic amplitude anomalies that may correspond to a leakage zone; (2) interpret these anomalies individually; and (3) group the leakage related anomalies into a leakage zone characterized by the root, the top, vertical extent, width and shape. The origin and upper termination of leakage anomalies are identified by the root and the top respectively. The width of leakage zone is measured by edge to edge identifying the distortion zone and then area is calculated by the formula of ellipse **(longest radius x shortest radius x π).**

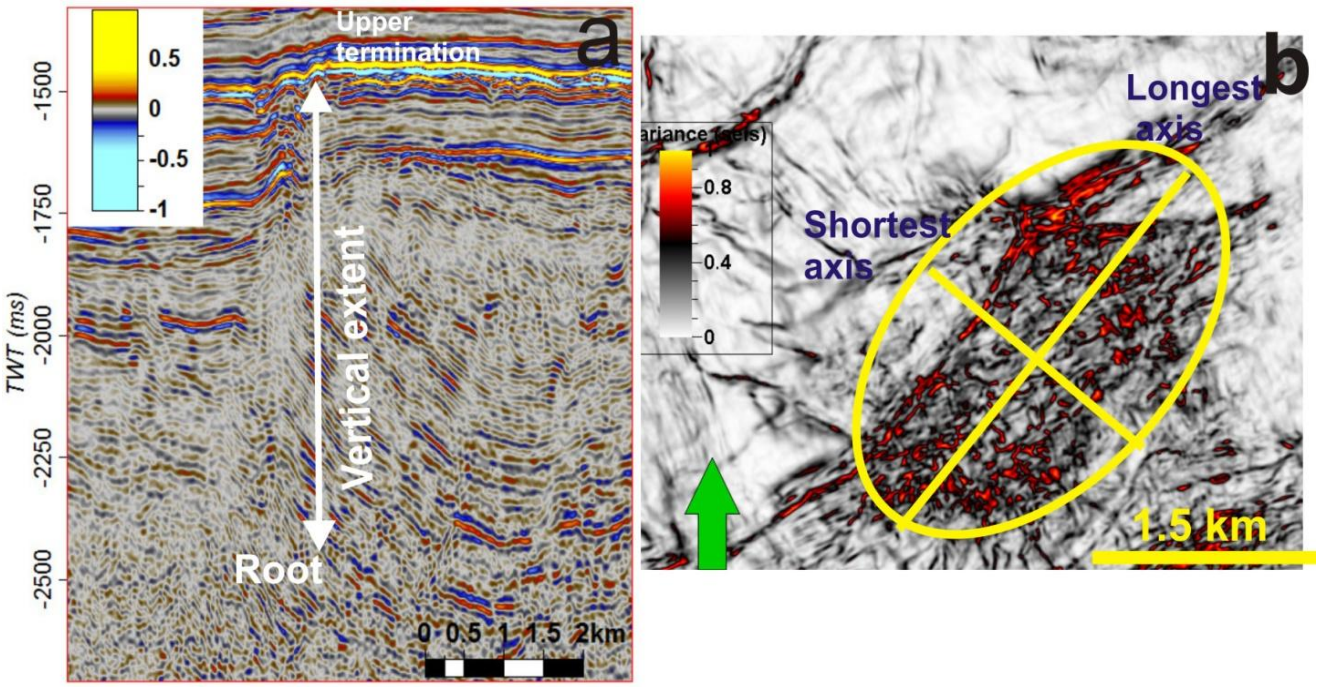


**Figure 3.6: Example of a leakage zone mapping: a) leakage zone with root and upper termination on seismic section b) longest and shortest axis of leakage zone from variance time slice at 1724 ms TWT.**

The associated anomalies and their pattern are described in table 2 and 3.

***Table 2: Descriptive of amplitude anomalies terms. (Table from Løseth et al., 2009)***

| *Term* | *Definition* |
|---|---|
| ***Bright Spot*** | Local increase in positive or negative amplitudes along a reflection for any reason. |
| ***Dim Spot*** | Local decrease in positive or negative amplitude along a reflection or in a zone for any reason. |
| ***V-shaped bright*** | High amplitude V-shaped reflection in vertical section that is discordant to reflection from deposition surfaces. Seldom more that 2-3 km wide. |
| ***Flat Spot*** | Relatively flat seismic reflection with an angle to the stratigraphic reflections. |
| ***Phase Reversal*** | Phase shift of 180° along a continuous reflection, so that peak become a trough and vice versa. |
| ***AVO*** | Amplitude variation with offset. |
| ***Reduced Continuity*** | Local reduction of continuity of a seismic event. |
| ***Increased Continuity*** | Local increase of continuity of a seismic event. |
| ***Reduced Frequency*** | Local decrease of frequency. |
| ***Bottom Simulating Reflector (BSR)*** | High amplitude reflection that often is parallel to seabed. |

***Table 3: Describes the anomalous pattern on seismic pattern. (Table from Løseth et al., 2009).***

| *Term* | *Definition* |
|---|---|
| ***Vertical wipe-out zone*** | The area on a seismic section where the reflections from the stratigraphic layers are deteriorated so the primary reflections either are absent or very weak. |
| ***Vertical dim zone*** | The area on a seismic section where the reflections from the stratigraphic layers are visible but have lower continuity and amplitude than in adjacent areas. |
| ***Vertical high amplitude*** | The area on a seismic section where several high amplitude reflection anomalies occur that naturally can be grouped together |
| ***Discontinuity zone*** | The area on a seismic section where the reflections from the stratigraphic layers are more discontinuous than in adjacent areas. |
| ***Chaotic reflection zone*** | The area on a seismic section where the reflection pattern is chaotic compared to adjacent areas. |
| ***Local depression features*** | Negative real down-bending or sag of a seismic reflection. The underlying reflections can be truncated, be parallel to the described structure or they can have any type of reflection pattern (e.g. chaotic). |
| ***Push down*** | Apparent down-bending produced by a local, shallower low-velocity region. |
| ***Pull up*** | Apparent uplift produced by a local, shallower high-velocity region. |
| ***Mounds*** | Positive structure of any shape rising above the normal top of a reflection. The reflection pattern below the mound can be of any type. |

## 3.3 Interpretation of data set SH9602

Petrel Geophysics software 2011 by Schlumberger (2011) is the tool used for 3D volume interpretation. It identifies stratigraphic and structural features, and then allows interpreting the horizon and faults through the volume.

For horizon interpretation, tracking parameters are set for better tracking results. The wavelet tracker uses the signal features like peak, trough, S-crossing or Z-crossing. The minimum value of correlation quality is set to 0.75 as it correlates threshold where tracking will fail and identical neighboring traces give a value of 1.0. The sample value is set 8 above and below in symmetrical window which determines whether the wavelet window is symmetrical (ON) or asymmetrical (OFF). Depending upon the continuity and lateral extent of strong reflections signal features peak or trough are normally set. The seed confidence value is set to 80% to utilize the minimum tracking value for seismic amplitude as a percentage of the seed point. The expansion quality is set to validated 5x5 which checks the 24 closest points against the seed point and their neighbors. The maximum vertical delta which controls the vertical position to change from one trace to the next in 2D guided and seed tracking modes is set to 3. During interpreting horizons the interval between inline or cross line is set to 5-8 depending upon the continuity of the reflection then paintbrush Autotracking tracked the points outwards from the seed point for complete horizon volume for detailed study (Schlumberger, 2011).

## 3.4 Seismic Attribute

An attribute is necessarily a derivative of a basic seismic measurement. There are different horizon and formation attributes independent of each other and there are different ways of presenting and studying various amounts of basic information. The basic information is time, amplitude, frequency and attenuation and this form the basis of our attribute classification. Time –derived attributes provide the structural information, amplitude –derived attributes provides stratigraphic and reservoir information. Frequency-derived also provide additional useful stratigraphic and reservoir information. Attenuation is not used today but probably in future (Brown, 1999). Thus **"Seismic Attributes"** are all of the measured, computed or implied quantities obtained from the seismic data. The use of color is very important in attribute displays. The attribute color scales can be modified so that the display is using the full dynamic range of the data.

**Seismic Surface attributes**

The surface attribute maps allow computation of interval attributes relative to a single horizon, between two horizons or within a constant time window.

**RMS Amplitude**

It is the measure of reflectivity within a time window where the square root of the sum of the squared amplitude is divided by the number of live samples. It is the classical attribute for bright spot detection. It is expressed mathematically as:

$$\sqrt{\frac{\sum_i^n amp^2}{k}}$$

Equation 3

Where k is the number of samples (Schlumberger, 2010). The color scale of RMS amplitude is adjusted to map out the desirable amplitude anomalies.

**Minimum Amplitude**

This amplitude map measure the maximum negative amplitude of a trace and potential low velocity medium within a time or depth window. It is a good indicators of hydrocarbon accumulations (Schlumberger, 2010).

**Instantaneous Frequency**

It is the time derivative of the phase of the seismic trace. It indicates the bed thickness and can detect lateral changes in lithologies due to changes in instantaneous frequency, which indicate the bed thinning or pinch outs. It also acts as a fracture zone indicator as the fracture may appear as lower frequency zone or as hydrocarbon indicator due to significant lower frequencies (Schlumberger, 2010).

**Instantaneous Phase**

It is the description of the phase angle at any instant along a trace independent of the amplitude. It also reveals weak and strong events with equal strength. It also acts as discriminator for geometrical shapes and is a good indicator of continuities, angular unconformities, faults, pinch-out, sequence boundaries and onlap patterns (Schlumberger, 2010).

**Reflection Strength**

It mainly represents the acoustic impedance contrast, hence reflectively. It detects the lithological changes, sequences boundaries and bed thinning effects. It is also allows for a spatial correlation to porosity and other lithological variations. It also detects bright spots (Schlumberger, 2010).

**Chaos**

It maps the chaoticness of the local seismic signal from the statistical analysis of dip/azimuth estimate. It is used for fault and fracture identifications. It provides a stratigraphic tool and is useful for identifying channel infill, gas chimneys, reef internal texture, sink holes, salt diapers and shale diapers. It is good discriminators for seismic facies analysis (Schlumberger, 2010).

**Variance (Edge Method)**

It uses a signal coherence analysis which estimates trace to trace variance. It will produce the same response for the same seismic signature in both high and low amplitude signals. It reveals discontinuities in seismic data either related to stratigraphic terminations or structural lineaments. It is useful for fault detection from continuous variance response where high variance can suggest faults and fracture swarms. It is helpful for gas chimney mapping and for discrimination between high and low continuity of seismic reflections (Schlumberger, 2010).

**Ant Tracking**

Ant tracking extracts faults, fractures, distorted pattern, chaoticness, internal amplitude variation, processing effects and other linear anomalies through edge enhancement within the seismic data volume (Pedersen et al., 2002 & 2005). A quality faults attribute (edge) volume

such as Variance or Chaos is needed to be generated for executing the Ant Tracking attribute. There are primarily three steps in the workflow such as, seismic conditioning, edge detection, and edge enhancement (the Ant Tracking attribute). The Ant Tracking utilizes an edge volume such as variance or chaos as an input data and generates the edge enhancement volume as output volume (Schlumberger, 2010).

### Structural Smoothing

It is a smoothing technique (Fig. 3.7) of the input seismic data to reduce noise and to increase the continuity of seismic reflection without the degradation of fault expressions contained in the regional data. It can also be used to illuminate "flat spots" within the seismic volume and to emphasize a fluid contact (Schlumberger, 2010).

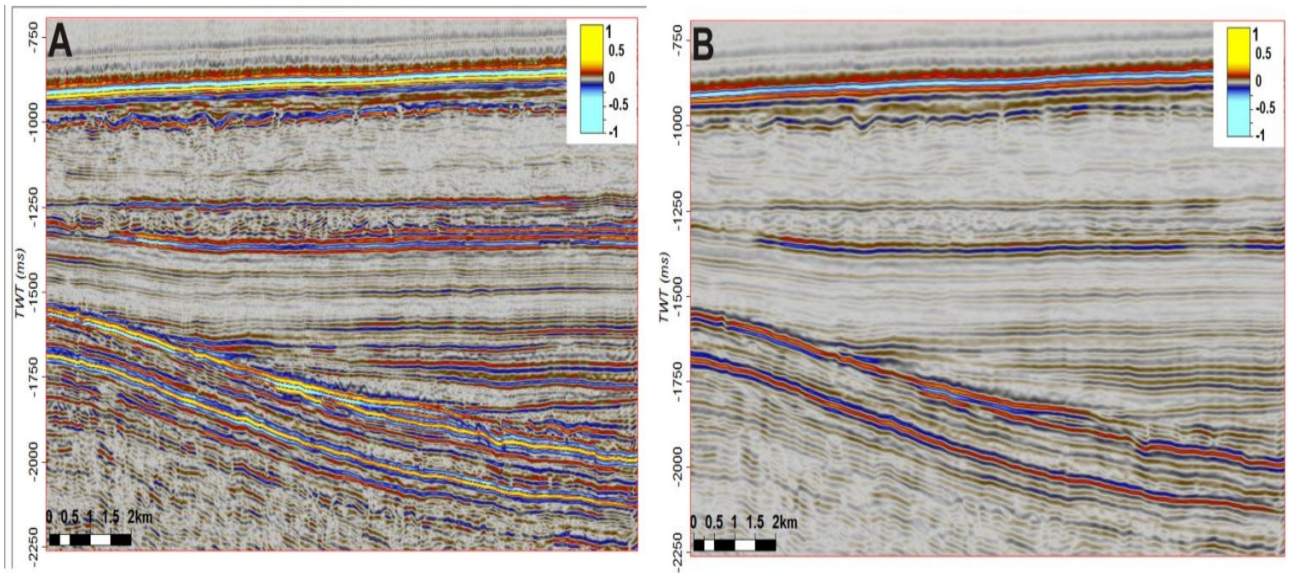


**Figure 3.7: Structural smoothing applied to data from SH9602 :a) Original seismic data. b) After structural smoothing seismic data.**

# 4 Results

## 4.1. Seismic Stratigraphy

The survey area comprises mainly two thick sedimentary formations, Eocene-Oligocene (Brygge Formation) and Pliocene-Pleistocene (Naust Formation) (Fig. 4.1).

The Brygge Formation (Eocene-Oligocene) forms the Helland Hansen Arch (HHA) and is characterized by high amplitude seismic reflections. It acts as the base for the prograding glacial and interglacial Plio-Pleistocene sequences (Naust Formation). The prograding wedges of the Naust N and Naust A formations show onlapping along the eastern flank of Helland Hansen Arch. They are stratified and identified by medium reflection seismic amplitudes.

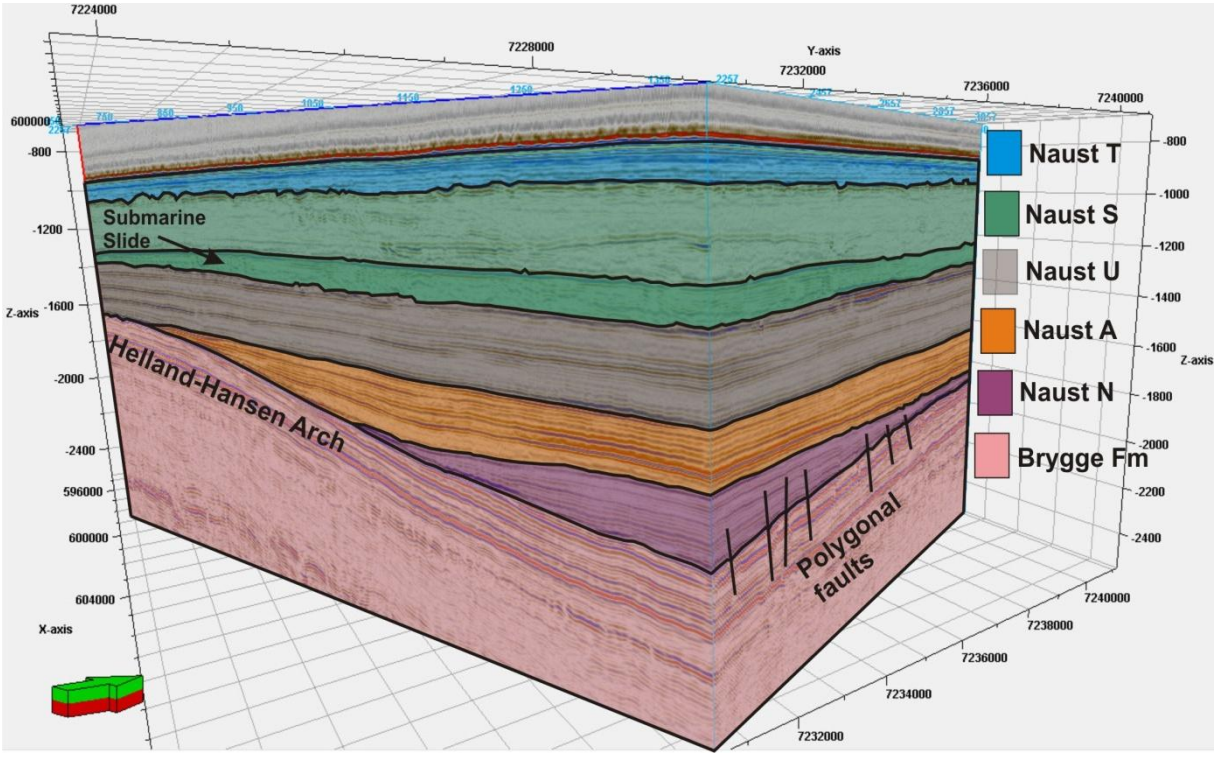


**Figure 4.1: 3D view of survey SH9602 seen from south-west. It shows the interpreted Formations, Brygge (Eocene- Oligocene) and Naust (late Pliocene-Pleistocene) with units Naust N, Naust A, Naust U, Naust S, Naust T and Seabed.**

The crest of the Helland Hansen Arch acts as a barrier for both Naust A and Naust U sediments. Naust A and U completely cover the Helland Hansen Arch and are identified by the low to medium seismic reflection amplitude. Naust S shows submarine sliding identified by disturbed seismic reflectors and transparent seismic units. Naust T characterizes the high amplitude seismic reflection of flat lying aggradational units. The interpreted seismic horizons in the 3D cube (Fig. 4.1) are based on 2D seismic interpretations (Rise et al., 2010., Chand et al., 2011., Ottesen et al., 2009) shown in figure 4.2.

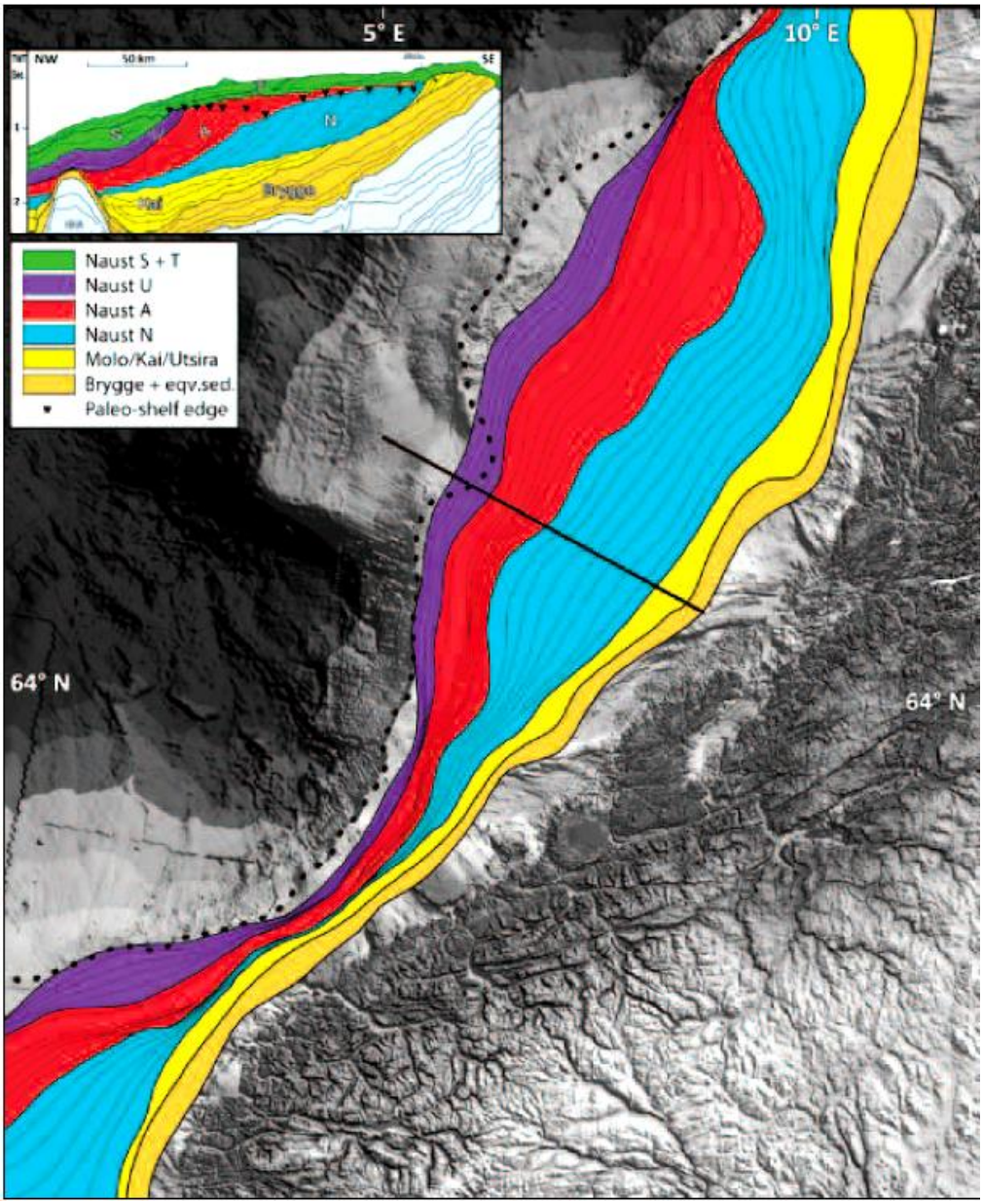


**Figure 4.2: Seismic profile showing the progradational pattern of palaeo-shelf break through Naust N, A, U across the Haltenbanken and the location of Brygge and Kai formations. (Figure from Ottesen et al., 2009).**

## 4.2 Seismic Interpretation of Eocene-Oligocene formations

The Brygge Formation (Eocene-Oligocene) shows a dome structure in the study area and forms the Helland Hansen Arch (HHA) (Fig. 4.3). The lateral extent of the thickness of the Brygge formation decreases both in north and south direction. It is more symmetrical in the south and becomes asymmetrical in the north due to the rotation of the northwestern flank of HHA. On the crest of HHA major several tens of kilometers long faults developed in approx. N-S direction (Figs. 4.3 and 4.4).

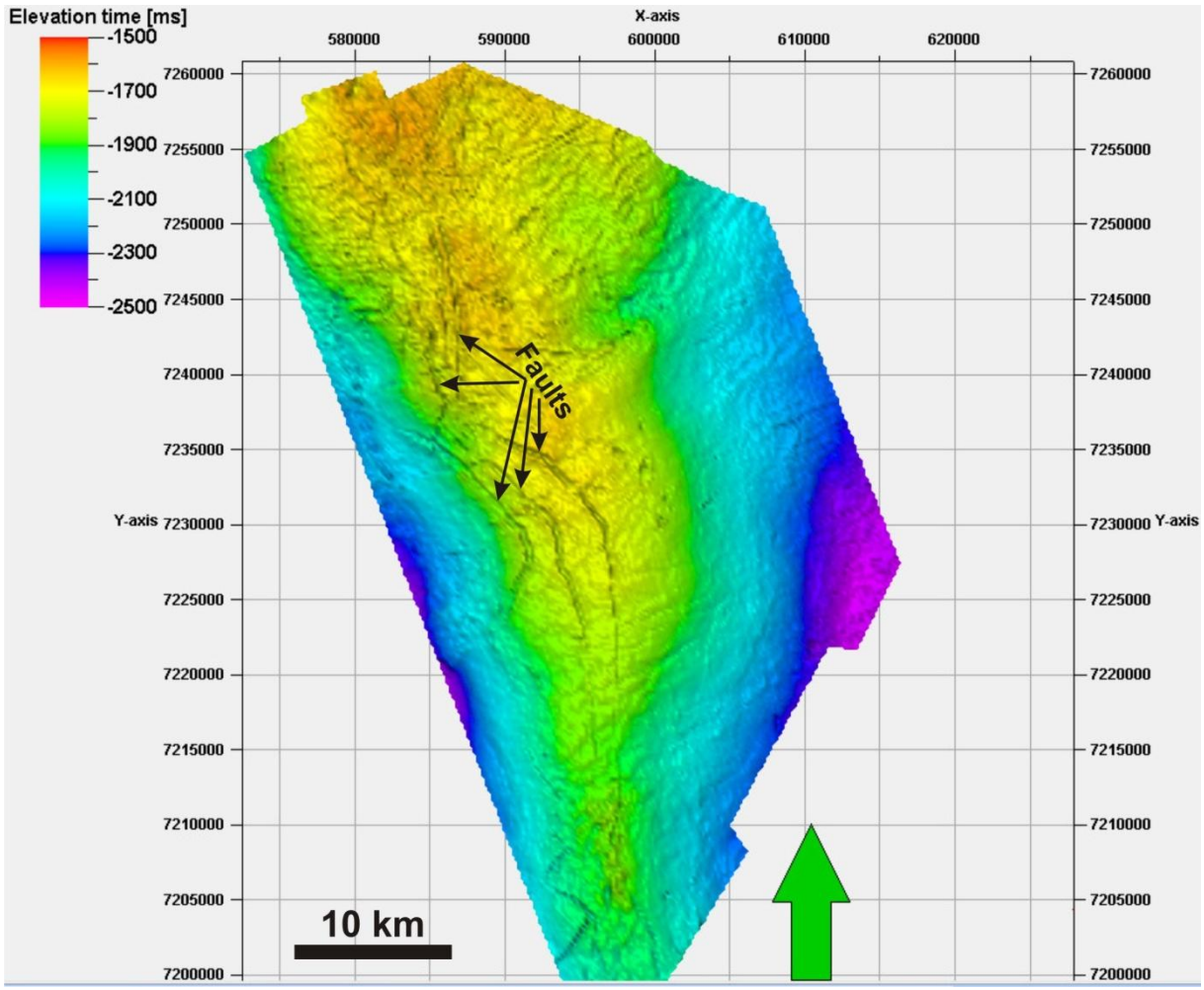


**Figure 4.3: The surface map in time domains of interpreted Brygge Formation shows the domal structure and major faults at the crest of Helland Hansen Arch (HHA).**

The Brygge Formation acts a surface for westward prograding NAUST formations (Naust N, A and U) and produces a strong reflection event caused by different physical properties, lithologies and hence acoustic impedance contrast from overlying beds. The seismic reflection generated by Brygge Formation is generally diachronous because it represents the hiatus in sedimentation record (Veeken et al., 2007). On both the eastern and western flanks of HHA, the younger Plio-Pleistocene formations are forming onlap patterns along Brygge Formation (Fig. 4.4).

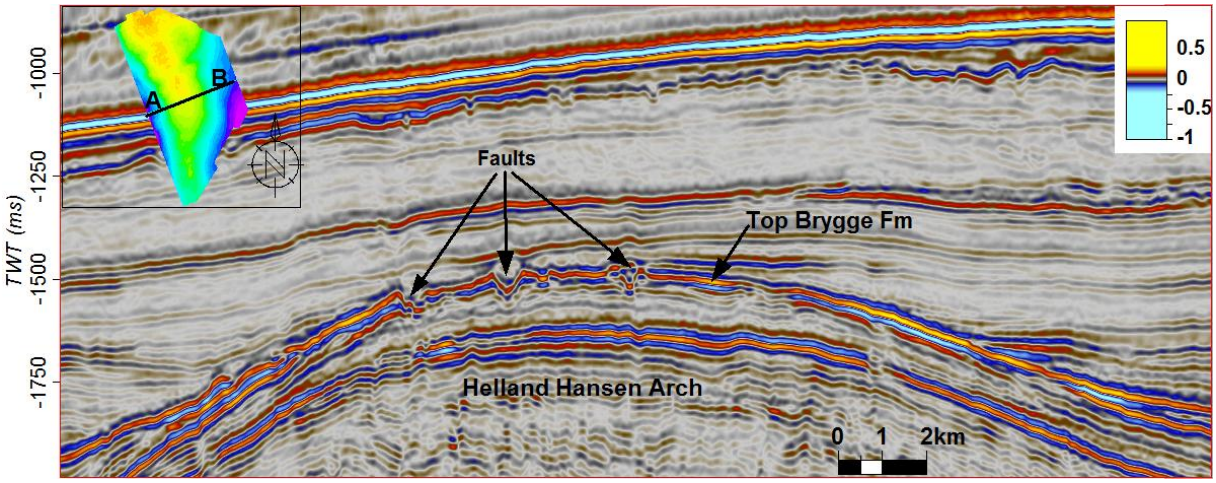


**Figure 4.4: A seismic profile of the survey shows the major faults at the crest and reflector onlapping on both the eastern and western flanks of Helland Hansen Arch (HHA).**

### 4.2.1 Evidence for gas accumulation in Brygge Formation

A strong reflection exists at the top of the Brygge Formation along the whole HHA due to an appreciable acoustic impedance contrast. High amplitude anomalies are widely distributed at the top of the Brygge Formation. The high amplitude anomaly shows a reversed polarity relative to the seabed and a distorted seismic pattern beneath it indication possibly gas accumulation. There may be a dramatic reduction of Vp (P-wave velocity) in gas the accumulation zone which produces the anomalously high amplitude. This high amplitude anomaly is interpreted as a bright spot, which forms above the acoustic masking zone of distorted and disturbed seismic reflection signals (Fig. 4.5).

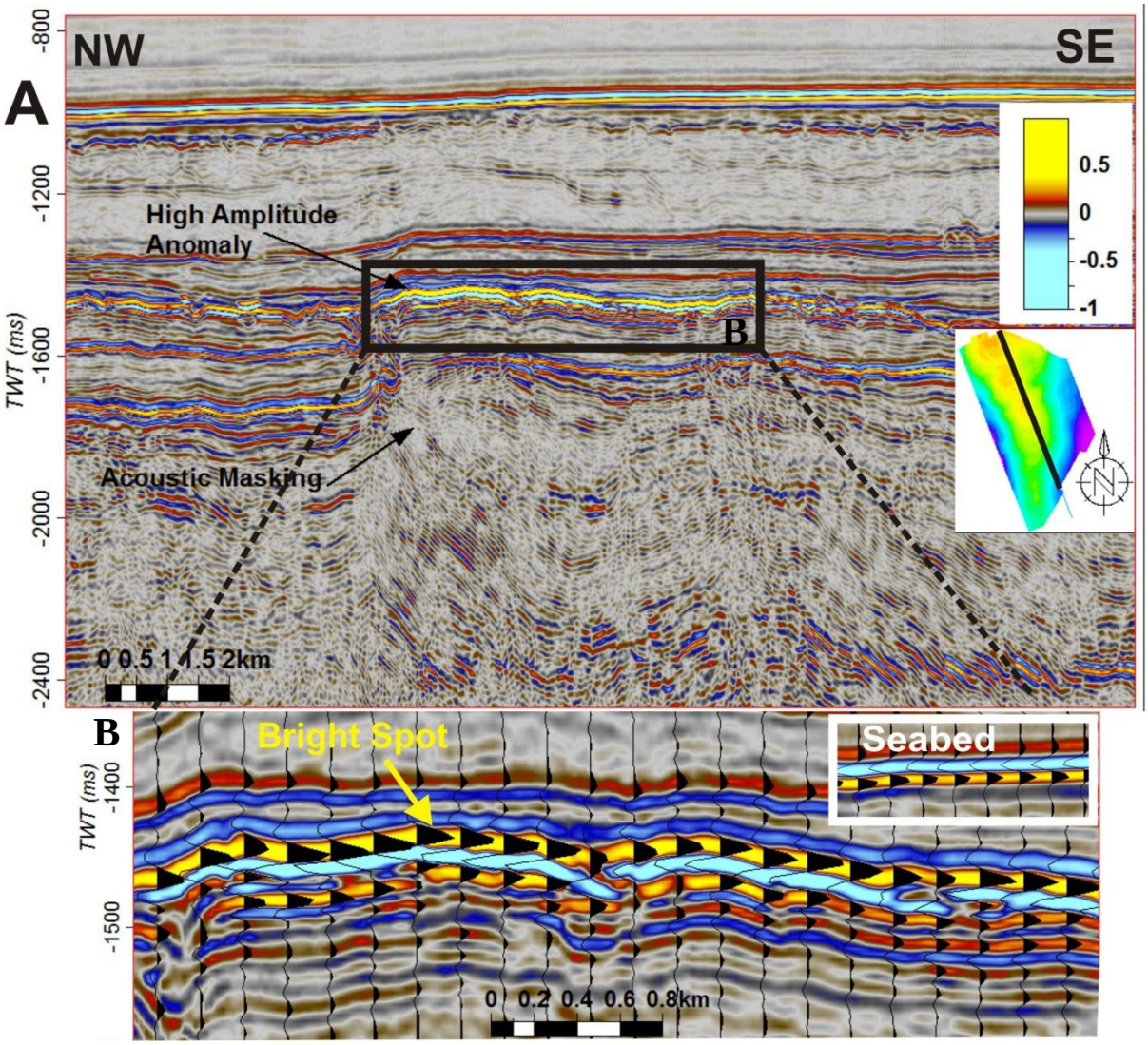


**Figure 4.5: A) A seismic section shows the high amplitude anomaly on inline 691. B) Wiggle display of high amplitude anomaly shows the polarity reversal relative to seabed.**

In the central part of the survey, at the crest of HHA, high amplitude anomalies B1 and B2 with reversed polarity relative to the seabed are observed at ~1450 ms TWT on inline 691 (Fig. 4.6). Beneath the high amplitude anomalies a disturbed and distorted seismic pattern of acoustic masking exists where reflections are absent or weak. The appearance of high amplitude anomalies right above the acoustic masking zone is interpreted as gas migration (acoustic dim zone) and accumulation (high amplitude zone) at the crest of HHA (Fig. 4.6).

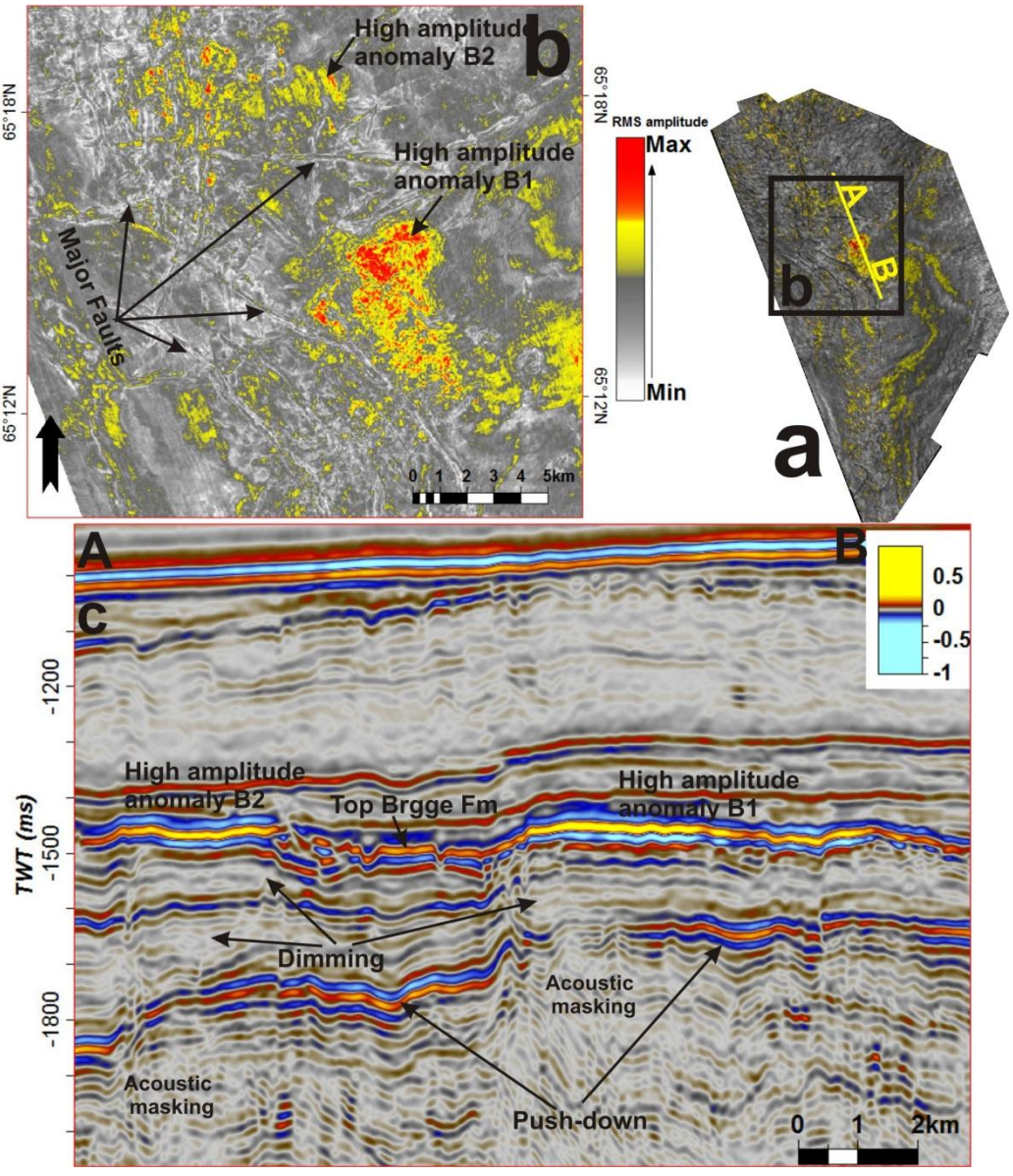


**Figure 4.6: a) RMS map shows the distribution high amplitude anomalies along the whole arch of HHA in Brygge Fm. b) RMS map indicates the high amplitude anomalies B1 and B2 and major faults in the central part of the survey c) A seismic section through theses high amplitude anomalies shows the acoustic masking and some minor push-down effects.**

A vertical dim zone is identified where the reflections are visible but with low continuity and amplitude in comparison to adjacent reflectors. Both push down effect and vertical dim zones suggest low velocity anomalies produced by the absorption and scattering of seismic energy below the gas accumulation area.

Several vertical high amplitude anomalies are grouped together indicating gas accumulations (Fig. 4.6). The high amplitudes anomalies are based on an RMS amplitude map (Fig.4.6). The RMS map gives the measure of square roots of the sum of the squared amplitude of B1 and B2 within a time window of 20 ms below the Brygge Formation. High amplitude anomaly B1 is more significant and distributed over a larger area at the crest of HHA .While B2 represents a smaller area.

On the eastern flank of Helland Hansen Arch (HHA) many high amplitude anomalies are observed at the Top Brygge Formation (Fig. 4.7). These high amplitude anomalies are accompanied by a polarity reversal relative to seabed, and are termed as bright spot. Different vertical features are observed beneath these high amplitudes such as polygonal faults and acoustic masking effects on seismic profile AB and CD (Fig. 4.7). These features and high amplitude anomalies with reversed polarity suggest gas accumulations in the Brygge Formation on the eastern flank of Helland Hansen Arch (HHA). RMS amplitude map is generated to map out these high anomalies below 20ms from Brygge Formation (Fig. 4.7).

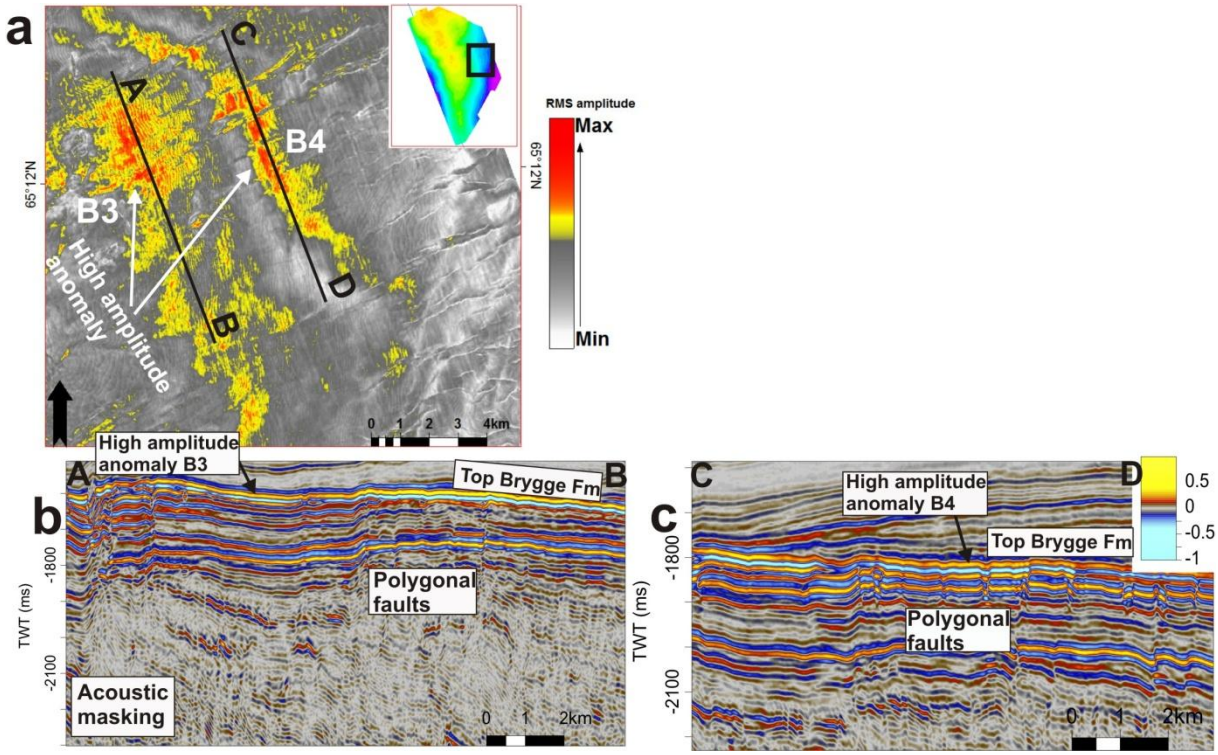


**Figure 4.7: a) RMS amplitude map of Brygge Formation shows the extension of high amplitude anomalies B3 and B4. b, c) Seismic profiles AB and CD shows the faulted high amplitude anomalies B3 and B4 respectively along Brygge Formation, polygonal faults and acoustic masking underneath it.**

High amplitude anomaly B3 is observed at 1590-1665ms TWT on seismic section inline 889 (Fig. 4.7). On RMS high amplitude map anomalies B3 shows an ellipsoidal shape. On seismic profile inline 1058 high amplitude anomalies B4 is located at 1747-1798ms TWT on eastern flank of HHA (Fig. 4.7). High amplitude anomaly B4 is disturbed by faults (Fig. 4.7).

On the northeastern part of HHA a cluster of high amplitude anomalies B5 is observed in the Brygge Formation (Fig. 4.8) on seismic profile IL 1130 at 1686-1885ms TWT. The high amplitudes anomalies are mapped using on RMS amplitude below 50 ms (Fig. 4.8). The high amplitudes anomalies are randomly distributed over a large area. A polarity reversal relative to sea floor suggests a bright spot that corresponds to gas accumulation along the eastern flank of HHA in the Brygge Formation. A vertical dim zone of low reflection continuity exists at depth 1955ms TWT right below the high amplitude anomalies. Polygonal faults and acoustic masking underneath these high amplitudes suggest vertical fluid flow features (Fig. 4.8).

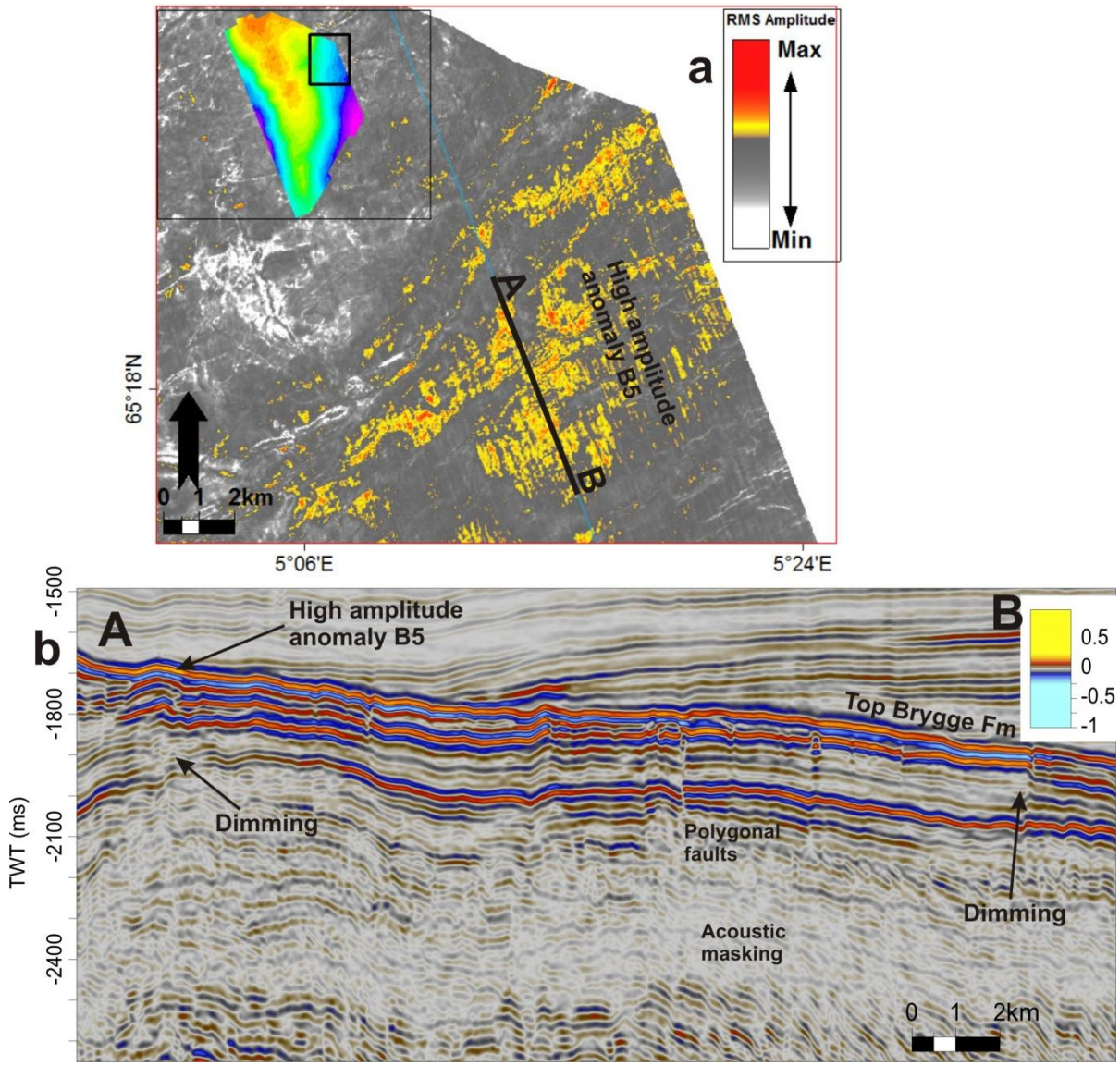


**Figure 4.8:a) RMS amplitude map of Brygge Formation shows the distribution of high amplitude anomalies. b) Seismic profile shows the extension of high amplitudes anomalies, polygonal faults and dimming effects.**

At the southern part of the 3D cube a high amplitude anomaly B6 is observed at 1517-1540ms TWT on inline 548 (Fig. 4.9). It shows a polarity reversal relative to the seabed. A vertical acoustic dim zone is observed right below B6 at 1580-1650ms TWT (Fig. 4.9).

On the western flank of HHA at the top of Brygge Formation at 1716-1738ms TWT a high amplitude anomaly B7 is observed on seismic profile inline 278 (Fig. 4.9). This high amplitude anomaly consists of a cluster of various amplitude anomalies scattered on the RMS amplitude map of the Brygge Formation. A push down effect apparently occurs at 1943ms

TWT and a vertical dim zone can be observed beneath the high amplitude anomaly at 1750-2000ms TWT (Fig. 4.9).

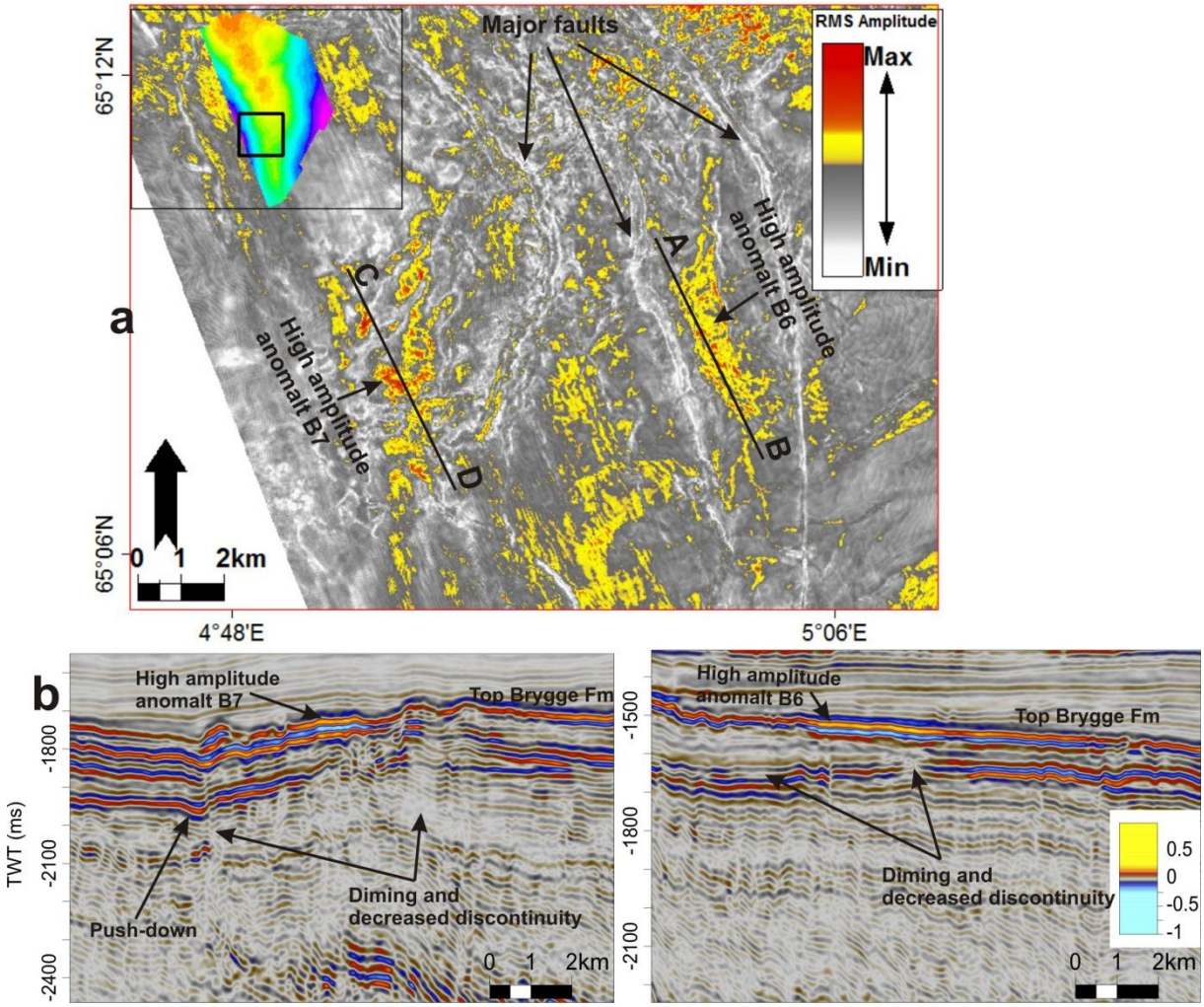


**Figure 4.9: a) RMS amplitude map of Brygge Formation shows the distribution of high amplitude anomalies B6 and B7. b) Seismic profiles indicate the B6 and B7 and related vertical dim zone and possible push down effects.**

At the northern part of the survey, high amplitude anomalies are randomly distributed and occur at shallower depth. High amplitude anomaly B8 shows a reversed polarity relative to the seabed suggesting a bright spot on seismic section inline 443 at 1450ms TWT (Fig. 4.10). The high amplitude anomaly B8 is centered above two wipe-out zones where primary reflections from stratigraphic layers are absent or weakened. High amplitude anomalies B9 and B10 are found further north and are observed at ~1430ms TWT (Fig. 4.10). Both high amplitude anomalies show reversed polarity relative to the seabed. Acoustic masking and a low continuity of seismic reflection beneath the high amplitude anomalies suggest gas accumulation at the crest of HHA at the top of Brygge Formation.

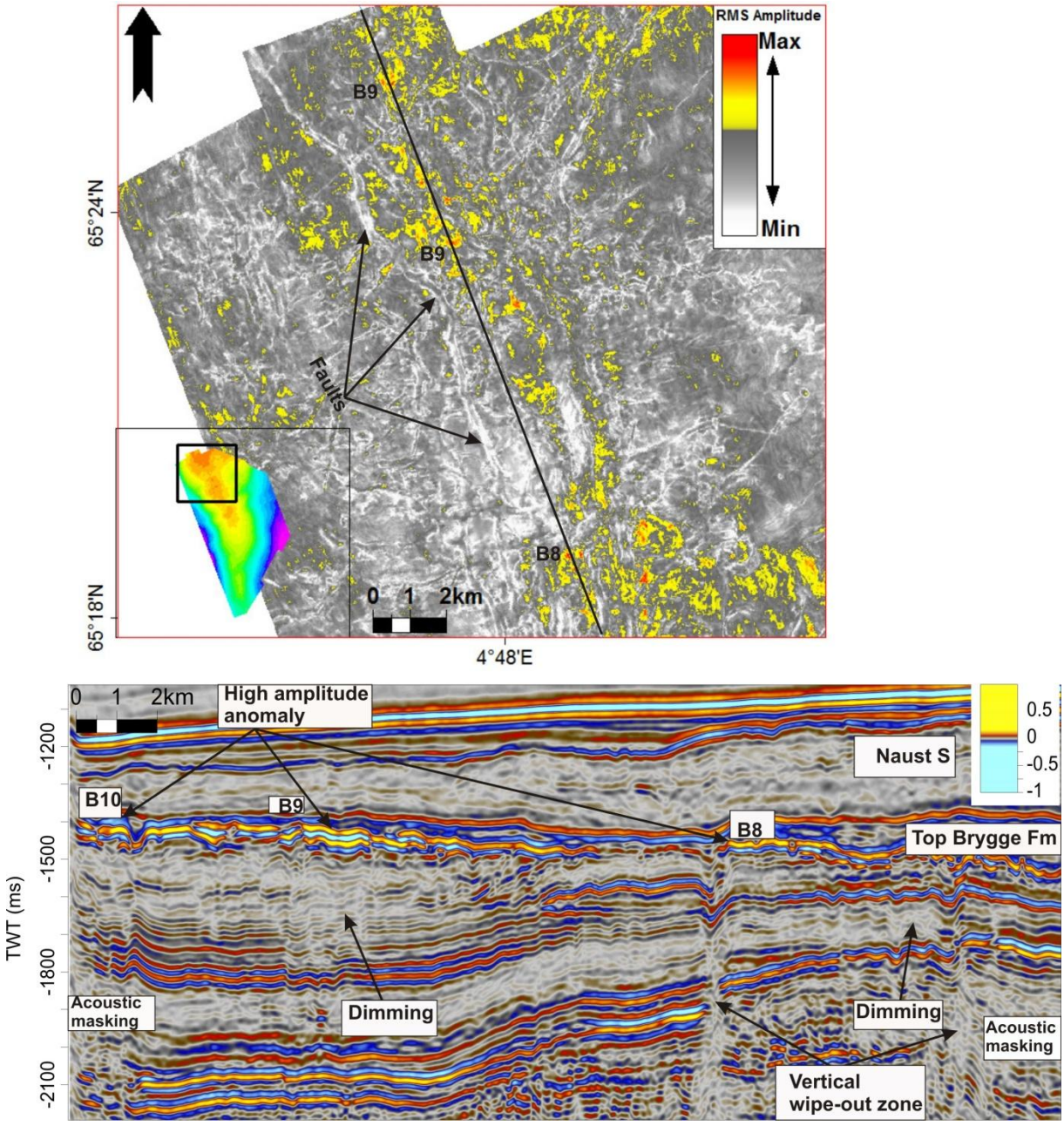


**Figure 4.10: a) RMS amplitude of Brygge Formation shows the distribution of high amplitude anomalies B8, B9 and B10. b) Seismic profile shows the depth of high amplitude anomalies and vertical wipe out zone, acoustic masking and vertical zone of dimming or push down effects.**

### 4.2.2 Tracing vertical fluid migration pathways in the Brygge Formation

Patchy distributions of high amplitudes anomalies are observable in seismic sections and corresponding attribute maps along the whole HHA within the Brygge Formation. They are mostly found at the upper termination of acoustic masking zones. The acoustic masking zone is identified as a vertical wipe-out zone of deteriorated and distorted seismic reflection of low amplitude. It may occur along with other features such as push-down effects and vertical dim zones. Acoustic masking zones at the HHA are often related to polygonal faults which are identified by low coherency on variance maps. The presence of high amplitude anomalies with reversed polarity right above acoustic masking zones and push-down effects strongly suggests that these zone act as vertical leakage zone for fluids.

Acoustic masking zone 1 is the combination of two prominent chaotic reflections B1.1 and B1.2 which appear on variance time slice at 1736ms TWT (Fig. 4.11). High amplitude anomaly B1 interpreted as bright spot seated above the upper termination of this zones at ~ 1450ms TWT (Fig. 4.6). The lateral extension of the acoustic masking zone is approx. 6.5 km. Due to the fact that the chaotic zone increases with depth it is difficult to define its lower termination.

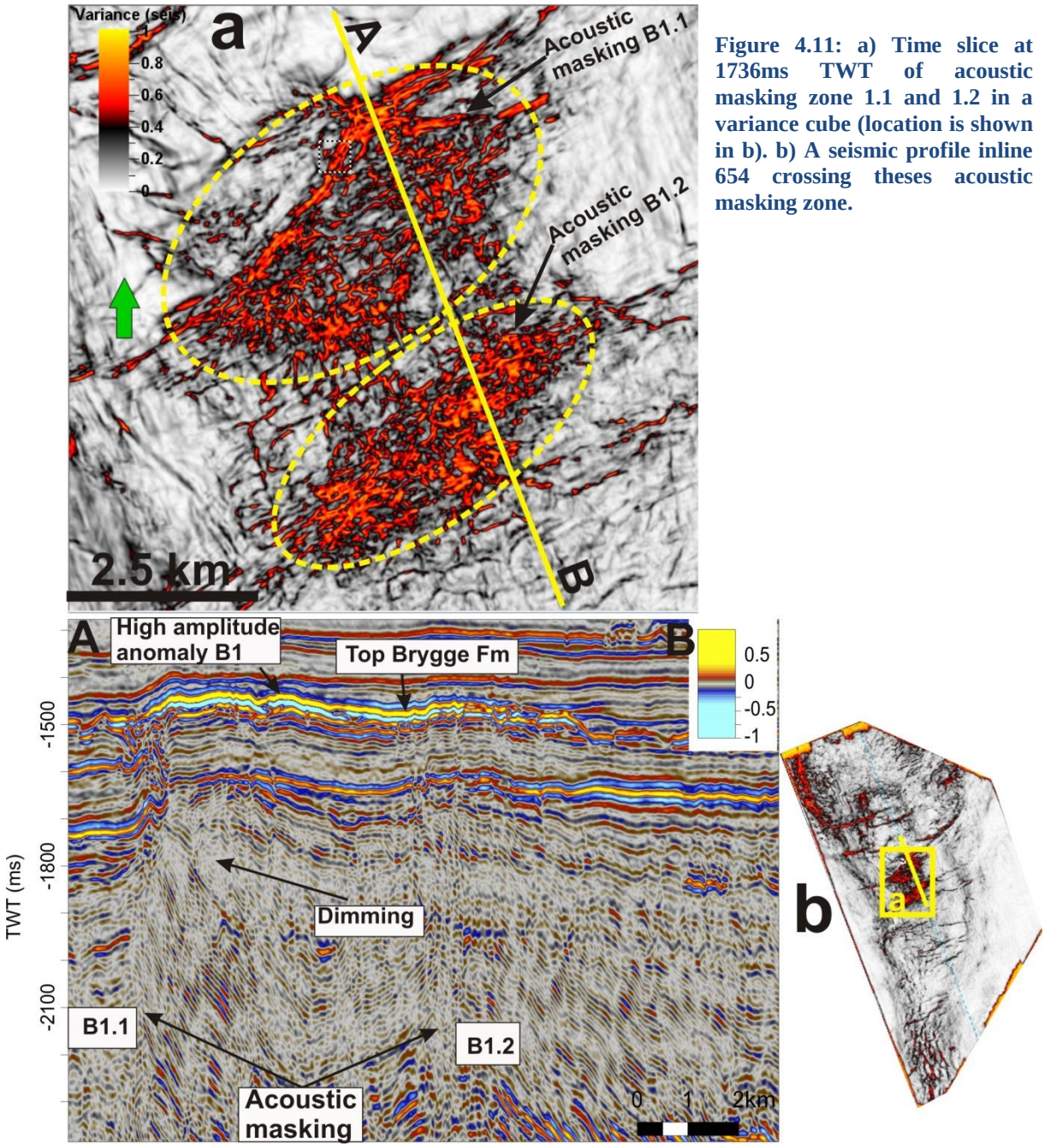


**Figure 4.11: a) Time slice at 1736ms TWT of acoustic masking zone 1.1 and 1.2 in a variance cube (location is shown in b). b) A seismic profile inline 654 crossing theses acoustic masking zone.**

The chaotic reflection areas B1 and B2 constituting the acoustic masking zone 1 are easily differentiated and separated between 1650ms-1740ms TWT time slices in the variance cube shown in figure 4.12. The line AB in figures 4.12 represents the seismic section (Fig. 4.11 b). The chaotic areas increase with depth and merge with each other to become one acoustic masking area below 1740ms TWT (Fig. 4.12).

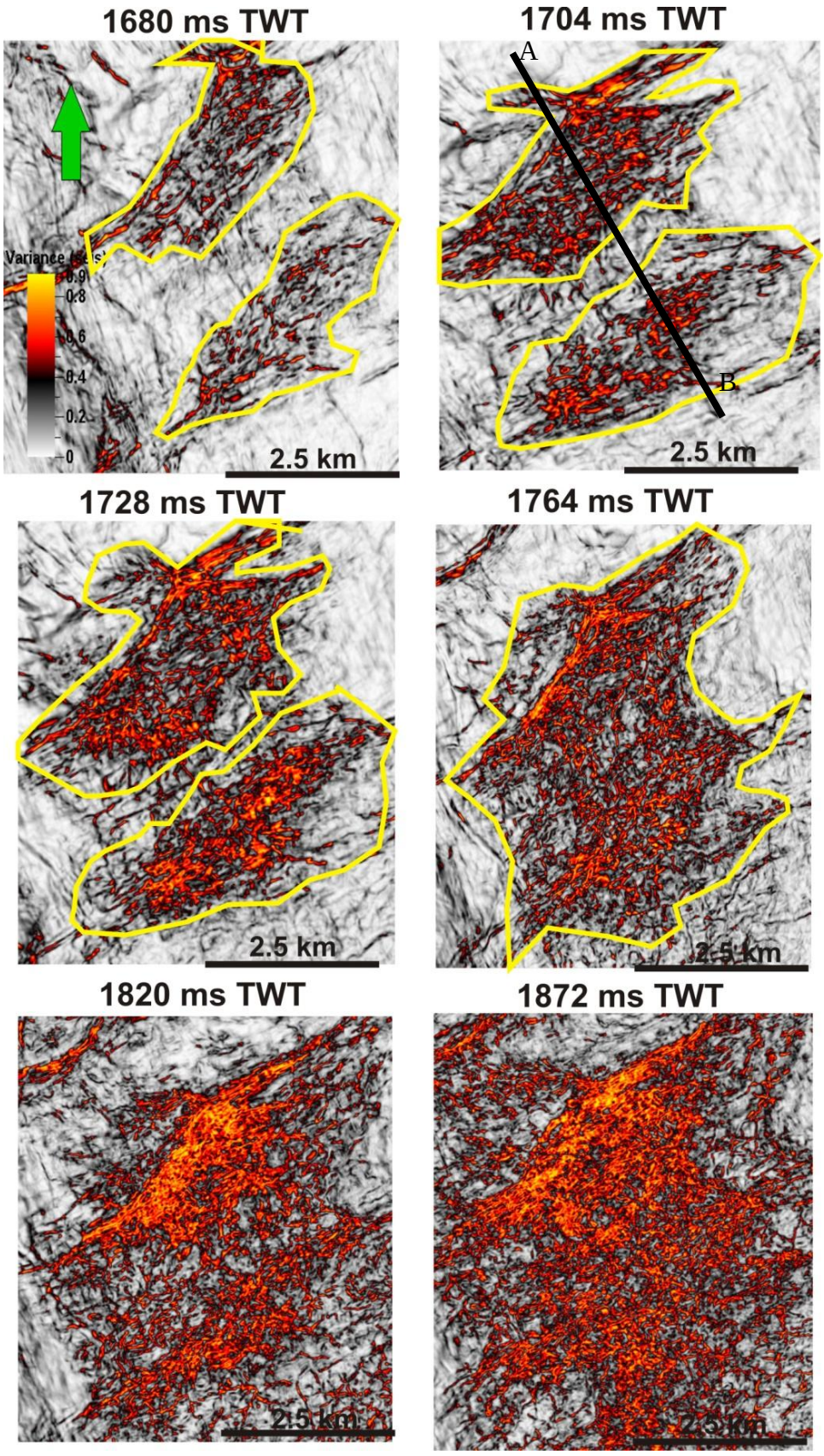


**Figure 4.12: The increases in area of chaotic reflection 1 and 2 with depth using time slices from the variance cube.**

Acoustic masking B3 occurs on the eastern flank of HHA in the Brygge Formation (Fig. 4.13). It shows a curvilinear appearance and EW orientation on variance time slice at 1628ms TWT (Fig. 4.13a). The zone of acoustic masking B3 can be followed from 2430ms TWT to ~1608 ms TWT where the high amplitude anomaly 3 with reverse polarity creates its upper termination (Fig. 4.13). Beneath the high amplitude anomaly 3 polygonal faults may be identified on seismic at 1630ms-1750ms TWT (Fig. 4.13).

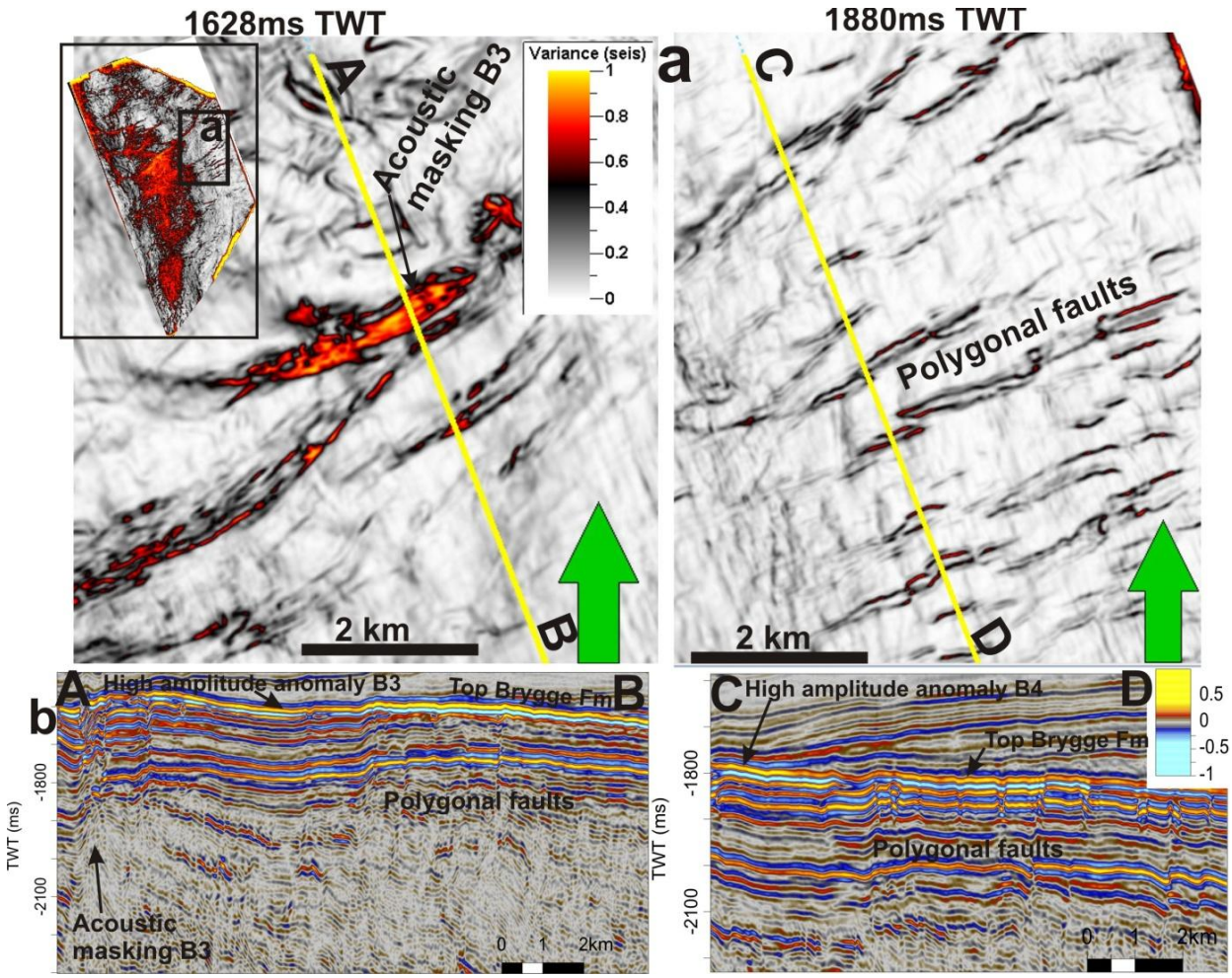


**Figure 4.13: a) Variance time slice at 1880ms shows polygonal faults and time slice at 1628 represents gas leakage routes 3. b) Seismic profile CD may indicate polygonal faults.**

A network of faults that may relate to polygonal faults is observed on the eastern flank of HHA in the Brygge Formation (Fig. 4.14). The anticipated polygonal faults show a linear to curvilinear geometry and an EW orientation on variance time slice at 1880ms TWT in figures 4.13 and 4.14. These concentrate on the seismic section between 1744ms-2150ms TWT (Fig. 4.14). High amplitude anomaly B4 with reverse polarity, interpreted as bright spot occur at ~1754ms TWT right above polygonal faults (Fig. 4.7). Polygonal faults exist beneath the

bright spot. The polygonal faults act as vertical fluid migration routes and are interpreted as leaking fault systems on the eastern flank of HHA in the Brygge Formation (Figs. 4.13 and 4.14).

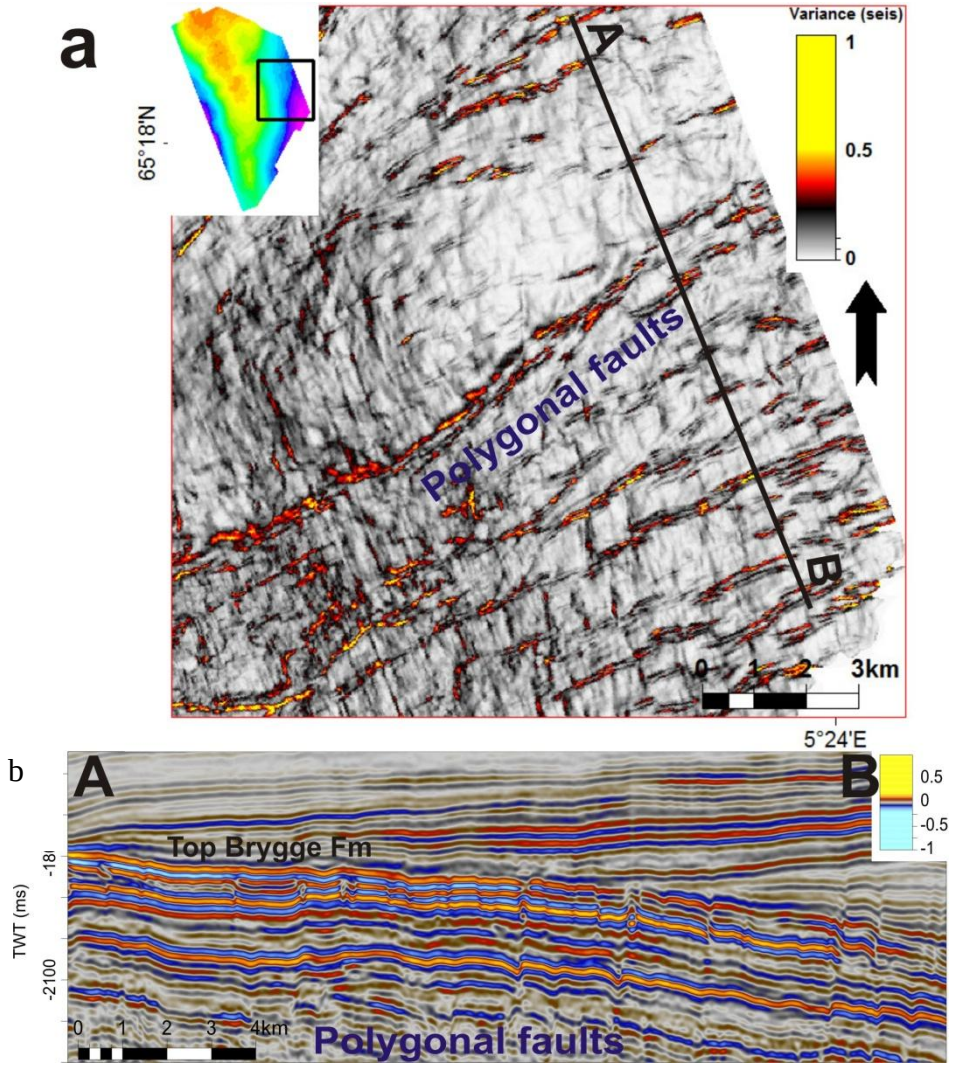


**Figure 4.14: a) Variance map 50ms below the top Brygge Formation shows the extension of faults. b) Seismic profile inline 1274 may indicate polygonal faults.**

Acoustic masking 5 is identified on the seismic section and occurs along the eastern flank of HHA in the Brygge Formation (Fig. 4.15). The chaotic area increases with depth. It shows a significant vertical extent and terminates at ~1690ms TWT at high amplitude anomaly 5, which shows a reverse polarity relative to the sea floor. Acoustic masking area 5 shows a low coherency of irregular shape on variance time slice at 2000ms TWT (Fig. 4.15). Polygonal faults may be observed between 1741ms-2078ms TWT (Fig. 4.15). There are two vertical dim zones at ~2000ms TWT and 2290ms TWT. The acoustic masking zone 5 with a bright spot at

its top and chaotic reflections and polygonal faults and dim amplitude anomalies beneath it suggests vertical fluid migration and accumulation along the eastern flank of HHA) at the top of Brygge Formation (Fig. 4.15).

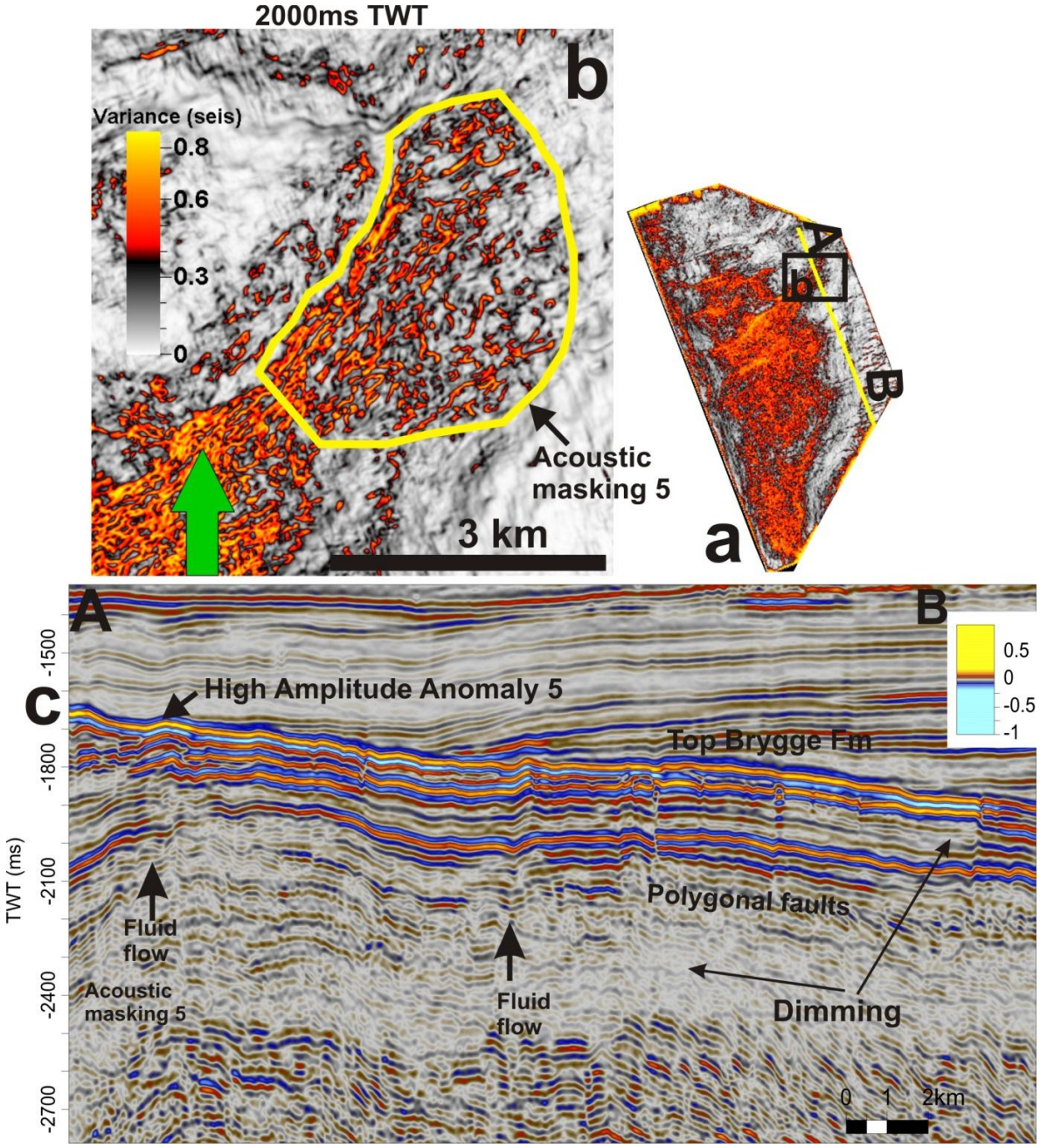


**Figure 4.15: a) Variance cube at time slice 2000ms TWT showing the location of acoustic masking zone 5 and the location of a seismic section. b) Zoomed part of the acoustic masking zone 5 at 2000ms TWT time slice of variance cube. c) Seismic section crossing acoustic masking zone 5 shows chaotic reflections and vertical dim zone.**

At the northern and northwestern part of the 3D cube seven curvilinear acoustic masking zones are identified. The acoustic masking zones are narrow and mapped out 50 ms below the top of Brygge Formation on the variance map (Fig. 4.16). The acoustic masking zones are partly interconnected with each other.

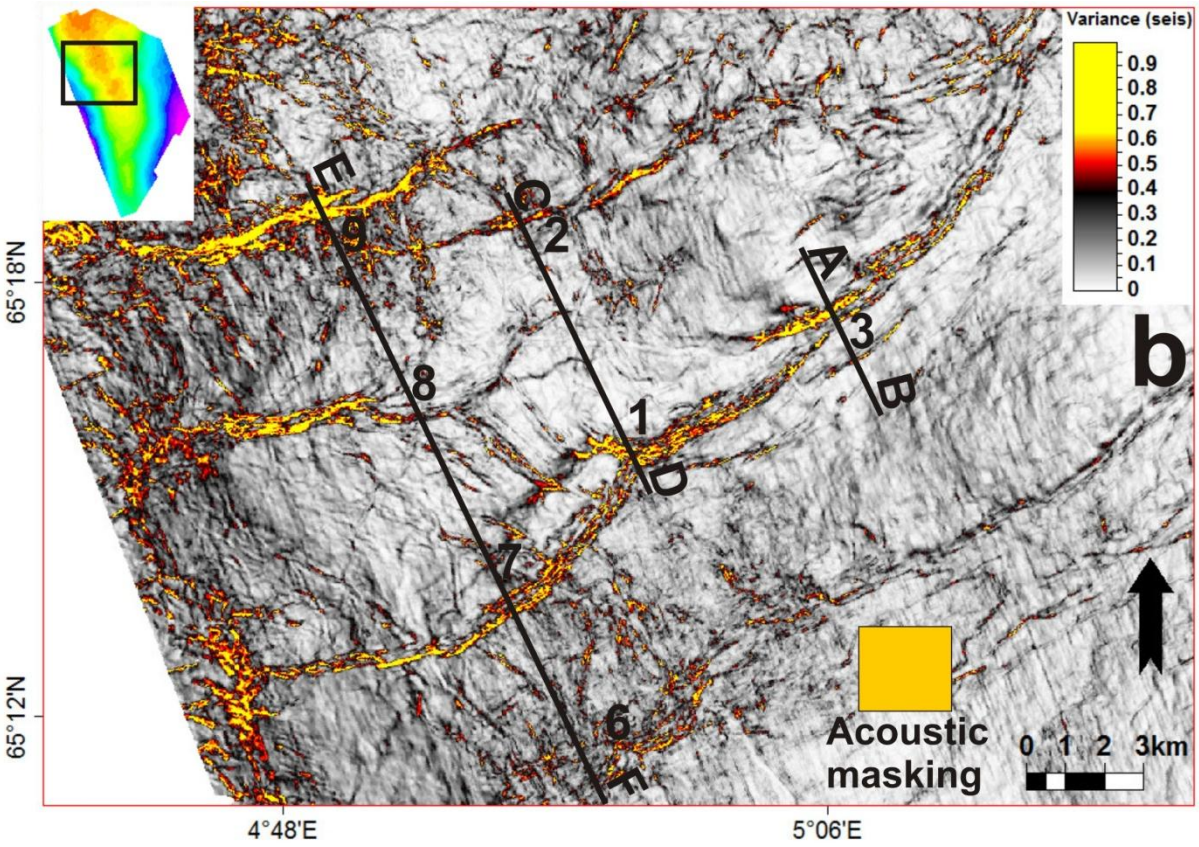


**Figure 4.16: Variance map 50ms below top Brygge Formation shows prominent crescent shape acoustic masking zones. The location of seismic sections is indicated and the sections are shown in Fig.4.17 and 4.18.**

The seismic profile AB and CD shown in figure 4.17 illustrates the prominent acoustic masking zone B1, B2 and B3. These acoustic masking zones can be recognized on seismic profile by their deteriorated and distorted seismic signal of low trace to trace coherency. Possible low velocity anomalies such as velocity sags (push-down) and dim zones are also associated with acoustic masking zones (Fig. 17). High amplitude anomalies with reverse polarity are seated above the upper termination of these acoustic masking zones.

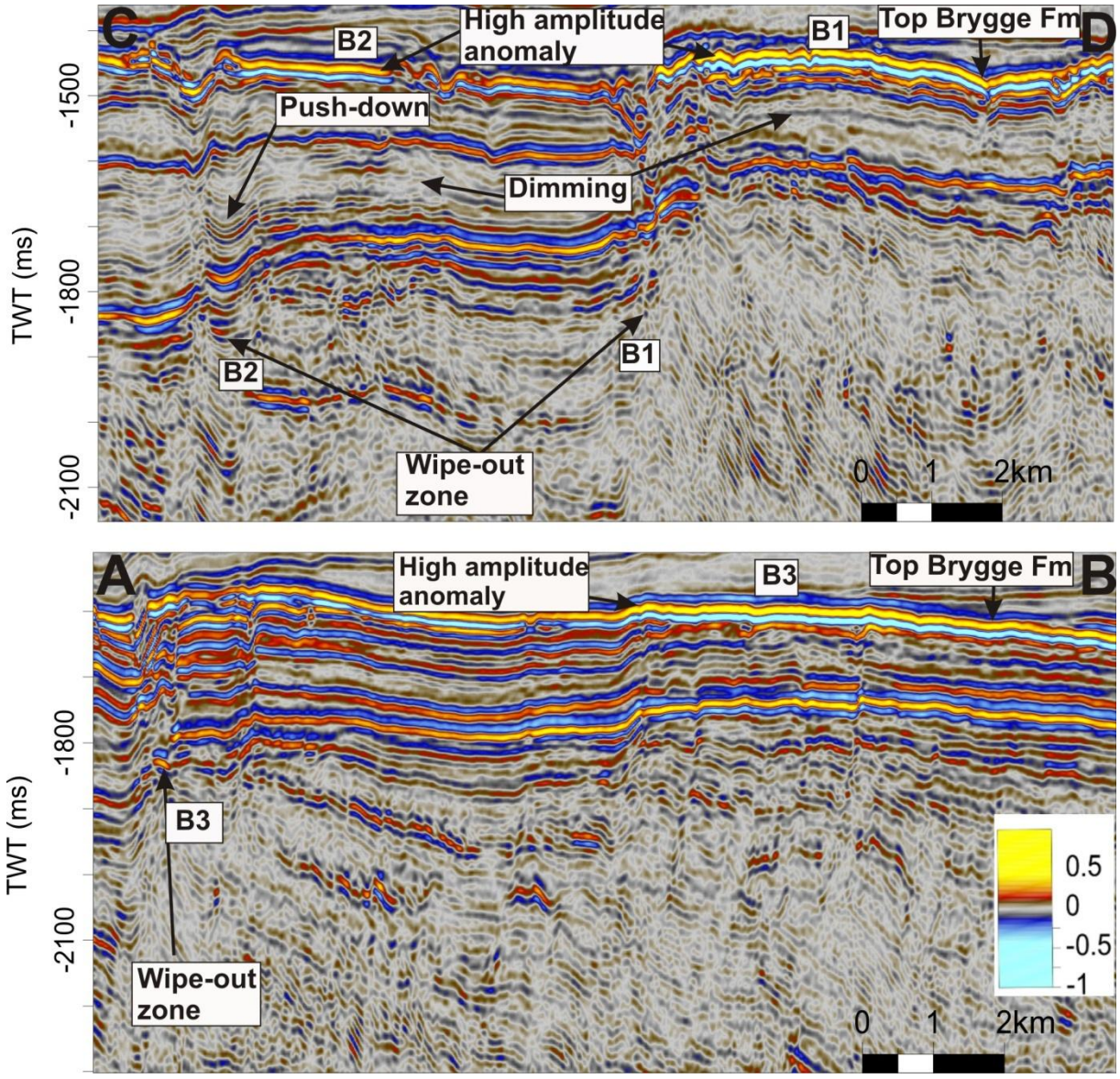


**Figure 4.17: Seismic profiles AB and CD show the high amplitude anomaly. For location see figure 4.16.**

Acoustic masking zones 6-9 are visible on the variance map in figure 4.16 and on seismic profile inline 441 in Figure 4.18. These acoustic masking zones are identified as major fault related vertical wipe-out zones of deteriorated seismic reflection where primary reflections are absent or very weak. Bright spots encountered in form of high amplitude anomalies occur at the upper termination of acoustic masking zones 6-9 (Figs. 4.16 and 4.18).

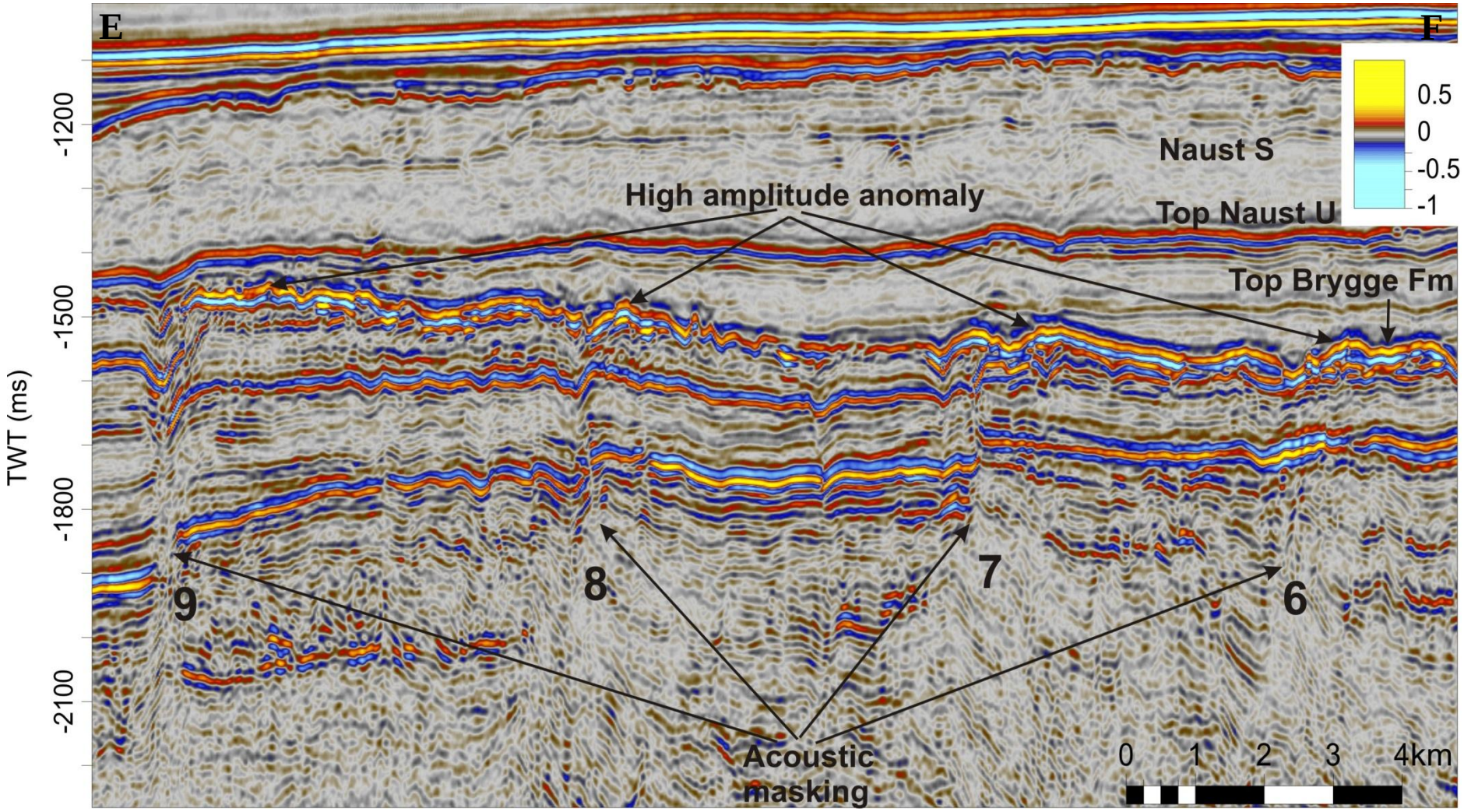


**Figure 4.18: Seismic profile EF shows high amplitudes anomalies and acoustic masking zones beneath it. For location see figure 4.16.**

## 4.3 Seismic evidence for variation in Pliocene-Pleistocene sediment thickness at HHA

Plio-Pleistocene formations show a progradation from east to west forming an onlap pattern on the flanks of the Helland Hansen Arch. The Plio-Pleistocene sediments completely buried the HHA (Fig. 4.19). The variation in thickness is significant from the eastern to the western flank of the arch (Fig. 4.19). The maximum thickness of the Plio-Pleistocene sediment accumulation exists at the eastern flank of HHA while the minimum thickness exists at the NW (Fig. 4.19).

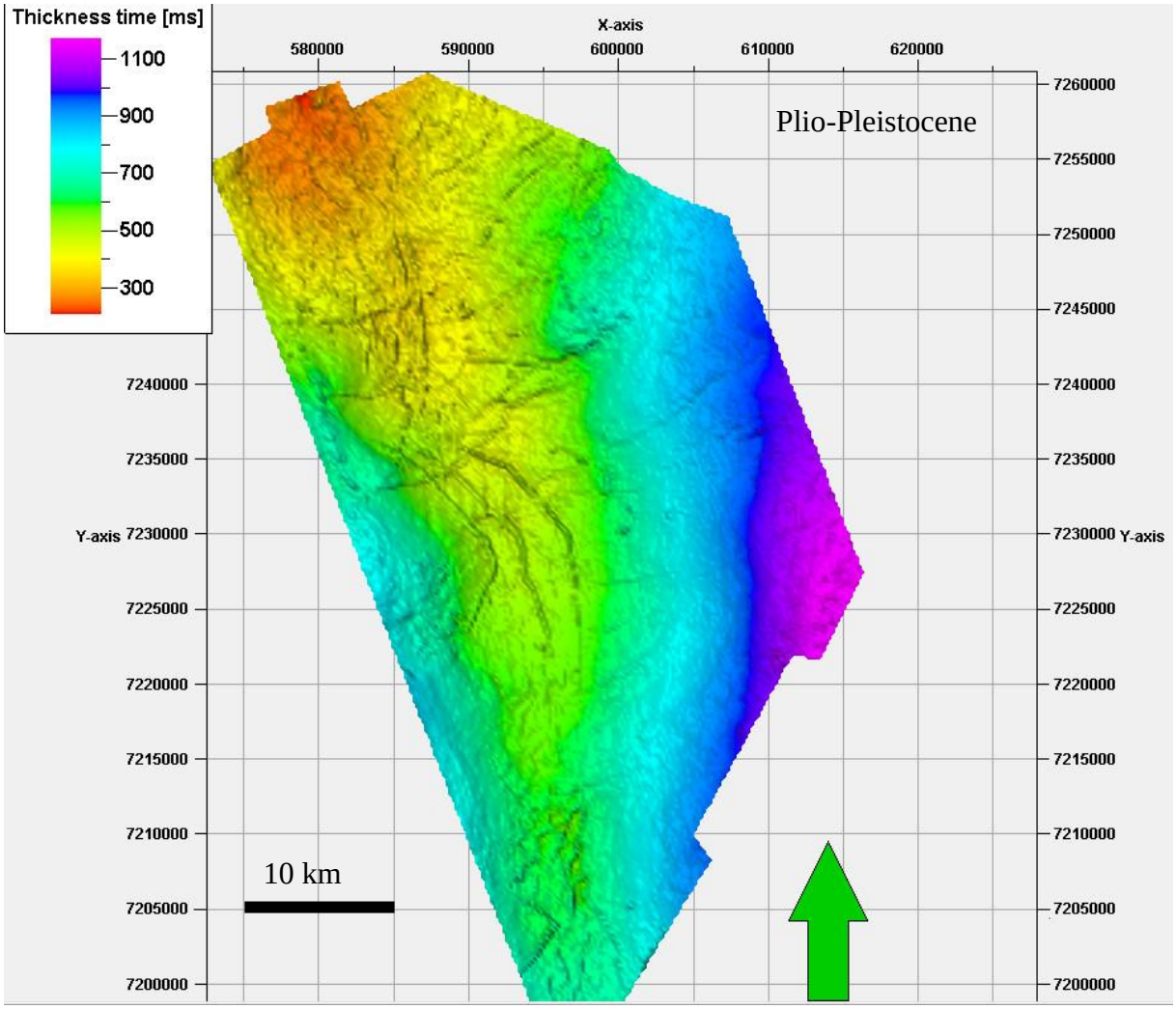


**Figure 4.19: Thickness map of whole Plio-Pleistocene sequence.**

### 4.3.1 Seismic amplitude anomalies in Naust N

Naust N is a westerly prograding wedge forming sequence onlap structures only along the eastern flank of Helland Hansen Arch (HHA) in southeastern part of the survey (Fig. 4.1). Its thickness decreases both northward and southward (Fig. 4.20). It is characterized by high amplitudes at its top and mostly transparent reflection pattern within it (Fig. 4.21).

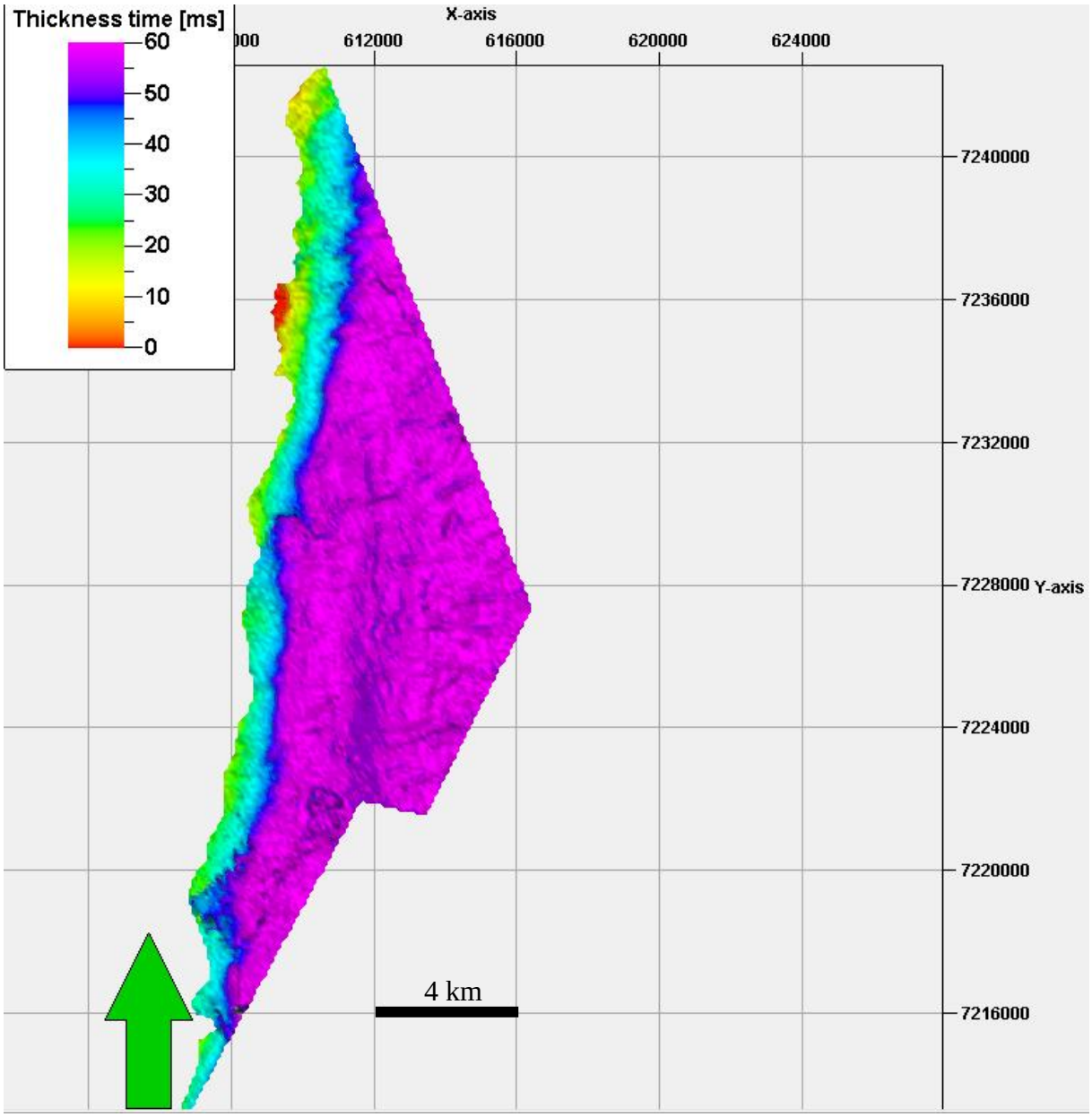


**Figure 4.20: Thickness map of Naust N unit.**

High amplitude anomaly N1 occurs close to the eastern flank of HHA at ~1767ms TWT on seismic profile inline 1375 (Fig. 4.21). High amplitude anomaly N1 shows a reverse polarity relative to the sea floor reflection (Fig. 4.21 a, c). There is a vertical dim zone beneath the high amplitude anomaly N1 (Fig.4.21c). A series of possible polygonal faults are identified beneath N1 on seismic profile IL 1375 as line-ups of reflection discontinuities (Fig. 4.21). The polygonal faults may act as vertical fluid migration routes for gas accumulation at the top of Naust N.

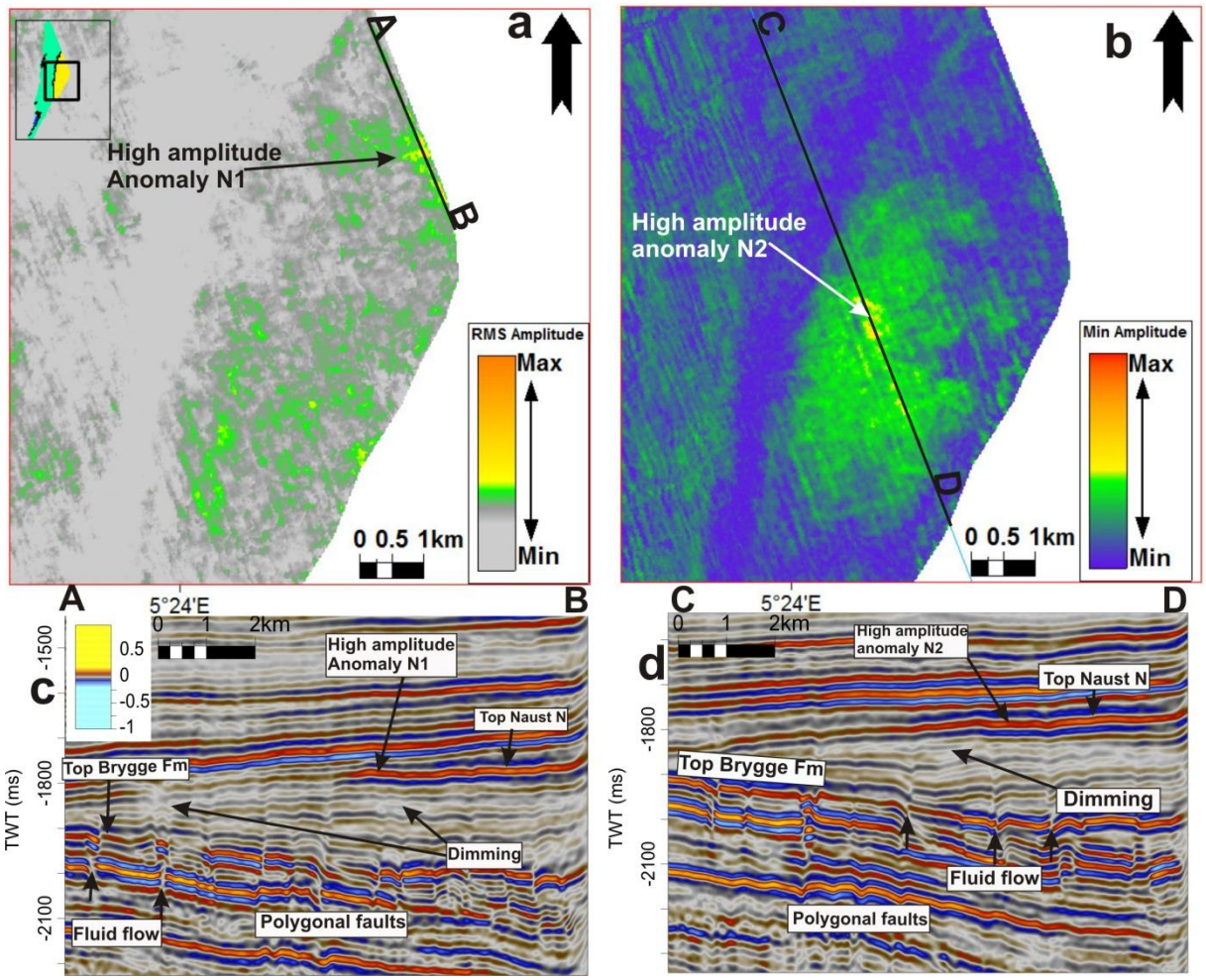


**Figure 4.21: a) RMS amplitude map 30ms below the top of Naust N shows high amplitude anomaly N1 with the location of seismic profile AB. b) Minimum amplitude map shows the extension of high amplitude anomaly N2 with the location of seismic profile CD. c) Seismic profile AB. d) Seismic profile CD.**

High amplitude anomaly N2 is identified in the southeastern part of the survey at the top Naust N unit (Fig. 4.21 b, d). It shows a reverse polarity relative to the seafloor (Fig. 4.21 b and d). A dim zone is identified at ~1850ms TWT. Polygonal faults appear to provide the vertical fluid migration pathways (Fig. 4.21d).

The polygonal faults extensively developed along the eastern flank of the HHA as shown in figures 4.13 and 4.14. They terminate in Naust N. The polygonal faults show the linear to curvilinear E-W extension on the variance map of top Naust N unit shown in figure 4.22.

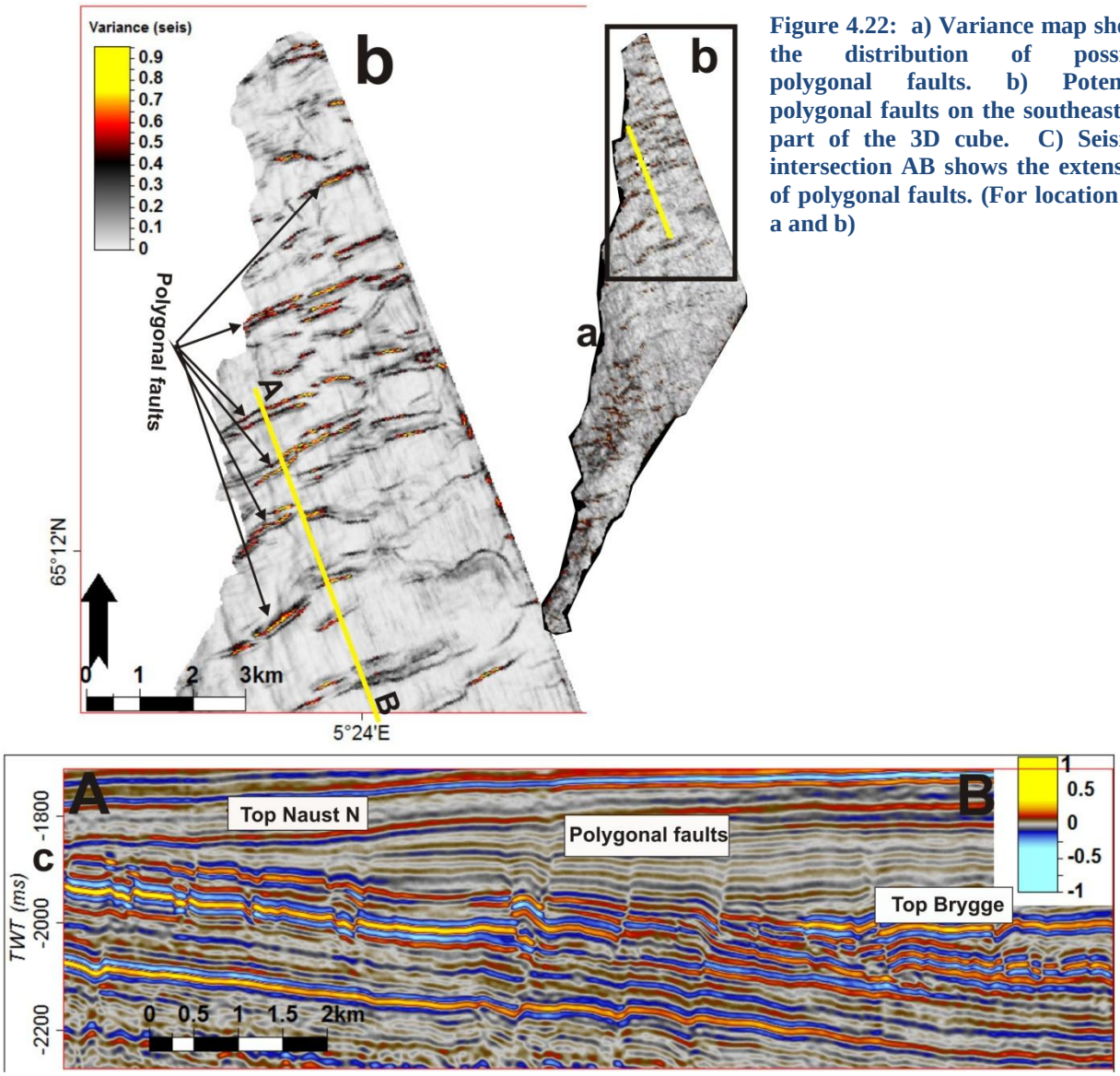


**Figure 4.22: a) Variance map shows the distribution of possible polygonal faults. b) Potential polygonal faults on the southeastern part of the 3D cube. C) Seismic intersection AB shows the extension of polygonal faults. (For location see a and b)**

### 4.3.2 Seismic Amplitude anomalies in Naust A

Naust A is also forming the onlapping and progradational wedges on the flanks of HHA but only in the southern part of the survey.

High amplitude anomalies are observed on the RMS map of Naust A unit in southeastern part at the top of Naust A right above the crest and eastern flank of HHA (Fig. 4.23). The high amplitudes anomalies are distributed over a large area.

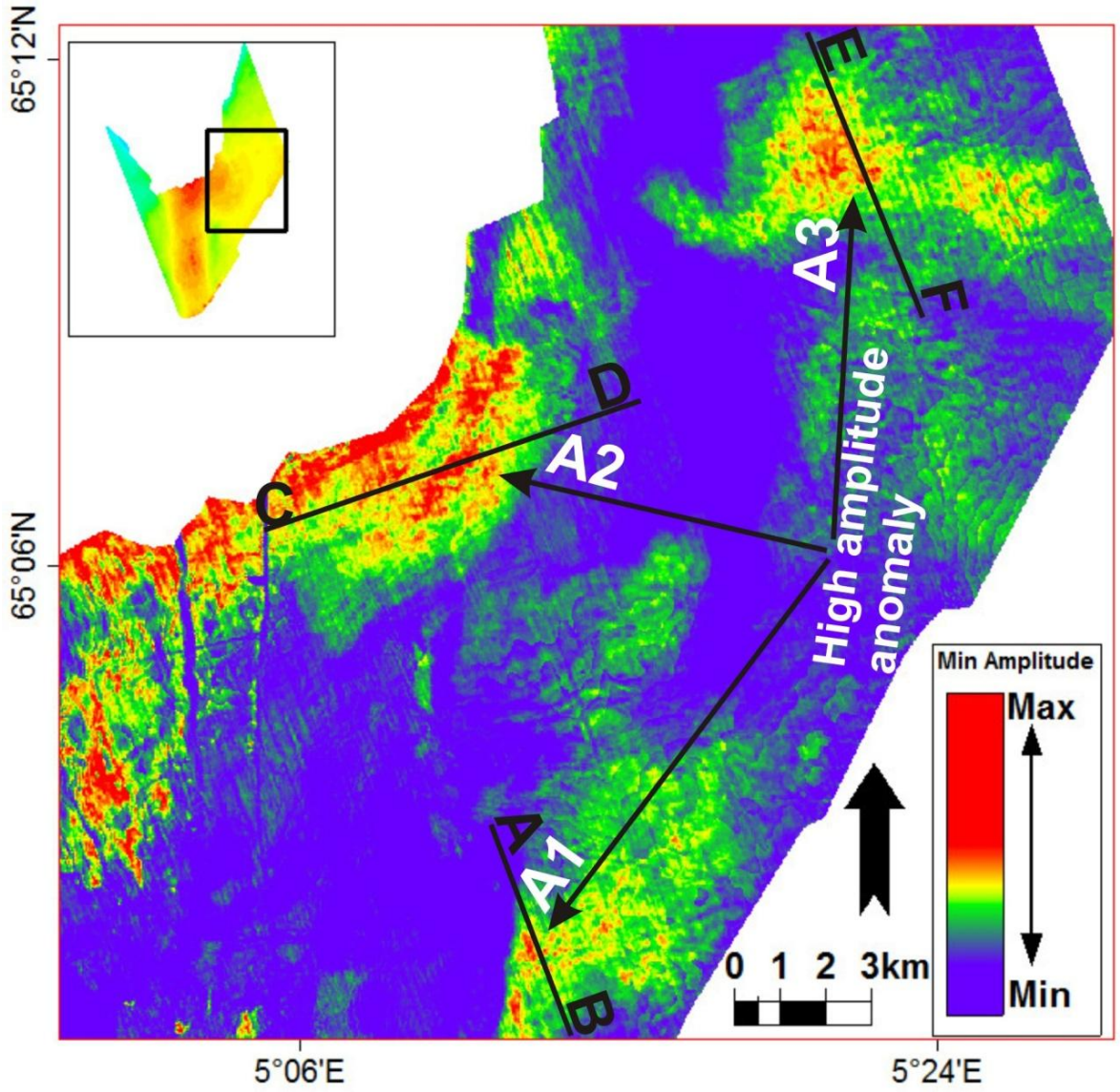


**Figure 4.23: RMS amplitude map from below 30ms of top Naust A. Black lines indicate the location of seismic sections.**

High amplitude anomaly A1 is found on the southern part of the survey close to the crest of HHA and at the progradational wedge at ~1552ms TWT on seismic profile inline 667 (Figs. 4.24a and 4.23). The high amplitude anomaly shows a reverse polarity relative to seabed. Beneath the high amplitude anomaly A1 polygonal faults terminate into sub-vertical and distorted line-up of discontinuous reflections. They may indicate acoustic pipes. They are starting at ~2089ms TWT and terminate at ~1665ms TWT at the base of the high amplitude anomaly A1 (Fig. 4.24a). High amplitude anomaly A2 occurs close to the crest of HHA (Fig. 4.23. It is part of the onlap formation of the progradational wedge at at ~1555ms TWT on the

seismic section cross line 2135 (Figs.4.24b & 4.23). It shows a reversed polarity relative to the seabed. .

High amplitude anomaly A3 is observed at the top Naust A unit above the eastern flank of HHA with a reversed polarity at ~1604ms TWT on seismic section inline 1181 (Figs. 4.24c & 4.23). Directly below the high amplitude A3 there are indications of the existence of polygonal faults, which terminate into sub-vertical, narrow zones of disrupted seismic reflection, known as acoustic pipes. The root area of the pipes is ~2105ms TWT and their upper termination ~1600msTWT at the base of potentially gas charged sediments (Fig. 4.24).

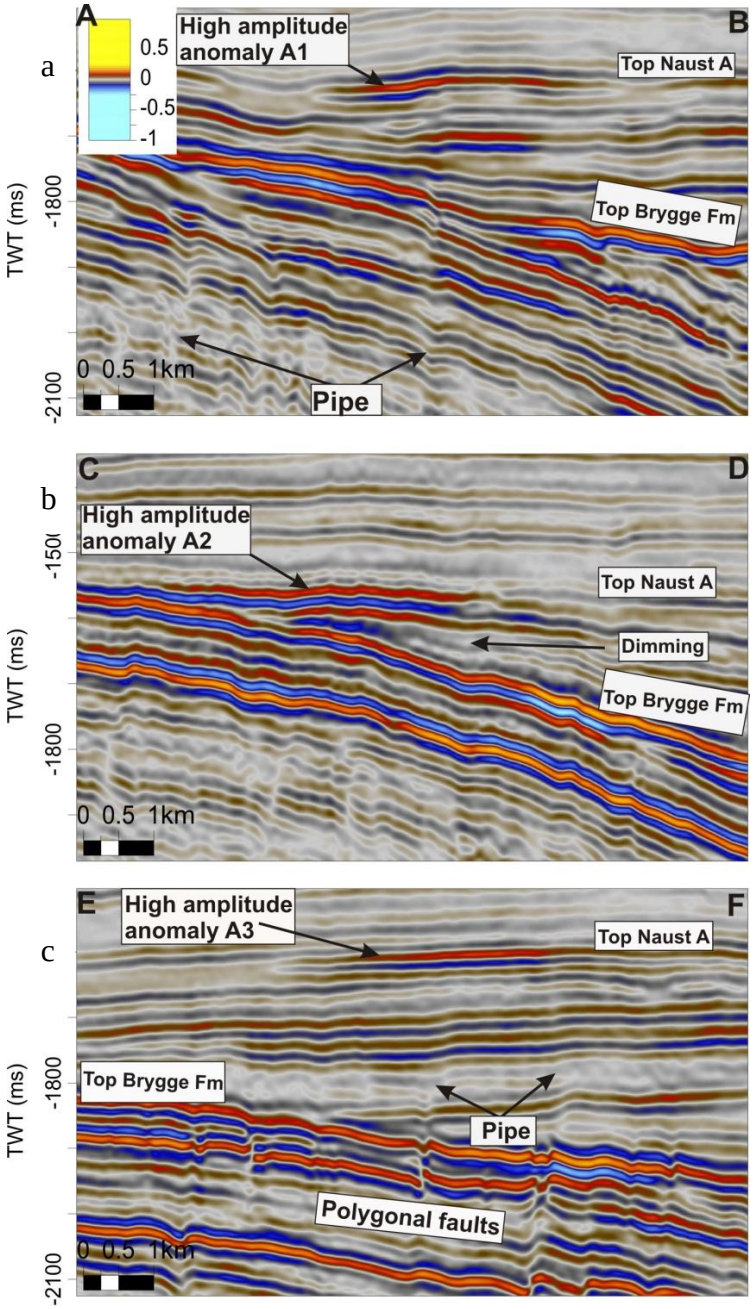


**Figure 4.24: Seismic cross-sections show the high amplitude anomalies and their related fluid flow pathways. (For location see figure 4.23)**

In the SW part of the survey and above the western flank of HHA a high amplitude anomaly A4 shows a reversed polarity relative to sea floor at 1646ms-1695ms TWT on inline 163 (Fig. 4.25a and b). The high amplitude anomaly A4 shows a large lateral extent (Figs. 4.25a and b). Corresponding polygonal faults in the Brygge Formation beneath are observed. Sub-vertical, narrow zones of disrupted and discontinuous seismic reflections are identified in the Brygge Formation just adjacent to the high amplitude anomaly A4.

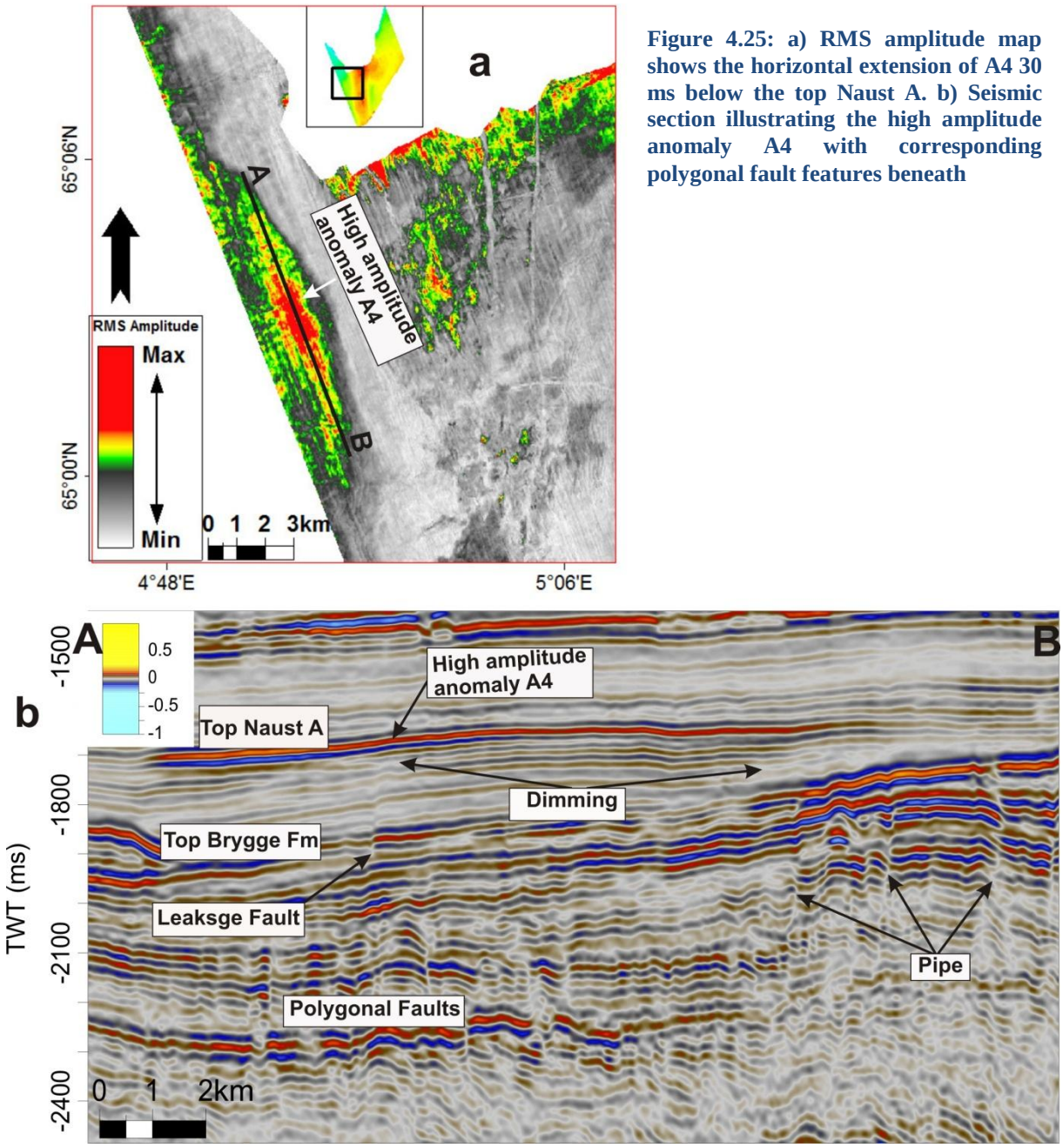


**Figure 4.25: a) RMS amplitude map shows the horizontal extension of A4 30 ms below the top Naust A. b) Seismic section illustrating the high amplitude anomaly A4 with corresponding polygonal fault features beneath**

### 4.3.3 Seismic amplitude anomalies in Naust U

The westward prograding Naust U unit shows high amplitude anomaly U1 in the southwestern part of the survey at ~1435ms TWT inline 279 (Fig. 4.26 a). High amplitude anomaly U1 shows a reverse polarity relative to the seabed. The RMS amplitude map shows a cluster of anomalies (Fig. 4.26 a). There are three zone of deteriorated and distorted seismic signals encountered along major faults beneath the high amplitude U1. The zones connect into the Brygge Formation and are interpreted as fluid migration pathways.

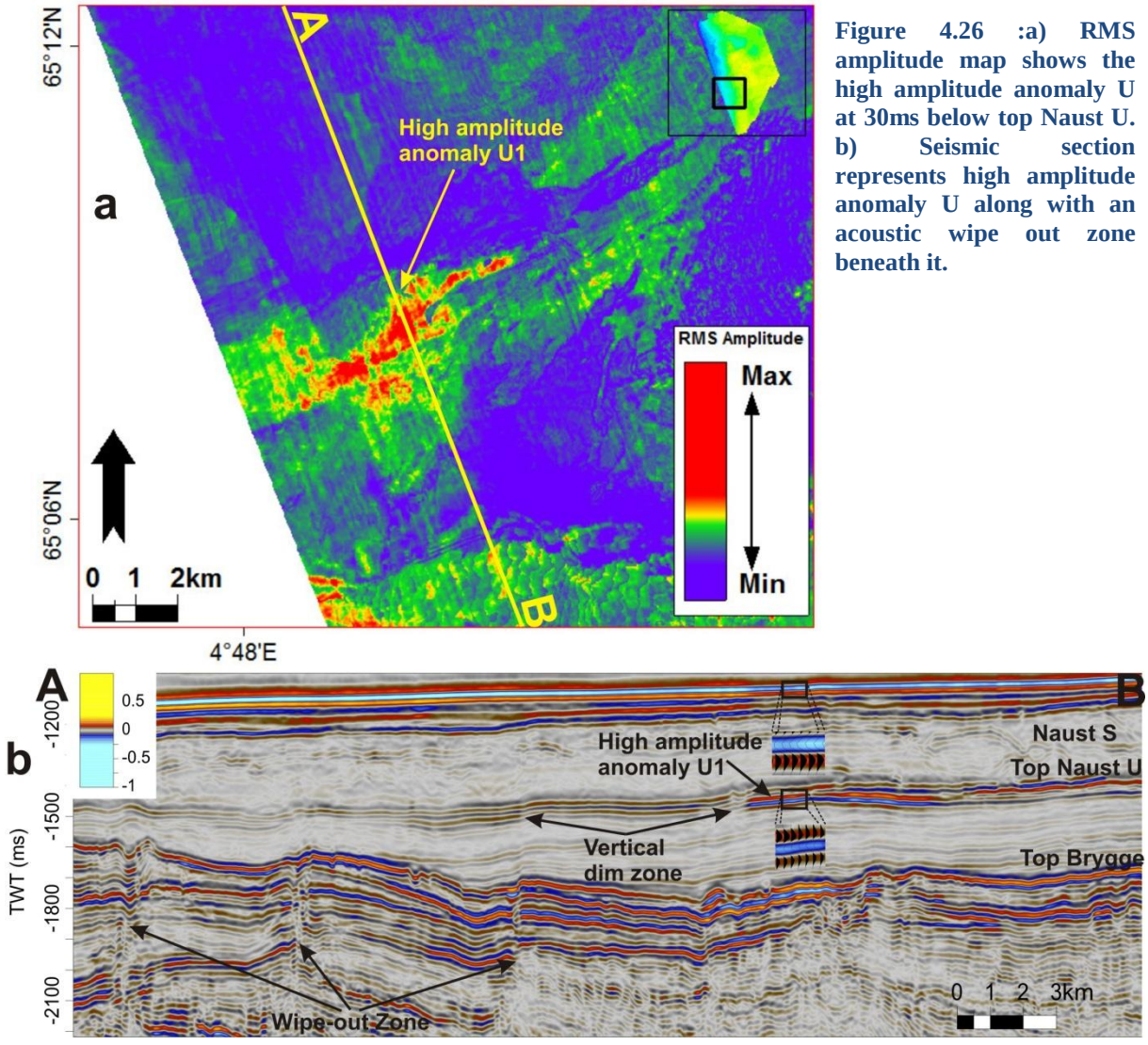


**Figure 4.26 :a) RMS amplitude map shows the high amplitude anomaly U at 30ms below top Naust U. b) Seismic section represents high amplitude anomaly U along with an acoustic wipe out zone beneath it.**

In the SW part of the 3D cube narrow sub-vertical zones of discontinuous reflections exists above the crest of the HHA. These zones may be the upper terminations of polygonal faults that developed in the Brygge Formation (Fig. 4.27).

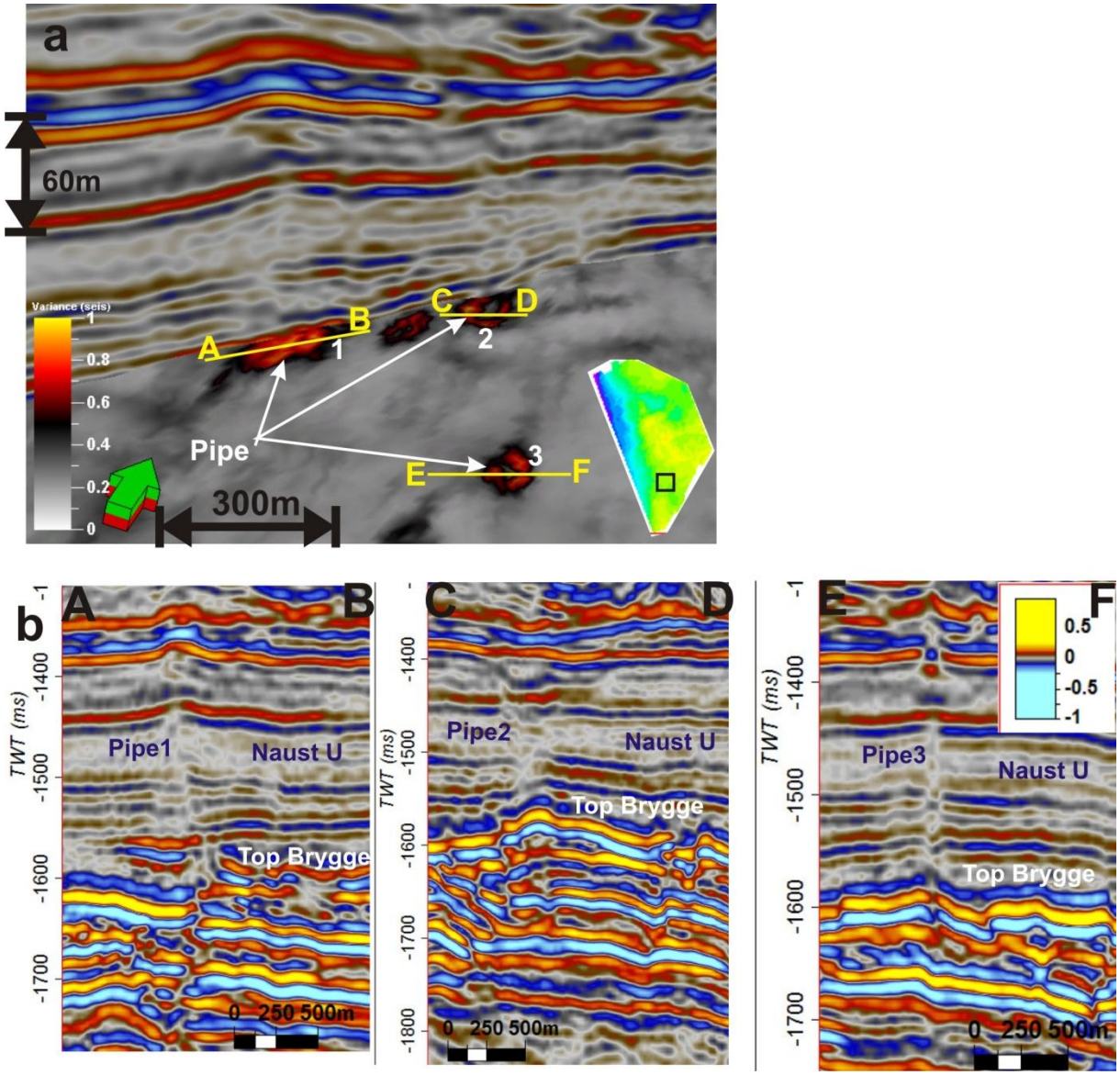


**Figure 4.27: a) 3D view of acoustic pipes in the variance map and in seismic sections. b) Seismic sections show the extension of pipes. (For location see Fig. 4.27 a).**

### 4.4.4 Seismic Character of Naust S

The seismic character of Naust S unit differs from the units beneath it in that, it shows very irregular configurations of reflectors (Fig.4.1). At the top of Naust S unit curvilinear features, grooves and depression that correspond to former iceberg plough marks and glacigenic debris flow deposits (Ottesen et al., 2005). Naust S unit shows the maximum thickness in the eastern part of the 3D cube with decreasing thickness towards West, NW and SW part of the survey where the Helland Hansen Arch (HHA) becomes narrow (Fig. 4.28).

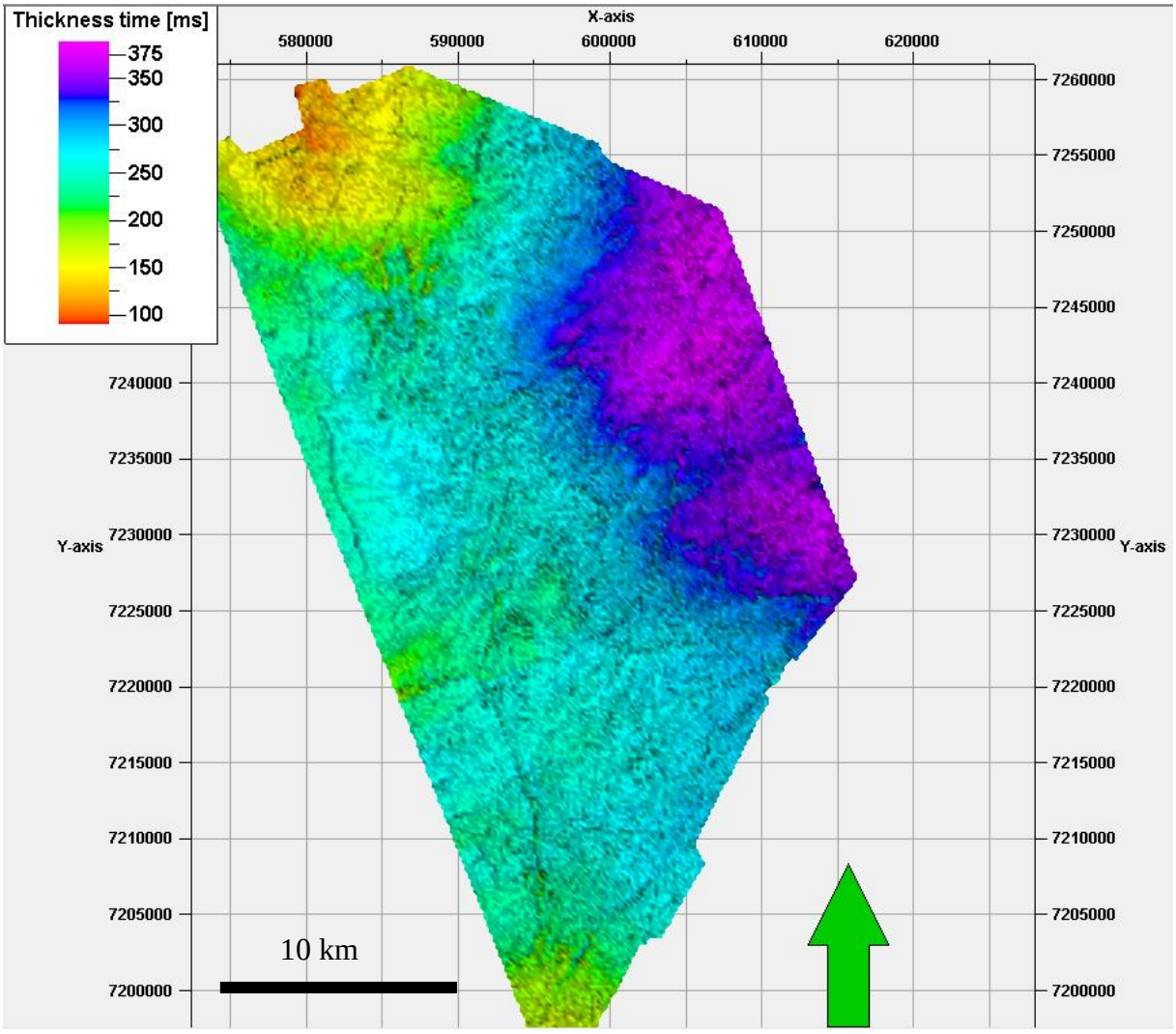


**Figure 4.28: Thickness map of Naust S unit.**

The base of Naust S shows internally chaotic and disturbed seismic reflections in the SE part of the 3D cube. The chaotic unit appears like an oblate form on variance maps of base Naust S. The feature is about 22 km long and 1l km wide (Figs. 4.29 – 4.30). On the variance map the chaotic unit forms elongated curved lineations which are interpreted as arcuate pressure ridges (Figs. 4.29 and 4.30). (Nygård). The arcuate pressures ridges may indicate a submarine slide (Gay & Berndt, 2007). Thus, Naust S may have been exposed to submarine slide activity.

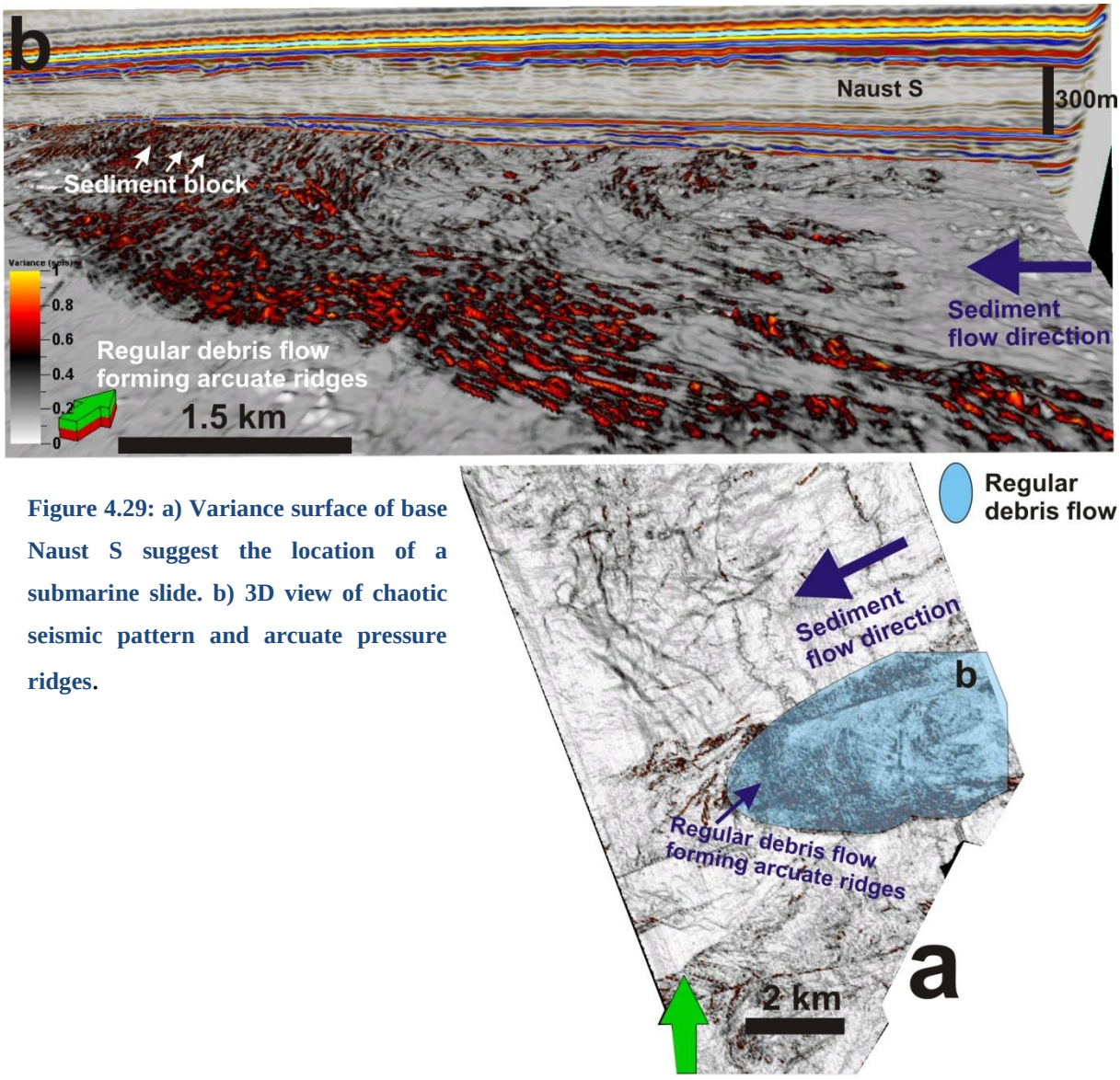


**Figure 4.29: a) Variance surface of base Naust S suggest the location of a submarine slide. b) 3D view of chaotic seismic pattern and arcuate pressure ridges.**

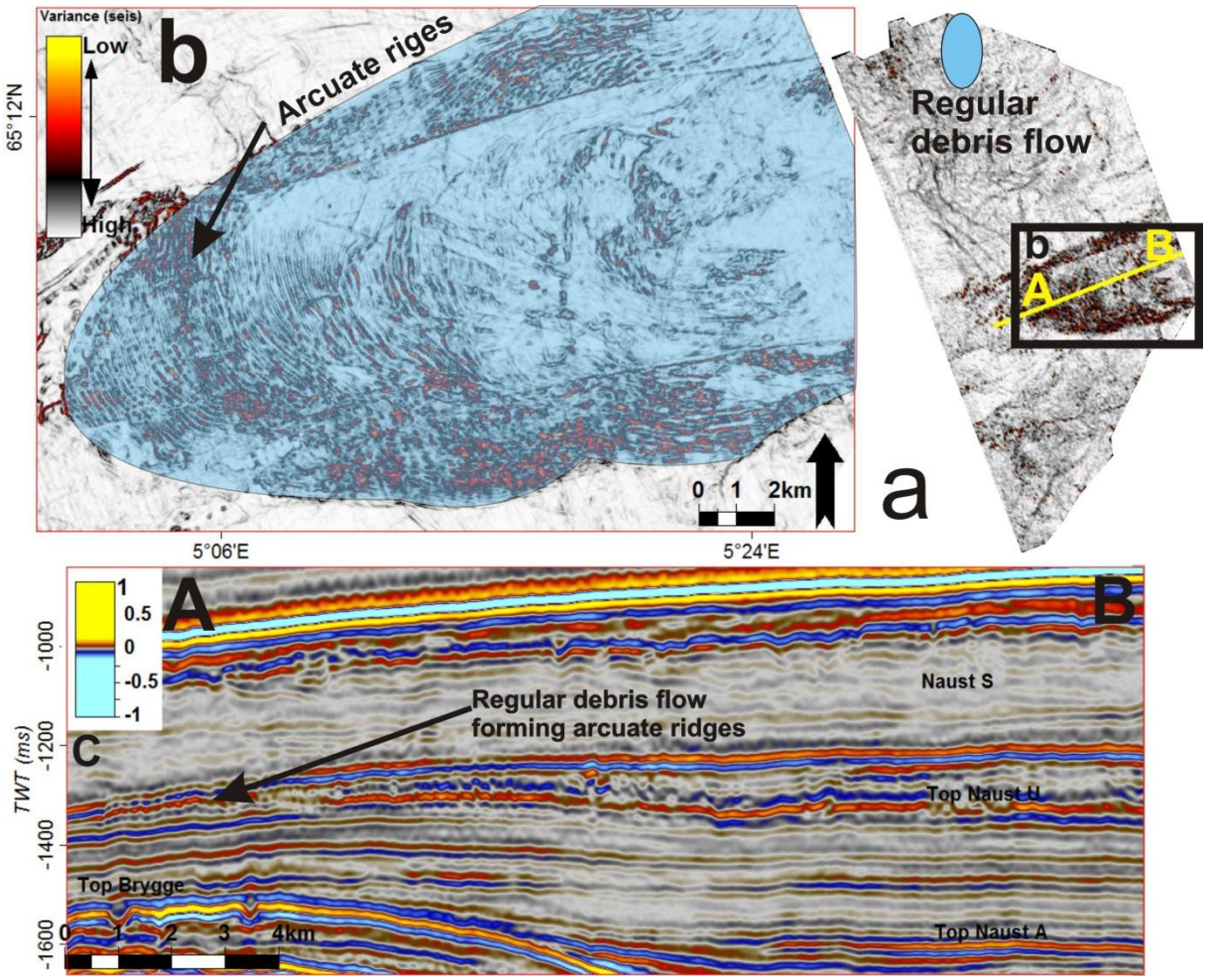


**Figure 4.30: a) Variance surface map showing the location of debris flow deposits and the seismic section. b) Debris flow deposit forming the arcuate pressure ridges. c) Seismic section shows the extension of debris flow deposits in the form of chaotic reflection pattern.**

High amplitudes anomalies S1-S5 are identified in Naust S unit in the SW part of the survey (Fig. 4.31). These high amplitude anomalies are clearly visible on the RMS amplitude map (Figs. 4.31 and 4.32). The high amplitude anomalies may be the result of lithological changes though fluids may also cause the seismic anomalies.

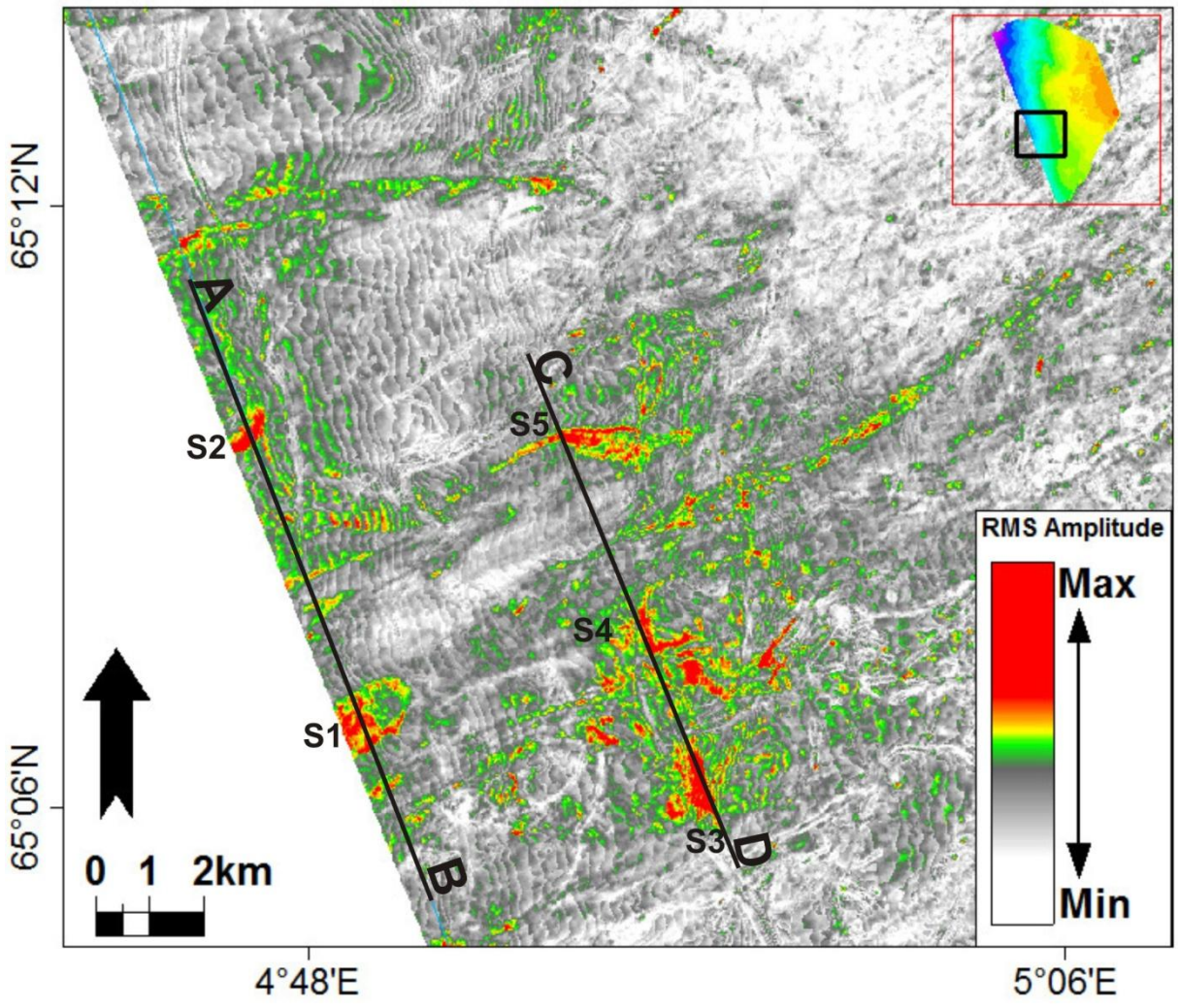


**Figure 4.31: RMS amplitude map of Naust S unit showing high amplitude anomalies up to 100 ms TWT from its top.**

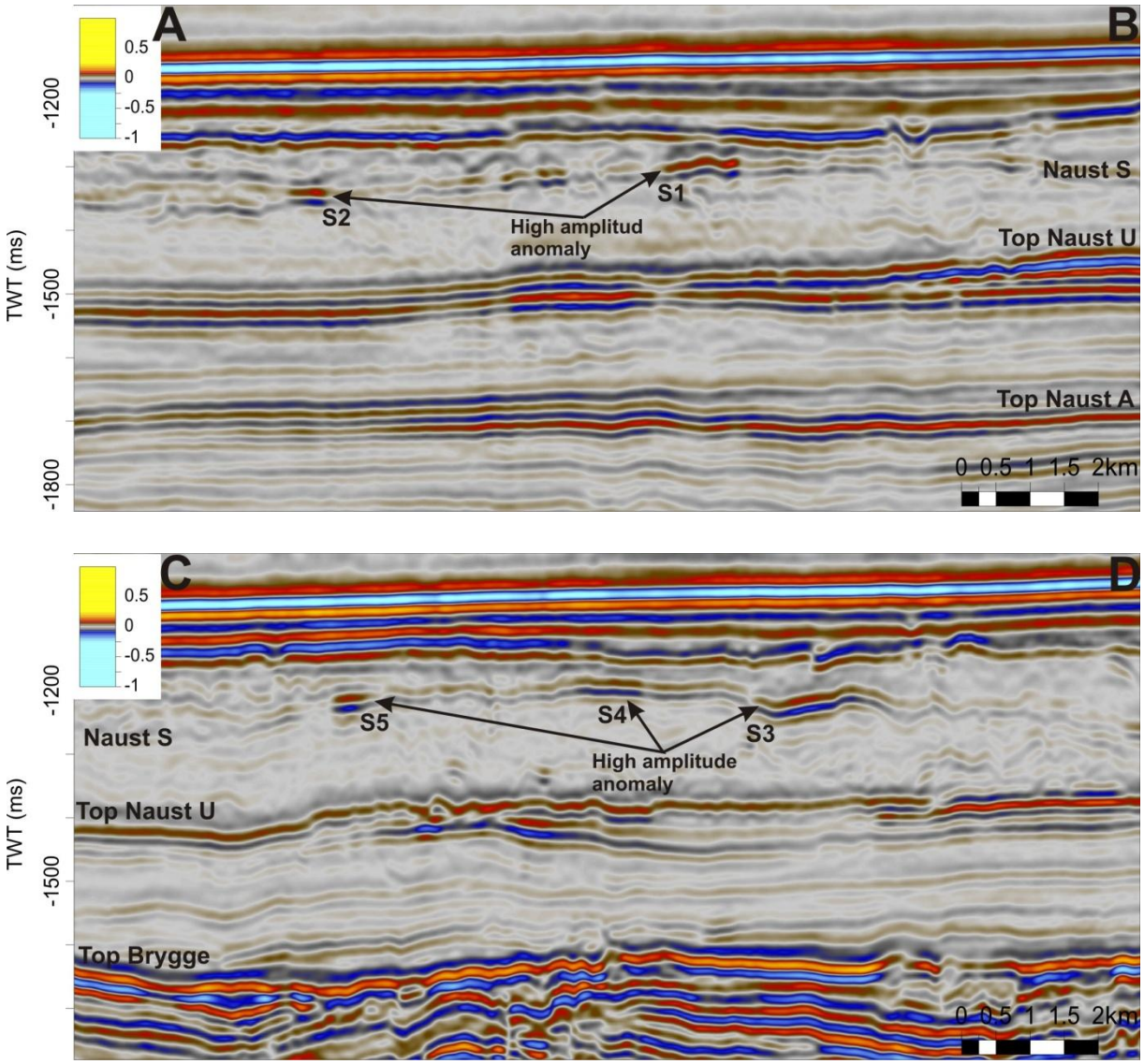


**Figure 4.32: Seismic profiles AB and CD shows the extension of high amplitude anomalies S1-S5. (For location see figure 4.33).**

# 5. Discussion

The discussion chapter concentrates on gas migration and accumulation processes in Brygge, Naust N, A and U formations. It describes the fluid migration mechanism, the geological process controlling the fluid migration, fluid release potential of polygonal faults and relationship between submarine slides and polygonal faults.

## 5.1 Hydrocarbon potential and trapping mechanism

Tertiary domes consist of reservoir rocks that have a potential for hydrocarbon accumulations where both tectonic and thermal subsidence have played a role in forming the hydrocarbon traps at the Helland Hansen Arch (e.g. Berg et al., 2005., Bryn et al., 2005).

Eocene-Oligocene clay-ooze dominated sediments of the Brygge Formation constitute the main sediments of the HHA (Fig.4.1, p. 40). The oozes provide a seal for vertical migrating gas and form a structural trap at the crest of HHA (Rokoengen et al., 1995., Stuevold et al., 2003., Hustoft et al., 2010).

## 5.2 Gas accumulation mechanism in Brygge Formation

High amplitudes anomalies are widely distributed at the top of Brygge Formation (Fig.4.6 a, p. 45). Some of the high amplitudes show a reverses polarity relative to the seabed suggesting gas accumulations (Fig.4.6-4.10, p. 45-50). Beneath the high amplitude anomalies fluid migration features appear as disturbed and distorted seismic zone and velocity sags (push down) beneath it suggests the accumulation of gas at the crest and along the eastern and western flanks of HHA (Figs. 4.6 and 4.7, p. 45-47). The vertical migrating gas is trapped by the impermeable ooze at the top of Brygge Formation (Figs. 5.1, 4.6 and 4.7, p. 45-47).

Beneath the bright spot at the crest of HHA the seismic energy is absorbed, which causes the depletion of higher frequencies (Fig. 5.1). This phenomenon is shown by a frequency analysis of seismic inline 691 (Fig.5.1). Area 2 shows an assumed gas free zone with a dominant frequency spectrum 27-45 Hz while area 1 indicates a loss of frequency with a dominant frequency spectrum 21-30Hz. The loss of higher frequency may suggest significant gas accumulation at the crest of HHA.

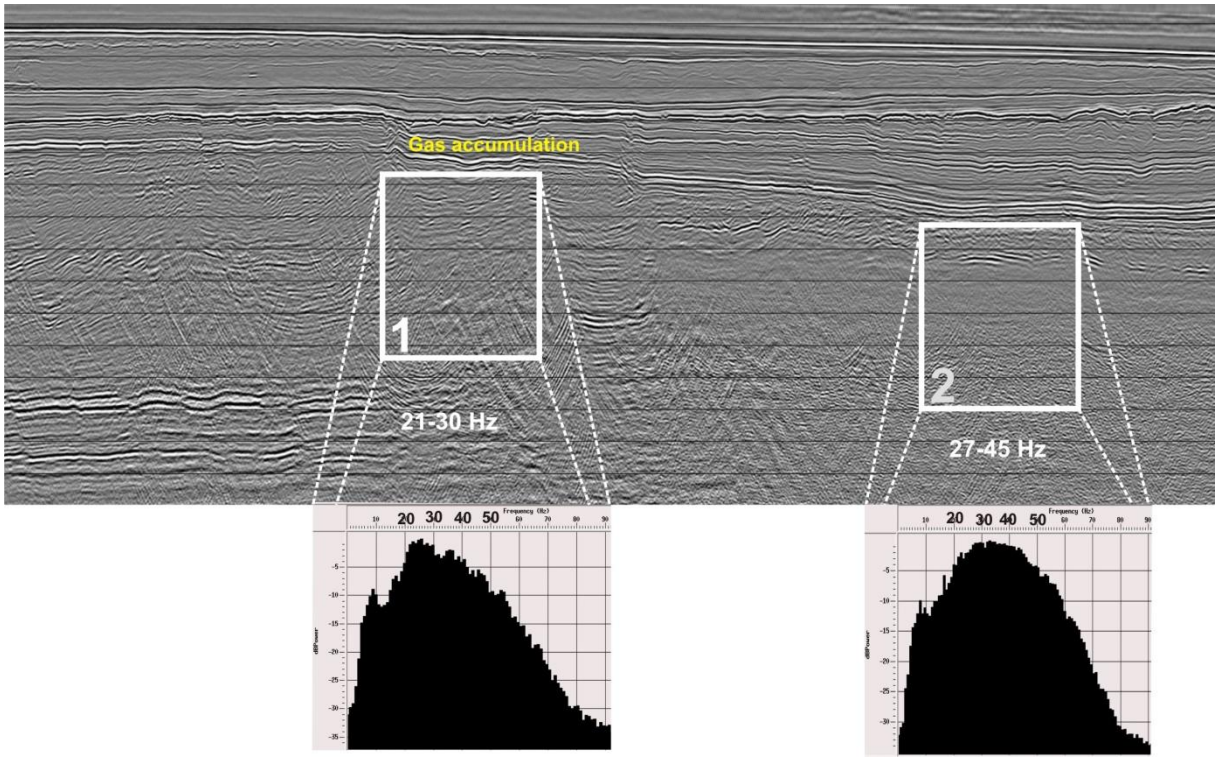


**Figure 5.1: Spectral analysis of inline 691. Area 2 shows the frequency spectrum 27-45Hz of gas free zone. Area 1 shows the loss of frequency where the spectrum lies at 21-30 Hz.**

Gas accumulation at the crest of HHA is also indicted by RMS maps distributed over a large area in the middle of the survey in which fluid migration features are shown by the low coherence values beneath gas accumulation areas (Fig 5.2, 4.6 and 4.11, p. 52). Along the eastern flanks of HHA gas accumulation zones are extensively disturbed by faulting where polygonal faults provide routes for gas migration and determine thus locations for gas accumulation (Fig. 4.7 and 4.8, p. 47-48). On the western flank of HHA gas accumulation occurs only in small patches with vertical fluid migration routes (Fig. 4.9, p. 49). At the northern part of the survey gas accumulated at shallower depth. Fluid migration features are connected to the gas accumulation area (Fig. 4.10, p. 50).

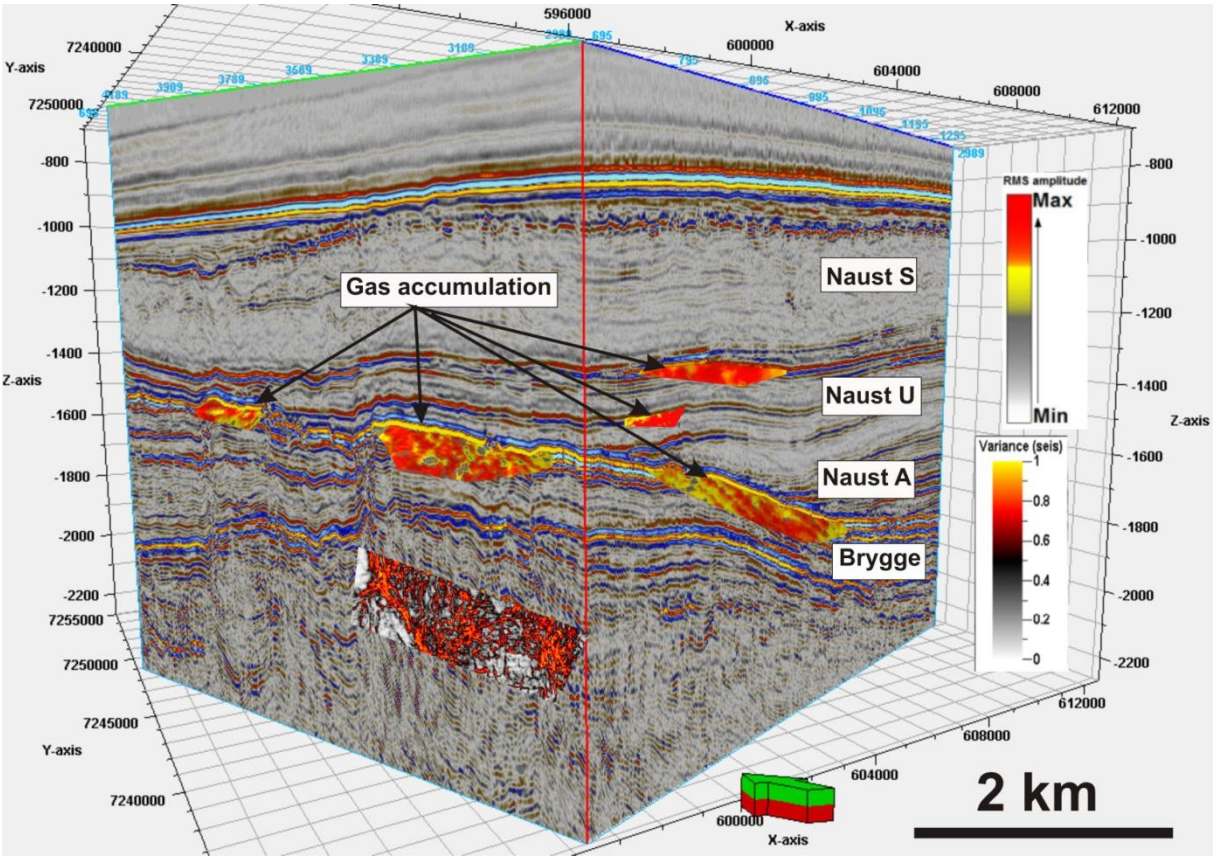


**Figure 5.2: 3D view of survey SH9602 shows the gas accumulation at the crest and along the eastern flank of HHA.**

## 5.3 Gas accumulation mechanism in Naust Formation

The top level of Naust N, A and U show high amplitude seismic reflections suggesting an increase in the concentration of free gas that mainly derives from Brygge Formation through acoustic pipes (Figs.4.21-4.26, p.62-67). The gas in these units distributes laterally. Below the high amplitude zones acoustic transparent zones exists which may be caused by the absorption and loss of seismic energy caused by the gassy sediments (Fig. 4.25, p. 66).

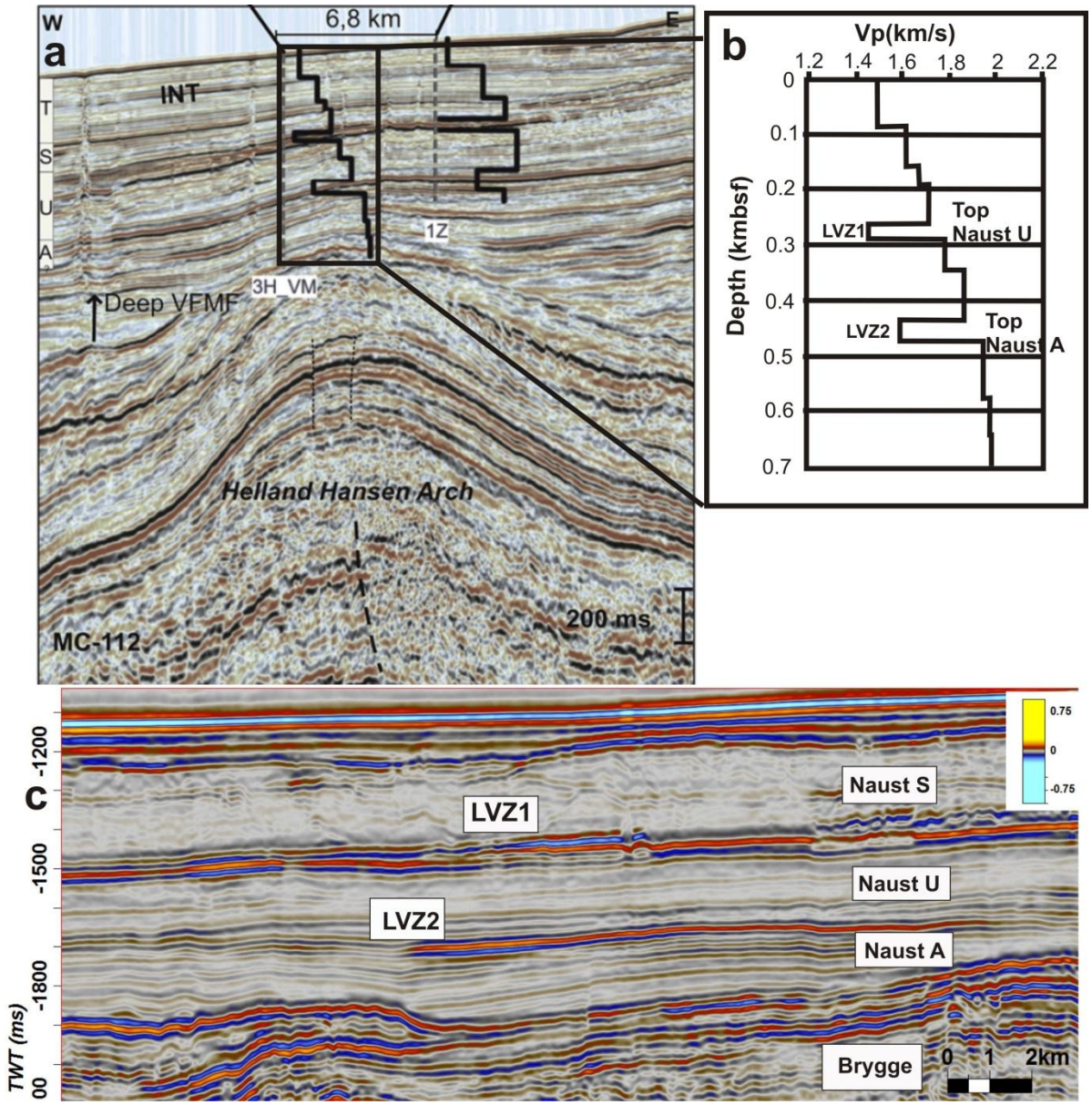


**Figure 5.3: a and b) Shallow seismic profile 06JM29S with projected velocity model taken from Plaza et al (2010) shows two anomalous low velocity zone LVZ1 and LVZ2 with high seismic amplitude. c) Seismic profile shows the same high amplitude anomaly caused by the LVZ1 and LVZ2 at top Naust U and Naust A respectively.**

The P-waves velocity model (Fig.5.3) from Plaza et al., (2010) was derived from the vertical component of an OBS (ocean-bottom seismometer) station in the investigated survey area where Brygge and Naust Fm exists (Rise et al., 2010). According to this model the P-wave velocity generally increases with depth due to compaction and depth of burial. Two low velocity anomalies are marked at the top of Naust A and U unit, termed as low velocity zone (LVZ). LVZ1 (Plaza et al., 2010) shows a marked decrease in velocity from 1710m/s to 1460m/s, i.e. 250 m/s. LVZ2 (Plaza et al., 2010) represents an velocity inversion of 280m/s

with a velocity decrease from 1720m/s to 1440m/s (Fig. 5.4 b). The velocity anomalies do not represent lithological changes but rather appreciable amounts of gas in the pore space of sediments, which causes the distinct reduction of P-wave velocity. (Plaza et al., 2010). Fluids are partly trapped at the top of Brygge formation and are seeping through faults upwards and accumulating at the top Naust A and Naust U where they produce velocity anomalies because of appreciable concentrations of gas in sediments.

The low velocity zone LVZ2 (Plaza et al., 2010) is encountered at top of Naust A unit where high amplitude anomalies A1-A4 are observed on seismic as well as on amplitude maps (Figs. 5.4, 4.23- 4.25, p. 64-66) with acoustic pipes beneath them, which presents the focused routes for fluid migration. The presence of high amplitude anomalies caused by the LVZ2 with acoustic pipes beneath suggests the concentration of gassy sediments at the top of Naust A close to the crest of HHA.

Similarly the high amplitude anomaly U1 with reverse polarity caused by the LVZ1 (Plaza et al., 2010) represents gas charged sediments (Figs. 5.4, 4.26, p. 67). The acoustic pipes are well developed along the reactivated faults in Naust U unit, which provide the focused routes for gas migration and related gas accumulation at the top of Naust U unit (Fig. 4.27, p. 68).

Naust S unit also shows high amplitude anomalies on RMS and on seismic profile (Figs. 4.31-4.32, p. 72-73). These high amplitudes anomalies are most likely the result of higher P-wave velocities due to debris flow deposits. The amplitude anomaly S1 (Figs.4.31-4.32, p. 72-73) could also be the result of lithological changes although vertical dim zones indicating fluids can be observed beneath S1. Thus, there may be a possibility that gas bearing sediments exists also in local areas of debris flow deposit of Naust S unit.

## 5.4 Origin of Thermogenic gas

Thermogenic gas can be produced at considerable depth where organic compounds undergo high temperature degradation and cracking of organic compounds (Welte et al., 1984). Thermogenic gas may migrate towards the surface due to large enough hydraulic gradients. It may be trapped as shallow gas accumulations (Fig. 1.2, p. 2). (Floodgate & Judd, 1992., Missiaen et al., 2002).

In our study area the root zone (where hydrocarbons may start to leak) of thermogenic gas and the fluid source is impossible to define due to acoustic masking and chaotic zones increasing with depth (Fig. 4.12 ,p. 53 ) (e.g. Hustoft et al., 2010).

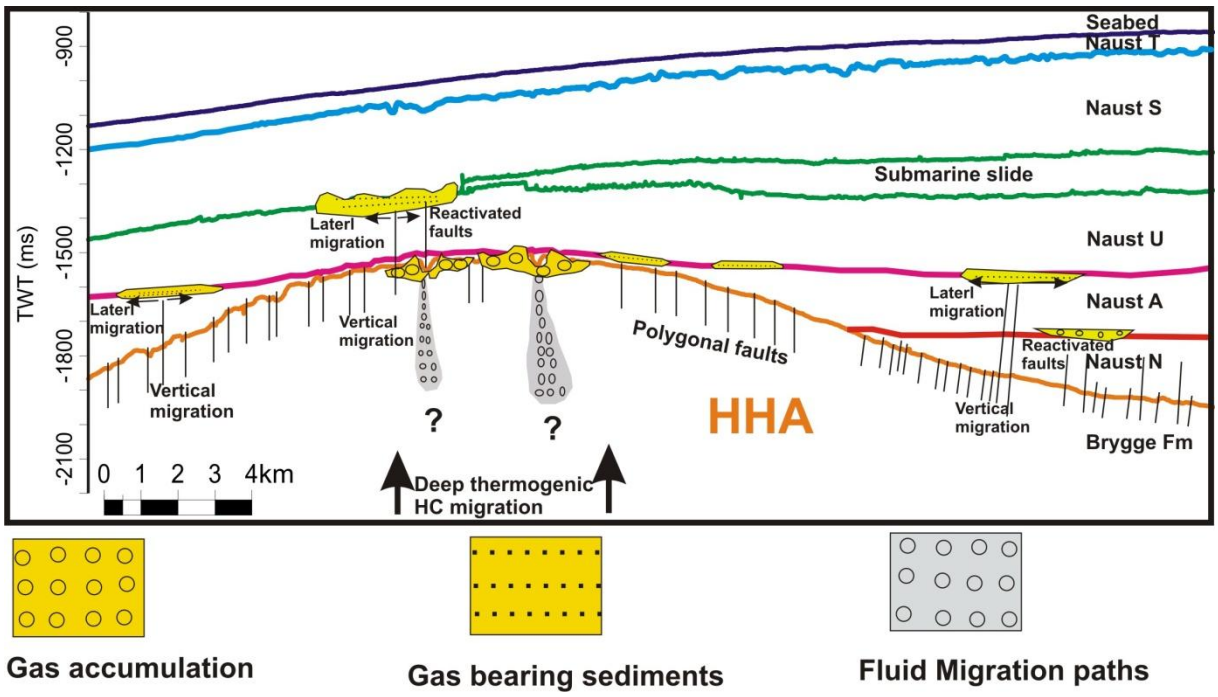


**Figure 5.4: Seismic conceptual model suggesting gas accumulation at the crest of HHA, gas bearing sediments at the top of Naust A and U unit, vertical fluid migration paths and unknown root zones of thermogenic gas.**

## 5.5 The Submarine debris-flow deposit acting as a seal

A thin layer of Naust U unit covers the shallowest crest of HHA and therefore may not act as a good seal for vertical migrating fluid (Figs. 2.8, p. 26, 4.27, p. 68). At the end of the Elsterian glaciations the deposition of Naust S covered the entire HHA and may have created an excessive pore pressure in Brygge Formation (Fig. 4.10, p. 50). As a result, vertical migration of gas started and accumulated at the crest of HHA due to impermeable sediment at the top of Brygge formation. At the crest of HHA the accumulation occurred mostly in the north and northwestern part of the survey (Fig. 4.10, p. 50). (Rise et al., 2006).

Glacigenic debris flow deposit and submarine slides consist of materials (Diamakis et al., 2000 ., De Blasio et al., 2005) that may be less sensitive than marine sediments ( Berg et al., 2005., Kvalstad et al., 2005) due to their unsorted grain size distribution and high plasticity index and low water content (Mitchell et al., 1993). All these characteristics make debris flow deposit a good seal for the vertical migrating fluid from the Brygge Formation (Fig. 4.10, p. 50). Upward migrating fluids accumulate at the base of debris flow deposit of Naust S (Figs. 4.26, p. 67 & 5.3, p. 78). Therefore a sufficient acoustic impedance between over consolidated and impermeable thicker debris flow deposit (Naust S) and gas bearing sediments beneath produce the high amplitude anomalies (Figs.4.10, p. 50 & 4.26, p. 67) (e.g. Gay & Berndt, 2007).

Debris flow deposits further prevent vertical fluid migration and may cause lateral migration of fluids and up-slope along strata. (Bunz & Mienert, 2004). These upward migrating fluids may get trapped beneath the gas hydrate stability zone and as a result a BSR may develop (Gay & Berndt, 2007).

## 5.6 Geological process controlling the Fluid Migration

There are various geological processes that may trigger vertical fluid expulsion associated with excess pore-fluid pressure. A common geological process is rapid sediment loading (Dugan and Flemings, 2000) and/or polygonal faulting (Cartwright et al., 2007).

The survey area investigated shows prograding sedimentary sequences and sediment loading during Plio-Pleistocene (Rise et al., 2006). The Plio-Pleistocene sequences consist of westerly prograded units of Naust Formations. Naust S unit comprises 300-350m (Rise, 2006) thick glacigenic debris flow deposits above the crest of HHA, which completely buried the HHA (Fig. 4.28, p. 69). This thick unit consists of high content of silt/ clay and low permeability, and this may not only increase the excess pore pressure within the Naust S unit but also in base Naust and underlying ooze-dominated siliceous sediments of Brygge Formation along the crest of HHA. This sedimentary loading of glacigenic debris flow deposits is more pronounced at the flank area than the at the crest of HHA. During the deposition (Fig. 4.28, p. 69) it may have caused not only the vertical fluid migration but also triggered the movement of low density ooze material towards the crest of the HHA at the top of Brygge (Fig. 4.18, p. 59) (Rise et al., 2006). The vertical fluid migration is identified along the major faults at the crest of HHA (Figs. 4.16-4.18, p. 57-59). The presences of high amplitude anomalies with reversed polarity at these locations suggest vertical fault related leakage zones (Figs. 4.11, p. 52 and 4.18, p. 59).

In my study area vertical fluid migration (Fig. 4.18, p. 59) mostly takes place along the major faults at the crest of HHA which are clearly visible on the time structure map of Brygge Formation and on seismic sections (Figs. 4.3-4.4, p. 42-43). Three of the faults are tens of kilometers long and hundreds of meters wide showing approx. N-S strike direction (Fig.4.3, p. 42). They are more prominent in the middle and southwestern part of the survey. The faults may have developed during post break up and/or compressional deformation. In the northern part of the survey where the HHA becomes narrow these faults were reactivated as indicated by reverse faulting due to sediment loading by debris flow deposits. The majority of the faults show a curvilinear appearance on the variance map (Fig. 4.16, p. 57) and they are partially interconnected with each other.

**Polygonal faults**

Polygonal faults are important in reservoir geology because they may provide a high drainage potential for pore fluid and for vertically migrating fluid from deep sources (Figs. 4.13-4.15,p. 54-56). (Stuevold et al., 2003., Berndt et al., 2003 & 2005 ., Hustoft et al., 2007., Gay and Berndt, 2007).

Polygonal faults developed in Brygge Formation along the whole arch of HHA (Figs. 5.6, 4.7, p. 47). The polygonal faults are identified by the discontinuous line-up of low amplitude reflection on seismic profile and low coherency values on variance map (Figs 5.6, 4.13, p. 54). The polygonal faults terminate into pipe structures showing distorted sub-vertical seismic pattern which allows the vertical fluid migration (Berndt et al., 2003 & 2005). At the top of Brygge Formation the vertical migrating fluids are stopped by more impermeable sediments along the eastern flank of HHA (Fig. 4.7, p. 47). The trapped fluid can be identified by the high amplitude anomalies (B3 and B4) accompanied by polarity reversal relative to seabed at the top of Brygge Formation along the eastern flank of HHA (Figs. 4.7 -4.8, p. 47-48).

The polygonal faults influenced the fluid expulsion from Brygge Formation to top Naust N unit where the gas accumulated, which is represented by the high amplitude anomalies N1 and N2 (Fig. 4.21, p. 62 ).

**Relationship between submarine slide and Polygonal faults**

In study area two processes accounts for the development of polygonal faults. The first process includes syneresis of colloidal sediment which involves the compaction by the volumetric contraction due to gravitational sediment loading (Scheree et al., 1986., Van Vielt et al., 1991., Goulty and Swarbrick et al, 2005., Gay and Berndt, 2007). The second process accounts the instantaneous compaction caused by the rapid loading by debris-flow deposit during submarine sliding. Due to this instantaneous character, polygonal faults developed at the base of Naust Formation. Thus the development of submarine sliding not only reactivated the polygonal faults within the underlying the Brygge Formation but also caused a propagation of the polygonal faults upward within the base of the Naust Formation. (Gay and Berndt, 2007) (Fig. 5.6).

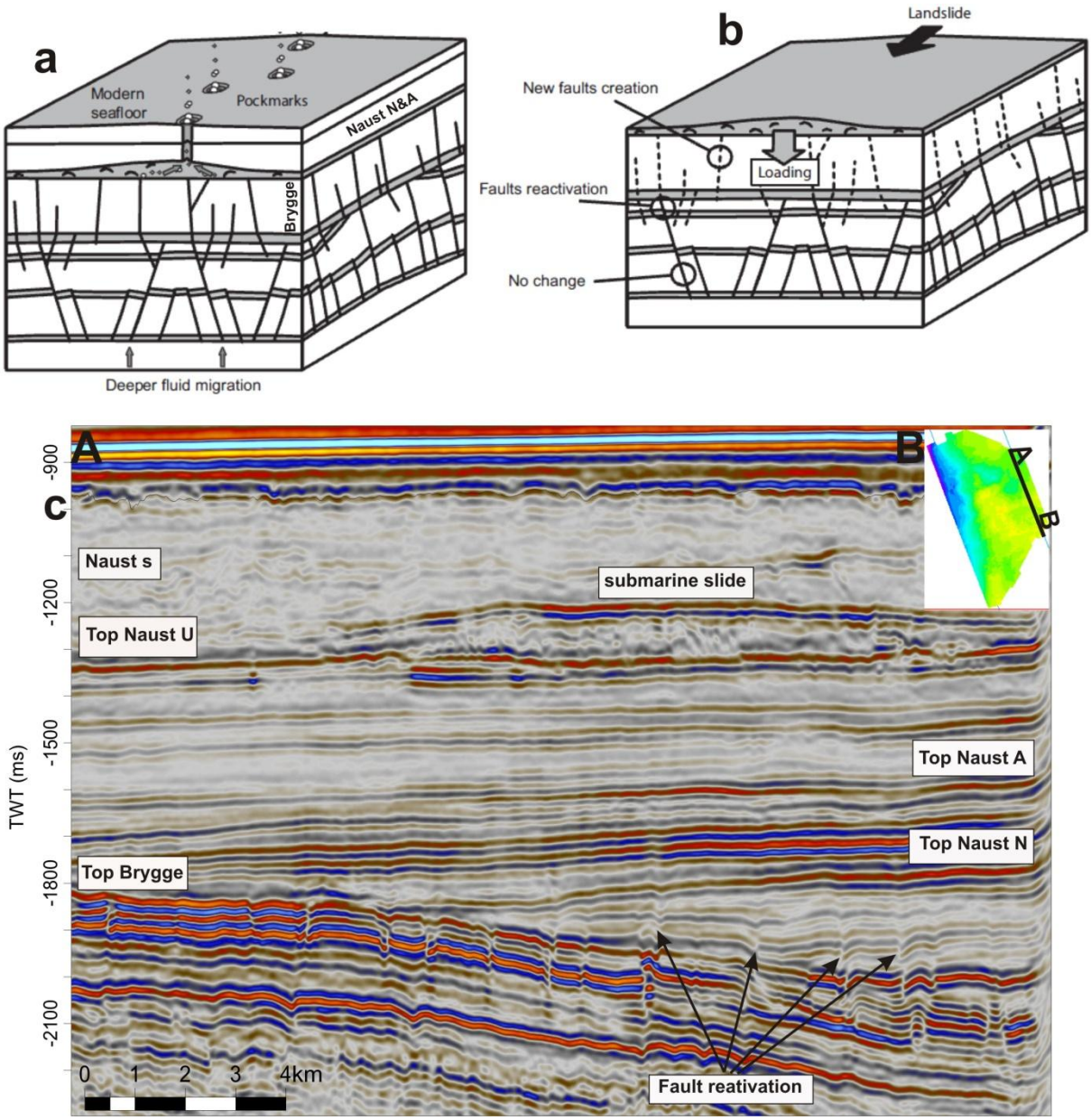


**Figure 5.6: a, b) Schematic model (form Gay & Berndt, 2007) illustrates the process of formation and reactivation polygonal faults in Base Naust units. c) A seismic profile shows the fault reactivation by discontinuous line-up reflection.**

The submarine slide which has created the reactivated faults is identified by a flat to concave base incorporating the internally chaotic unit due to extensive erosion and remoulding of the underlying sediments. It shows an oblate shape on the variance map forming elongated curved lineations interpreted as arcuate pressure ridges (Figs. 4.29-4.30, p. 70-71). This submarine slide comprises of regular debris flow deposit and is not the glacigenic origin (Nygård).

On the eastern flank of HHA polygonal faults in the Brygge Formation do not act as seal because they are reactivated within the base of Naust Formation by the load of overlying debris flow deposit during instantaneous processes (Fig. 4.21, p. 62). These reactivated polygonal faults terminate into pipe structure (Fig. 5.6), which provide the routes for deeper (? thermogenic) gas and intra-formation fluids to migrate vertically and accumulate at the top of Naust N, A and U units. The gas accumulation at the top of Naust A and U is identified by the high amplitude anomalies accompanied by the reverse polarity relative to seabed and LVZs (Plaza et al., 2010) (Figs. 5.4, 4.24-4.25, p. 65-66).

# 6. Conclusion

3D seismic interpretation and acoustic attribute generation by using Petrel software helped to identify pathways of migrating fluid and their accumulation area within different sedimentary formations.

- The Brygge Formation shows areas of gas accumulation as inferred from both the existence of bright spots and the decrease of frequency. Beneath the suggested gas accumulation zones acoustic masking and vertical wipe-out zones exist indicating focused fluid flow pathways. Vertical fluid migration takes place along major faults at the crest of HHA but also at polygonal faults. They are identified by a discontinuous line-up of low amplitude reflections on seismic sections and low coherency values on the variance map. Polygonal faults provide routes for vertical fluid migration.
- The NAUST Formation shows high amplitude anomalies having a large lateral extent Naust N, A and U. Evidence for reverse amplitude polarity relative to the seabed are interpreted as gas bearing sediment. The presence of gassy sediments at the top of Naust A and U unit is accompanied by a distinct decrease in P-wave velocity. Reactivated polygonal faults in base Naust are connected to pipe structures that provide routes for further vertical fluid migration. The polygonal faults along the HHA suggest a reactivation by rapid and instantaneous sediment deposition. Submarine slide material deposition may have contributed to such sediment loading processes.
- At the base of Naust S debris flow deposit are identified by the internally chaotic seismic patterns and by elongated curved lineation termed as arcuate pressure ridges on the variance map.
- At the base of the debris flow deposit gas is trapped and accumulates. Debris flow deposit consists of stiffer materials and can make a god trap for the vertical migrating fluids from the Brygge Formation.

# 7 References

Andreassen, K., 2009. Marine Geophysics, lecture notes for Geo-3123.

Andreassen, K., Nilssen, E., Ødegaard, C., 2007. Analysis of shallow gas and fluid migration within the Plio-Pleistocene sedimentary succession of the SW Barents Sea continental margin using 3D seismic data. Geo-Marine Letters, 27(2), p. 155-171.

Barth, G.A., Scholl, D.W., Child, J.R., 2006. Possible deep-water gas hydrates accumulation in the Bering sea, U.S. Department of energy.

Berg, K., Solheim, A., Bryn, P., 2005. The Pleistocene to recent geological development of the Ormen Lange area. Marine and Petroleum Geology, v. 22, p. 45–56.

Berndt, C., 2005. Focused fluid flow in passive continental margins. Philos. Trans. R. Soc. Lond., v. 363, p. 2855–2871.

Berndt, C., Bunz, S., Mienert, J., 2003. Polygonal fault systems on the mid- Norwegian margin: a long-term source for fluid flow. In: Van Rensbergen, P., Hillis, R.R., Maltman, A.J. & Morley, C.K. (eds) Subsurface Sediment Mobilization. Geological Society, London, Special Publications. 216, p. 283–290.

Blystad, P., Brekke, H., Færseth, R.B., Larsen, B.T., Skogseid, J., Tørudbakken, B., 1995. Structural elements of the Norwegian continental shelf, Part II: The Norwegian Sea region. Nor. Pet. Direct. Bull. 8, 45 pp.

Brekke, H., Riss, F., 1987. Tectonic and basin evolution of the Norwegian shelf between 62° N and 72° N. Nor.Geol. Tidsskr. 67, p. 295-322.

Brown, A.R., 1999. Interpretation of three-dimensional seismic data: AAPG Memoir, v. 42.

Bryn, P., Berg, K., Lien, R., Solheim, A., 2005. Submarine slides on the mid-Norwegian continental margin – a challenge to the oil industry. Onshore–Offshore Relationships on the North Atlantic Margin, v. 12, p. 255–263.

Bukovics, C and Ziegler, P. A., 1985. Tectonic development of the Mid- Norway continental margin. Mar. Pet. Geo., 2: p. 2-22.

Bunz, S., Mienert, J., 2004. Acoustic imaging of gas hydrate and free gas at the Storegga slide. Journal of Geophysical Research, v. 109, p. 1-15.

Bunz, S., Mienert J., Berndt, C., 2003. Geological controls on the Storegga gas-hydrate system of the mid-Norwegian continental margin. Earth and Planetary Science Letter 209, p. 291-307.

Bøen, F., Eggen, S., Vollset, J., 1984. Structures and basins of the margin from 62–69ºN and their development. In: Spencer, A.M. et al. (Eds.), Petroleum Geology of the North European Margin. Norwegian Petroleum Society, Graham and Trotman, London, p. 3–28.

Cartwright, J., Huuse, M., Aplin, A., 2007. Seal bypass systems. AAPG Bull., 91, p. 1141-1166.

Cartwright, J.A., Lonergan, L., 1996. Volumetric contraction during the compaction of mud rocks: a mechanism for the development of regional-scale polygonal fault system. Basin Res. 8, p. 183–193.

Chand, S., Minshull, T.A., 2003. Seismic constraints on the effect of gas hydrate on sediment physical properties and fluid flow: a review. Geofluid3, p. 275-289.

Chand. S., Rise, L., Knies, K., Haflidason, H., Hjelstuen, B.O., Bøe, R., 2011. Stratigraphic development of the south Vøring margin (Mid-Norway) since early Cenozoic time and its influence on subsurface fluid flow. Marine and Petroleum Geology. V. 28, p. 1350-1363.

Dalland, A., Worsley, D., Ofstad, K., 1988. A lithostratigraphic scheme for the Mesozoic and Cenozoic succession offshore mid-and northern Norway. Nor. Pet. Direct. Bull. 8.

De Blasio, F.V., Elverhoi, A., Issler, D., Harbitz, C.B., Bryn, P. & Lien, R., 2005. On the dynamics of subaqueous clay rich gravity mass flows: the giant Storegga Slide, Norway. Marine and Petroleum Geology, v. 22, p. 179–186.

Detlev Leythaeuser. Encyclopedia of hydrocarbon.

Dillon, W.P., Max, M. D., 2000. Oceanic gas hydrate. In: Coastal system and continental margins, Natural gas hydrates in oceanic and permafrost environments. Kluwer Academic press London. P. 61-76.

Dimakis, P., Elverhoi, A., Hoeeg, K., 2000. Submarine slope stability on high-latitude glaciated Svalbard–Barents Sea margin. Marine Geology, v. 162, p.303–316.

Dugan, B., Flemings, P.B., 2000. Overpressure and fluid flow in the New Jersey continental slope: implications for slope failure and cold seeps. Science, v. 289, p. 288-291.

Doré, A.G., Lundin, E.R., 1996. Cenozoic compressional structures on the NE Atlantic margin: nature, origin and potential significance for hydrocarbon exploration. Pet. Geosci. 2, p. 299–311.

Eidvin, T., Jansen, E., Rundberg, Y., Brekke, H., Grogan, P., 2000. The upper Cenozoic of the Norwegian continental shelf correlated with the deep sea record of the Norwegian Sea and the North Atlantic. Mar. Pet. Geol. 17, p. 579– 600.

Eldholm, O., Theide, J. and Taylor, E., 1989. Evolution of the Vøring volcanic margin. Proc. ODP Sci. Res., 104, p. 1033-1065.

Floodgate, G. D., Judd, A.G; 1992. The origin of shallow gas. Continental shelf research. V, 12, No10, p. 1145-1156.

Gabrielsen, R.H., 1984. Long-lived fault zones and their influence on the tectonic development of the southwestern Barents Sea. J. Geol. Soc. London, 141: p. 651-662.

Gay, A., Berndt, C., 2007. Cessation/reactivation of polygonal faulting and effects on fluid flow in the Vøring Basin, Norwegian Margin. J. Geol. Soc. 164 (1), p. 129–141.

Goulty, N.R., Swarbrick, R.E., 2005. Development of polygonal fault systems: a test of hypotheses. Journal of the Geological Society, London, 162, p. 587–590.

Grunnaleite, I., Gabrielsen, R.H., 1995. The structure of the Møre Basin. Tectonophysics 252, p. 221–251.

Guliev, I.S., 1992. A Review of Mud Volcanism. Azerbaijan Academy of Sciences Institute of Geology, Naftra Press, Baku, 65.

Hamar, G.P., Hjelle, K., 1984. Tectonic framework of the Møre Basin and the northern North Sea. In: Spencer, A.M. et al. (Eds.), Petroleum Geology of the North European Margin. Norwegian Petroleum Society, Graham and Trotman, London, p. 349-358.

Heggland, R., 1999. Gas seepage as an indicator of deeper prospective reservoirs. A study based on exploration 3D seismic data. Mar. Petrol. Geol., 15, p. 1-9.

Hinz, K., Dostmann, H.J., Hanisch, J., 1982. Structural framework of the Norwegian Sea. In: The Geological Framework and Hydrocarbon Potential of the Basins in Northern Seas. Offshore North Sea Conference 1982, Norwegian Petroleum Society, Article E=4, 22.

Hjelstuen, B.O., Sjurp, H.P., Hafidason, H., Nygærd, A., Ceramicola, S., Bryan, P., 2005. Late Cenozoic glacial history and evolution of the Storegga Slide area and adjust slide flanks regions, Norwegian continental margin. Marine and Petroleum Geology 22.p. 57-69.

Hjelstuen, B.O., Sejrup, H.P., Haflidason, H., Berg, K., Bryn, P., 2004. Neogene and Quaternary depositional environments on the Norwegian continental margin, 628N–688N. Marine Geology 213. p. 257– 276.

Hoveland, M., Gardner. J. V., Judd. A.G., 2002. The significance of pockmarks to understanding fluid flow processes and geo hazards. Geofluids 2, p.127-136.

Hovland, M., Judd, A.G., 1988. Seabed Pockmarks and Seepages: Impact on Geology, Biology and the Marine Environment. Graham & Trotman Ltd., London. 293.

Hustoft, S., Mienert, J., Bunz, S., Nouze, H., 2007. High-resolution 3D-seismic data indicate focussed fluid migration pathways above polygonal fault systems of the mid-Norwegian margin. Marine Geology 245, p. 89–106.

Hustoft, S., Bünz, S., Mienert, J., 2010. Three-dimensional seismic analysis of the morphology and spatial distribution of chimneys beneath the Nyegga pockmark field, offshore mid-Norway, Basin Research, 22(4), p.465-480.

Judd, A., Hovland, M., 2007. Seabed fluid flow, the impact on geology, biology and the marine environment. Cambridge University Press, Cambridge, DOI 10.2277/0521819504.

Jørgensen, F., Navrestad, T., 1981. The geology of the Norwegian Shelf between 62ºN and the Lofoten islands. In: Illing, L.V., Hobson, G.D. (Eds.), Petroleum Geology of the Continental Shelf of Northwest Europe. Heyden, London, p. 407–413.

Kjeldstad, A., Skogseid, J., Langtangen, H. P., Bjørlykke,K., Høeg, K., 2003. Differential loading by prograding sedimentary wedges on continental margins: An arch-forming mechanism. Journal of geophysical research, Vol.108. p. 4-3.

Kvalstad, T.J., Andresen, L., Forsberg, C.F., Berg, K., Bryn, P., Wangen, M., 2005. The Storegga slide: evaluation of triggering sources and slide mechanics. Marine and Petroleum Geology, 22, p. 245–256.

Larsen, V. B., 1987. A synthesis of tectonically related stratigraphy in the North Atlantic-Arctic region from Aalenian to Cenomanian time. Nor.Geol. Tidsskr. 67. p. 281-294.

Leverson, A. I., 1967. Geology of Petroleum. 2nd Edition. Freeman, San Francisco.

Lightenberg, J. H., 2003. Unraveling the petroleum system by enhancing the fluid migration paths in seismic data using neutral network based pattern recognition technique. Geofluids, p. 355-261.

Ligtenberg, J.H., 2005. Detection of fluid migration pathways in seismic data: implications for fault seal analysis. Basin Research17, p. 141–153.

Løseth, H., Gading, M., Wensaas, L., 2009. Hydrocarbon leakage interpreted on seismic data. Marine and Petroleum Geology 26, p. 1304-1319.

Ludin, E., Dore, A. G., 2002. Mid-Cenozoic post-break up deformation in the "passive" margins bordening the Norwegian-Greenland Sea, Marine and Petroleum Geology 19, p. 79-93.

Magoon, L. B., Dow, W. G., 1994. The petroleum system: AAPG Memoir 60, p. 3-24.

Martinsen, O.J., Bben, F., Charnock, M.A., Mangerud, G., Nbttvedt, A., 1999. Cenozoic development of the Norwegian margin 60– 64 8N: sequences and sedimentary response to variable basin physiography and tectonic setting. In: Fleet, A.J., Boldy, S.A.R. (Eds.), Petroleum Geology of Northwest Europe. Proc. 5th Conf. p. 293–304.

Mienert, J., Posewang, J., Lukas, D., 2001. Changes in the hydrate stability zone on the Norwegian Margin and their consequence for methane and carbon releases into the ocean. In P. Schafer, W. Ritzrau, M. Schluter, & J. Thiede (Eds.), the Northern North Atlantic: A Changing environment (p. 259–280). Berlin, Germany: Springer.

Missiaem, T., Murphy, S., Loncke, L., Henriet, J.P., 2002.Very High-resolution seismic mapping of shallow gas in the Belgian coastal zone. Continentlal Shelf Research 22. p. 2291-2301.

Missiaen, T., Murphy, S., Loncke, L; Henriet. J. P., 2002. Very high-resolution seismic mapping of shallow gas in Belgian coastal zone. Continental Shelf Research 22. P. 2291-2301.

Mitchell, J.K., 1993. Fundamentals of Soil Behaviors, 2nd. Wiley, New York.

Nimblett, J., Ruppel, C.D., 2003. Permeability evolution during the formation of gas hydrates in marine sediments. J. Geophys. Res. 108 (B9), 2420.

Nygåard, A., Haflidason, H., Sejrup, H. P. Morphology of a Non-glacigenic Debris Flow Lobe in the Helland Hansen Area Investigated with 3D seismic Data.

Ottesen, D., Rise, L., Andersen, E.S., Bugge, T., Eidvin, T., 2009. Geological evolution of the Norwegian continental shelf between 61°N and 68°N during the last 3 million years. Norwegian Journal of Geology 89, p. 251-265.

Ottesen, D., Dowdeswell, J. A., Rise, L., 2005. Submarine landforms and the reconstruction of fast-flowing ice streams within a large Quaternary ice sheet: The 2500-km-long Norwegian Svalbard margin (57°–80°N). GSA bulletin. P. p. 1033-1050.

Paull, C. K., Ussler. W., Dillon, W. P., 2000. Potential role of gas hydrate decomposition in generating submarine slope failures, in: M.D. Max (Ed.), Natural Gas Hydrate in Oceanic Permafrost Environments, Coastal Systems and Continental Margins 5, Kluwer Academic, Dordrecht, p. 149-156.

Pedersen, S. I., Skov, T., Randen, T. & Sønneland, L., 2005. Automatic Fault Extraction Using Artificial Ants, Mathematical Methods and Modeling in Hydrocarbon Exploration and Production, p. 107-116.

Pedersen, S.I., Randen, T., Sonneland, L. & Steen, O., 2002. Automatic fault extraction using artificial ants. 72nd Annual International Meeting, SEG Expanded Abstracts, 21, p. 512-515.

Perez-Garcia, C., Berndt, C., Klaeschen, D., Mienert, J., Haffert, L., Depreiter, D., Haeckel, M., 2011. Linked halokinesis and mud volcanism at the Mercator mud volcano, Gulf of Cadiz J. Geophys. Res. 116(B05101): 17 PP.

Perez-Garcia, C., Feseker, T., Mienert, J., Berndt, C., 2009. The Håkon Mosby mud volcano: 330000 years of focused fluid flow activity at the SW Barents Sea slope. Marine Geology 262, p. 105–115.

Plaza-Faverola, A., Bunz, S., Mienert, J., 2010. Fluid distributions inferred from P-wave Velocity and reflection seismic amplitude anomalies beneath the Nyegga pockmark field of the mid-Norwegian margin. Marine and Petroleum Geology 27, p. 46-60.

Plaza-Faverola, A., Bünz, S., Mienert, J., 2012. The free gas zone beneath gas hydrate bearing sediments and its link to fluid flow: 3-D seismic imaging offshore mid-Norway. Marine Geology. 291-294, p. 211-226.

Rise, L., Chand. S., Hjelstuen, B. O., Haflidason, H., Bøe, R., 2010. Late Cenozoic geological development of the south Vøring margin, mid-Norway. Marine and Petroleum Geology 27. p. 1789-1803.

Rise, L., Ottesen, D., Longva, O., Solheim, A., Andersen, A.S., Ayers, S., 2006. The Sklinnadjupet slide and its relation to the Elsterian glaciations on the mid-Norwegian margin. Marine and Petroleum Geology 23, p. 569–583.

Rokoengen, K., Rise, L., Bryn, P., Frenstad, B.,Gustavsen, B., Nygaard, E., Sættem, J., 1995. Upper Cenozoic Stratigraphy on the Mid-Norwegian Continental Shelf. Norsk Geol. Tidsskr., 75, p. 88-104.

Rønnevik, H., Navrestad, H., 1976. Geology of the Norwegian shelf between 62ºN and 69ºN. Offshore North Sea. Technology Conference and Exhibition, Stavanger 1976, GIV=4, p. 1–24.

Scherer, G. W. 1986. Drying gels. I. General theory. Journal of Non-Crystalline Solids, 87, p. 199–225.

Schlumberger., 2010. Interpreter's Guide to Seismic Attribute.

Schlumberger., 2011. Petrel Geophysics Course.

Sejrup, H.P., Haflidason, H., Hjelstuen, B.O., Nygaard, A., Bryn, P., Lien, R., 2004. Pleistocene development of the SE Nordic Seas margin. Mar. Geol. 213, p. 169–200.

Selley, R.C., 1998. Elements of Petroleum Geology.

Sheriff, RE. 2006. Encyclopedia Dictionary of Exploration Geophysics, 5th Ed. Tulsa: Society of Exploration Geophysics.

Shipley, T.H., Houston, M. K., Buffler, R.T., Shaub, F. J., McMillan, K.J., Ladd, J.W., Worzel, J.L., 1979. Seismic reflection evidence for the widespread occurrence of possible gas hydrate horizons on continental slopes and rises. Am. Assoc. Pet. Geol. Bull. 63, p.2201–2213.

Skogseid, J., Eldholm, O., 1989. Vøring Plateau Continental Margin: seismic interpretation, stratigraphy, and vertical movements. Proc. ODP, Sci. Results 104, p. 993–1030.

Skogseid, J., Pedersen, T. and Larsen, V.B., 1992. Vøring Basin: subsidance and tectonic evolution. Nor. Pet. Soc. Spec. Publ1:55-82.

Sloan, E.D.J., 1998. Clathrate Hydrates of Natural Gases. Marcel Dekker Inc., New York & Basel. 705 pp.

Stuevold, L.M., Faerseth, R.B., Arnesen, L., Cartwright, J., Moller, N., 2003. Polygonal Faults in the Ormen Lange Field, More Basin, Offshore Mid Norway. Geological Society of London, London. Special publication216, p. 263-281.

Stuevold, L.M., Skogseid, J., Eldholm, O., 1992. Post-Cretaceous uplift events on the Vøring continental margin. Geology 20, p. 919-922.

Stuevold, L. M., Eldholm, O., 1996.Cenzoic uplift of Fennoscandia inferred from a study of the mid-Norwegian margin, Global and Planetary Change 12, p. 359-386.

Tissot, B.P., Welte, D. H, 1984. Petroleum formation and occurrence, springer Verlag.

Tsikalas, F., Eldholm, O., and Faleide, J.I., 2005. Crustal structure of the Lofoten-Vesterålen continental margin, off Norway: Tectonophysics, v. 404, p. 151–174.

Van Vliet, T., Van Dijk, H.J.M., Zoon, P. & Walstra, P; 1991. Relation between syneresis and rheological properties of particle gels. Colloid and Polymer Science, 269, p. 620–627.

Veeken, P., 2007. Seismic Stratigraphy, Basin analysis and reservoir characterization. In Helbig, K., Theitel, S. (Eds.) Handbook of Geophysics Exploration. Seismic Exploration, 3. Elservier, 509 pp.

Vågnes, E., Gabrielsen, R. H. Haremo, P., 1998. Late Cretaceous-Cenozoic intraplate constructional deformation at the Norwegian continental shelf: Timing, magnitude and regional implications. Tectonophysics 300, p. 29-46.

Welte, D. H., Yukler, M.A., 1984. Petroleum origin and accumulation in basin evolution-A quantitative model. AAPG mem.35, p. 27-78.

Yilmaz, Ö., 1987. Seismic Data Analysis, Vol II, Second Edition. Society of Exploration Geophysicists, Tulsa, Oklahoma, 2027 pp.